On the Development of a Far-Infrared Bolometric Detector Using a 2DEG as the Absorbing Medium

Ian Dean Bacchus

Cardiff University

Department of Physics and Astronomy

September 15, 2007

ProQuest LLC
789 East Eisenhower Parkway
P.O. Box 1346
Ann Arbor, MI 48106-1346

I dedicate this to my grandmother, the greatest human being I have ever known.

Contents

0.1 Abstract

This thesis describes the development of a far-infrared bolometric detector using a two-dimensional electron gas (2DEG) as the detecting medium. The 2DEG is formed at a AlGaAs/GaAs heterojunction made of layers of undoped GaAs and AlGaAs and highly doped ($\sim 5 \times 10^{12} \frac{electrons}{cm^2}$) AlGaAs. A 2DEG layer grown in this way in a molecular beam epitaxy (MBE) system is generally within ~100 nm of the surface of the wafer and is subsequently patterned by etching away the surrounding wafer material and leaving a mesa containing the buried 2DEG. Ohmic contact to the 2DEG is achieved either through a diffusion of charge carriers into the contact region.

Using a 2DEG as the absorbing medium in bolometers will yield detectors that are fast, sensitive, and frequency selective. The low electron densities in 2DEGs ($\sim 10^{11}$ cm^{-2}) allow large-area devices with extremely low thermal conductance between the electrons and the semiconductor lattice (e.g. Appleyard, *et al.* [1]). The fast time constant (on the order of 1 ps) of the electron relaxation time in the 2DEG would allow for very high bandwidth spectroscopy.

This thesis presents an overview of the use of 2DEG bolometers and a detailed study of their properties relevant for use as THz HEBs or CEBs. Chapter 1 briefly outlines the importance of Terahertz astronomy. Chapter 2 presents an introduction to bolometer theory. Chapter 3 provides a description of the electrical, thermal, and magnetic properties of 2DEGs. Chapter 4 outlines the equations governing the operation of 2DEG HEBs and CEBs and contains computer-simulated data. Chapter 5 describes our device fabrication, testing methods, and gives the results of our measurements. Finally, this thesis concludes with a discussion of the results of the tests and possible interpretations in terms of different physical models for electron-photon interactions in the 2DEG.

Chapter 1

Terahertz Radiation and Its Importance to Astronomy

1.1 What Terahertz Radiation Tells Us about the Universe

Terahertz (THz) radiation extends from about $10\mu m$ to 1 mm in the electromagnetic spectrum. It is a frequency range above microwave and below infrared radiation (it is frequently referred to as far-infrared radiation or FIR). Development of technology for astronomy has been approaching the THz band from both directions. We have reliable x-ray, ultraviolet, radio, and microwave telescopes (we started with optical), but this in-between band has remained elusive until very recently. The work to develop THz detectors has been spurred on by the fact that half of the non-cosmic microwave background (non-CMB) light in the universe is in the far infrared, and a good deal of information about the universe lies within this band.

One of the main areas for investigation for FIR astronomy is star formation. Stars form when clouds of dust and gas collapse under their own gravity. This

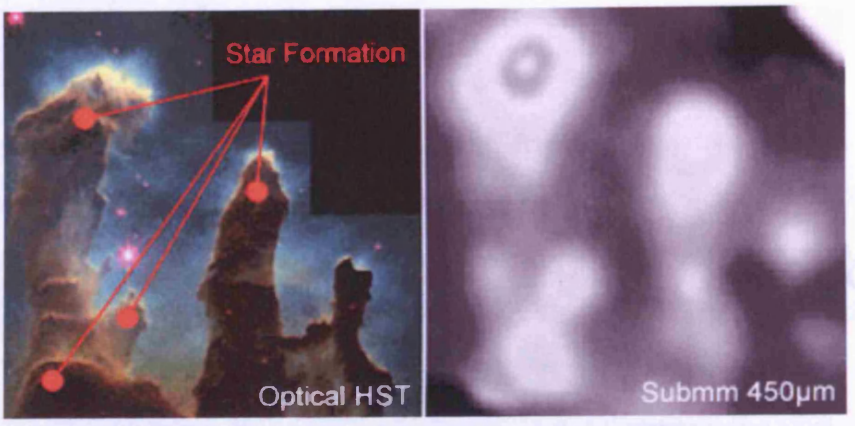

Figure 1.1: A comparison of images of the Eagle Nebula taken by Hubble in the optical and by SCUBA in the THz spectrum. Notice how the THz band shows the features of the star forming regions. (Taken from Mark Devlin's BLAST web site [2])

gravitational collapse generates the heat that ignites the proto-stars. Around these nascent stars, disks of dust and gas coalesce and within these disks new planets form. The planets' gravity disturbs the remaining dust in the disk causing ripples and lumps to form. Radiation emanating from the protostar is absorbed by the dust and reradiated in the far infrared. A good THz detector enables us to observe the star formation directly and the planet formation indirectly. In some instances, these processes are otherwise undetectable.

THz detectors also allow us to see the mechanics of early galaxy formation. Due to expansion, the light from the furthest galaxies has been red-shifted into the far infrared. A detector sensitive to these wavelengths would enable observation of galaxies billions of light years away. These would be the earliest galaxies from "just" after the Big Bang; we could study the very first galaxies in the universe as they form. Again, such events can be invisible to anything but THz detectors.

The processes described above are not well understood precisely because the technology to make precise observations has not been available. THz detectors have

the potential to show us the very beginnings of our universe and the mechanics of its evolution.

1.2 The Problem With Terahertz Detection

Making a THz detector is complicated because THz waves are non-ionizing, strongly absorbed by water, low energy, and produced as a component of blackbody radiation by anything with a temperature above 10K. Water's strong absorption of THz radiation means that the atmosphere will block most celestial signals unless we conduct far infrared observation in very dry, high environments; with the ideal being a space-borne detector. Putting a THz detection apparatus, or anything else, into orbit is extremely expensive and ground-based observation has to be conducted in very high, dry environments such as the Mount Lemmon Infrared Observatory in Utah [3], the airborne SOFIA (Stratospheric Observatory for Infrared Astronomy) [4] jointly run by NASA and the German Aerospace Center, and Antarctica.

Everything with a temperature of more than 10 K will be emitting THz waves so the environment is saturated with signal that will drown out that from stars. Any THz detector will have to be cooled to well below 10K (typically $\approx$300 mK for ground-based systems) for the duration of observation, necessitating the incorporation of cryogenic equipment into any design and the use of expensive (liquid helium) coolant. In the case of "ground-based" measurements, the detectors and cryogenic systems are sometimes lifted to high atmosphere via balloon (see Figure 1.4 showing the BOOMERANG- Balloon Observations Of Millimetric Extragalactic Radiation ANd Geophysics- system) to avoid atmospheric absorption of the signal.

The low energy of THz waves and photons necessitates very sensitive detectors. The required sensitivity is determined by the photon shot noise of the incoming

Measurement Type	Telescope Temp.	Required Sensitivity ($W/\sqrt{Hz}$)
Ground-Based Photometry	300 K	10^{-15}
Ground-Based Spectroscopy	300 K	10^{-17}
Satellite-Based Photometry	60 K	10^{-16}
Satellite-Based Spectroscopy	60 K	10^{-18}
Satellite-Based Mirror	7 K	10^{-19}
Satellite-Based Spectroscopy	7 K	10^{-20}

Table 1.1: Telescope types and their sensitivity requirements assuming an incoming wavelength of 200μm. These numbers are determined by the shot noise of the incoming radiation.

radiation: the detector's sensitivity must be at or below the photon shot noise (see Chapter 4 for a discussion of noise). Table 1.1 lists the sensitivity requirements of different detectors based on their operating temperature and an incoming wavelength of 200μm. The ground-based systems have lesser sensitivity requirements (higher numbers) because of the higher baseline of thermal noise in their systems due to the relative warmth of atmosphere compared to space. The detector must also contend with the power emanating from the detectors themselves, the atmosphere, and space. We calculate these numbers through the Planck blackbody formula:

$$Power = \int \frac{\epsilon(\nu) A\Omega(\frac{2h\nu^3}{c^2})}{\exp(\frac{h\nu}{k_B T}) - 1} d\nu, \tag{1.1}$$

where k_B is the Boltzmann constant, T is temperature, ν is the frequency, $\epsilon(\nu)$ is the frequency-dependent emissivity, A is area, and Ω is the solid angle. In instances in which $h\nu \ll kT$, we can use the expansion $\exp(h\nu/k_BT) \approx 1 + (h\nu/k_BT)$. This allows us to reduce Equation 1.1 to the Rayleigh-Jeans Law:

$$Power = 2k_B T \Delta\nu \epsilon(\nu) \frac{A\Omega}{\lambda^2}, \tag{1.2}$$

where λ is the wavelength and $\Delta\nu$ is the bandwidth. For our example, we need

only consider single-mode transmission [5], so the $A\Omega/\lambda^2$ term will go to one. The value of the emissivity would be given by

$$Emissivity = 1 - Transmission. \tag{1.3}$$

Transmission numbers would be specific to the region, elevation, temperature, etc. at which they were measured.

At lower temperatures, we do not use the expansion. Again, for single-mode, $A\Omega = c^2/\nu^2$ so Equation 1.1 reduces to

$$Power = 2h \int \frac{\epsilon(\nu)\nu}{\exp(\frac{h\nu}{k_B T}) - 1} d\nu. \tag{1.4}$$

Figure 1.2 shows a transmission graph taken on Cerro Sairecabur, Chile. We can get a good estimate of atmospheric power from the sky brightness, as shown in Figure 1.3. In calculating power, we often assume a constant throughput and a constant frequency resolution (i.e. $\Delta\nu/\nu = 1$). We can rewrite Equation 1.1 in terms of the intensity I_ν,

$$Power = \int I_\nu \epsilon(\nu) A\Omega(\nu) d\nu. \tag{1.5}$$

With our assumptions, the sky power is proportional to νI_ν. Table 1.2 shows examples of some power outputs. Compare the background power from atmosphere at 250K versus that from space. This relates back to Table 1.1 in that a ground-based detector is only going to be able to pick up whatever astronomical signal that can be seen above the thermal noise of the atmosphere, hence a detector sensitive enough to pick up anything less would be pointless.

Several different technologies are in use or being developed. Currently, the most often employed THz detector is the composite "spider web" bolometer. The pros and

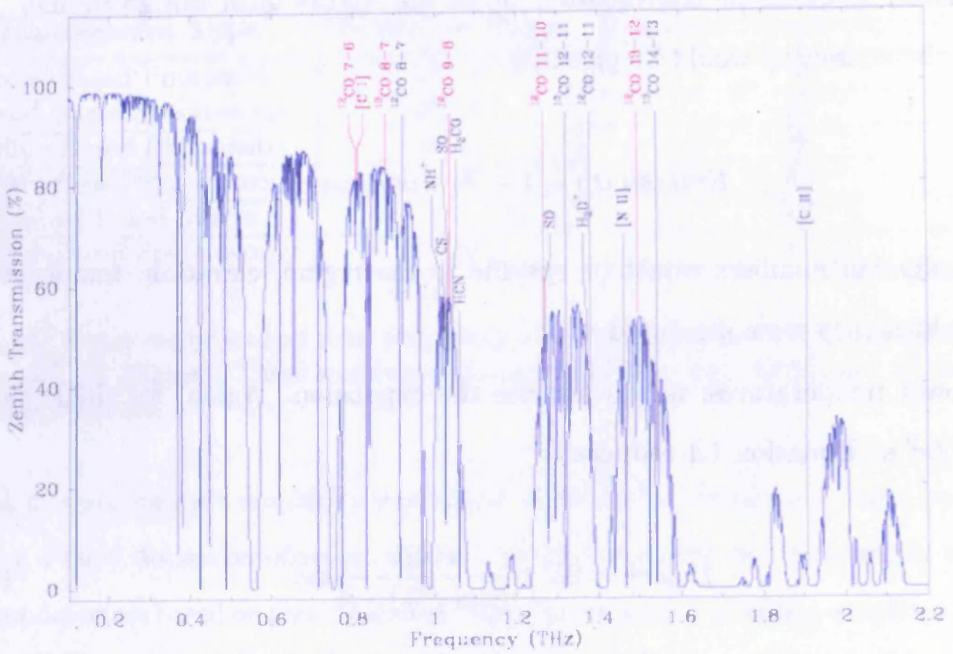

Figure 1.2: A plot of the transmission vs. frequency at Cerro Sairecabur, Chile. (taken from Marrone *et al.* [6])

	Background Power Loading (W) at...		
Source	$1\ THz$	$1.5\ THz$	$2\ THz$
300 K Blackbody	2.24×10^{-9}	1.86×10^{-9}	3.48×10^{-9}
300 K Blackbody w/ 10 % emissivity	2.24×10^{-10}	1.86×10^{-10}	3.48×10^{-10}
250 K atmosphere	1.86×10^{-9}	1.55×10^{-9}	4.83×10^{-9}
Background Power from Space	2.70×10^{-15}	8.00×10^{-15}	2.90×10^{-15}
	$0.6\ THz$	$0.8\ THz$	$1.2\ THz$
80 K telescope w/ 4% emissivity (SPIRE)	2.6×10^{-12}	3.0×10^{-12}	3.8×10^{-12}

Table 1.2: Background powers for detectors, atmosphere, and space followed by those generated by two space-based FIR telescopes. Detectors on these satellites are cooled by on-board helium cryostats in order to give them the sensitivity to detect FIR photons. When the supply of helium runs out, the detectors' temperatures will rise to meet that of their respective satellites and their own noise will drown out the target FIR signal. Values calculated from data in Marrone *et al.* [6] and taken from data in Griffin *et al.* [8]

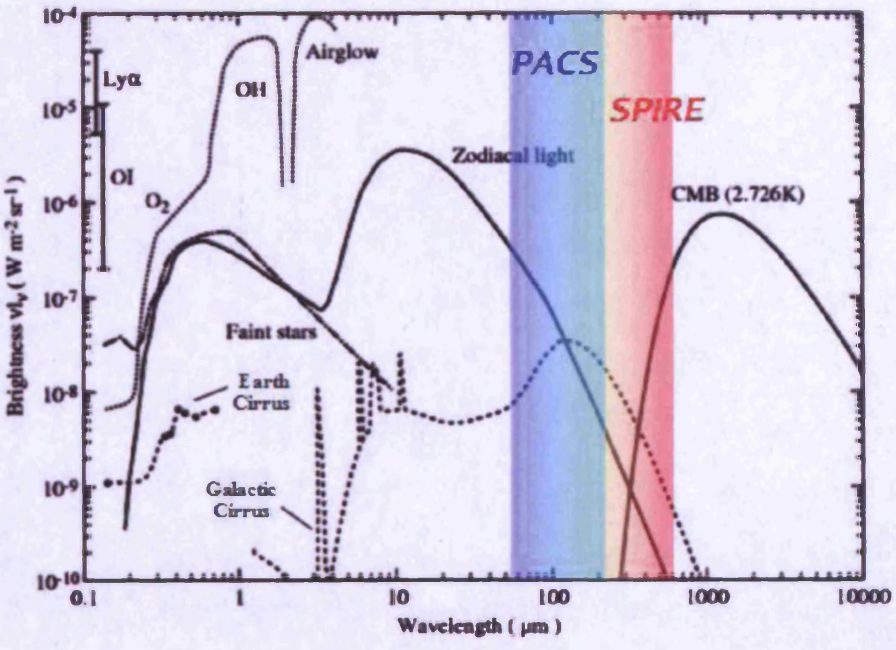

Figure 1.3: A plot of the night sky brightness from various sources vs. wavelength. Note how different sources dominate at different frequencies. The region in which dust emission dominates($\sim$ 1-3 THz, the FIR region) is covered by the PACS and SPIRE instrument in the Herschel Space Observatory. (adapted from image in Leinert *et al.* [7])

cons of each type of detector is covered in Chapter 2. When speaking of maximizing sensitivity, we speak of direct detectors rather than heterodyne detectors. The difference between the two is that a direct detector generates information about the source through absorption of the source's radiation while a heterodyne detector mixes the incoming radiation with a signal from a local oscillator and generates a beat frequency which the operator reads out. All following discussions will concern direct detectors exclusively.

1.3 Our Best Efforts So Far...

Spider web bolometers represent the most well-developed THz detectors at the time of this document's drafting. They detect from $\sim 300\mu$m to 3 mm and have been used extensively to map the sky in the far infrared. The output of each bolometer represents a pixel on the readout, each pixel covering a certain area of the sky. To maximize the amount of sky that can be simultaneously imaged, the bolometers are arranged in arrays. Multiple arrays are used in instances where several different bandwidths are being studied, with each array being tuned to a particular wavelength using appropriate filters. The arrays are mounted in a cryostat that will keep them at liquid helium temperature or lower. Ground-based THz astronomy is mostly done in Antarctica, the most arid environment on the planet. The coldness of the environment further eliminates moisture through freezing. There, bolometric arrays are flown via balloon into the high atmosphere to map the sky in the far infrared. Projects that have used spider web bolometric arrays in this fashion include BOOMERANG [9, 10], BLAST(Balloon-borne Large Aperture Submillimeter Telescope) [11], and Bolocam (Bolometric Camera) [12, 13].

An ideal location for THz detection is space and the satellites Herschel Space

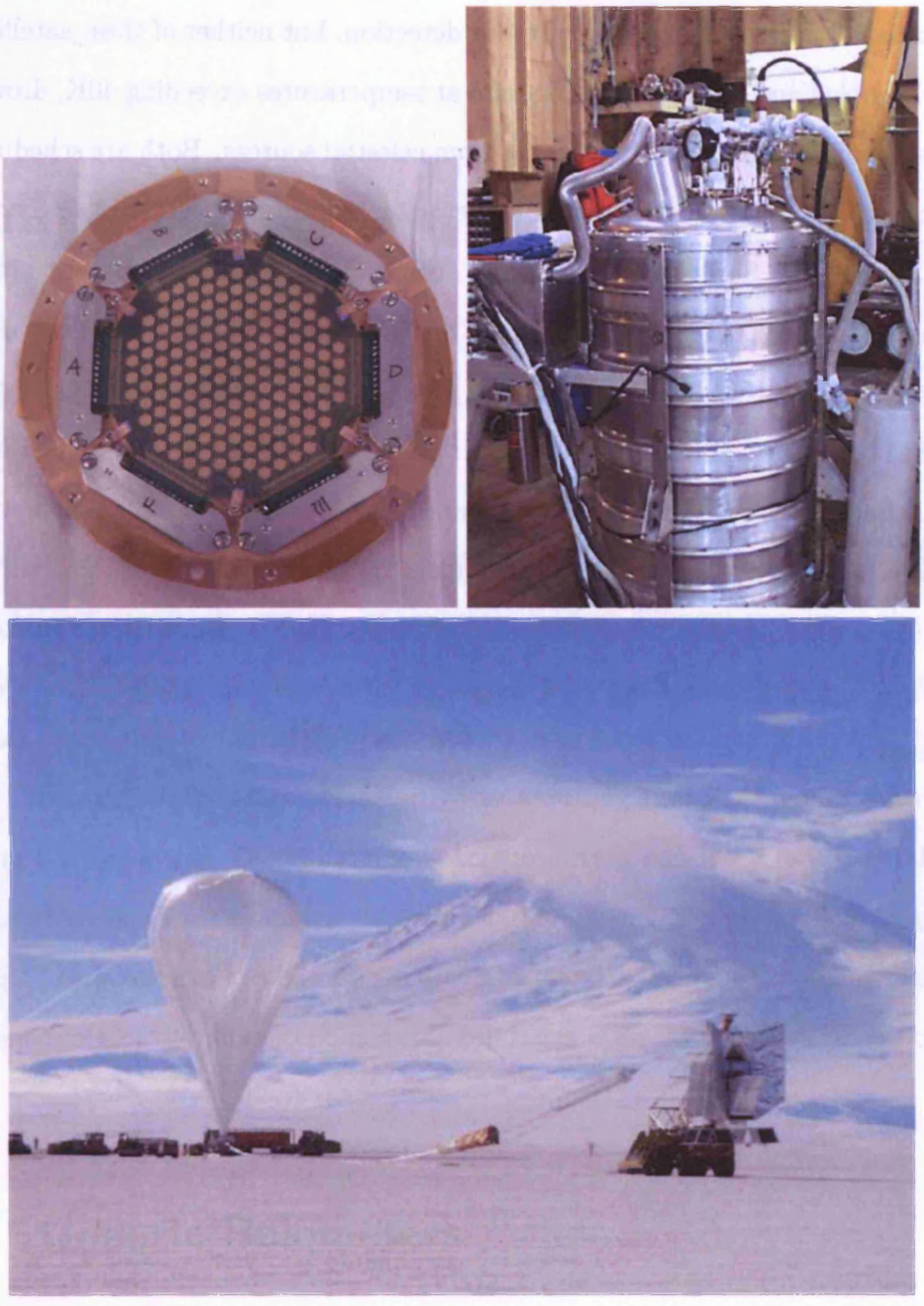

Figure 1.4: Showing (clockwise from top) a bolometric array, a cryostat, and the balloon used for BOOMERANG's launch. From the Astronomy and Instrumentation Group at Cardiff University's web site [14].

Observatory containing SPIRE (Spectral and Photometric Imaging REceiver) [8] and Planck [15] utilize bolometric arrays for detection, but neither of these satellites is actively cooled and the telescopes operate at temperatures exceeding 40K, drowning out a lot of the THz radiation coming from celestial sources. Both are scheduled to launch in July 2008. SPIRE has a detector sensitivity of $2\times10^{-17}W/\sqrt{Hz}$ [8]. as does Planck [15]. Several actively cooled orbital far infrared observatories are in the planning phases. These projects include SAFIR (Single Aperature Far-InfraRed observatory) [16, 17], SPECS(Submillimeter Probe of the Evolution of Cosmic Structure) [18, 17], SPIRIT (SPace InfraRed Interferometric Telescope) [19], and SPICA (Space Infrared Telescope for Cosmology and Astrophysics) [17, 20]. Achieving their design sensitivity requires the development of THz detectors with an NEP of $< 1 \times 10^{-19}$(see Chapter 2 for a discussion of NEP). 2DEG based detectors could realize this requirement and will be a viable option by the time the projects are in the construction phases.

Chapter 2

Bolometer Models

The basic definition of a bolometer is a detector whose electrical properties depend on its rate of energy absorption. In this section three different types of bolometers and the theories governing their operation are discussed, with a concentration on the theories applicable to our 2DEG bolometers. The word bolometer literally means "ray measurer." Bolometers are sensitive to anything that can generate heat, including EM radiation. Therefore, one of the important considerations for making a THz instrument with bolometric detectors is the filtering of high and low frequency signals. The bolometers to be discussed will be standard composite bolometers with different types of thermometers, hot electron bolometers, and cold electron bolometers.

2.1 Generic Bolometers

A generic bolometer consists of a medium to absorb thermal radiation (an absorber) connected to a heat sink through links with low thermal conductance. A resistor whose resistance value is very dependent on temperature (a thermistor) is put in good thermal contact with the absorber so it can be assumed that they are at

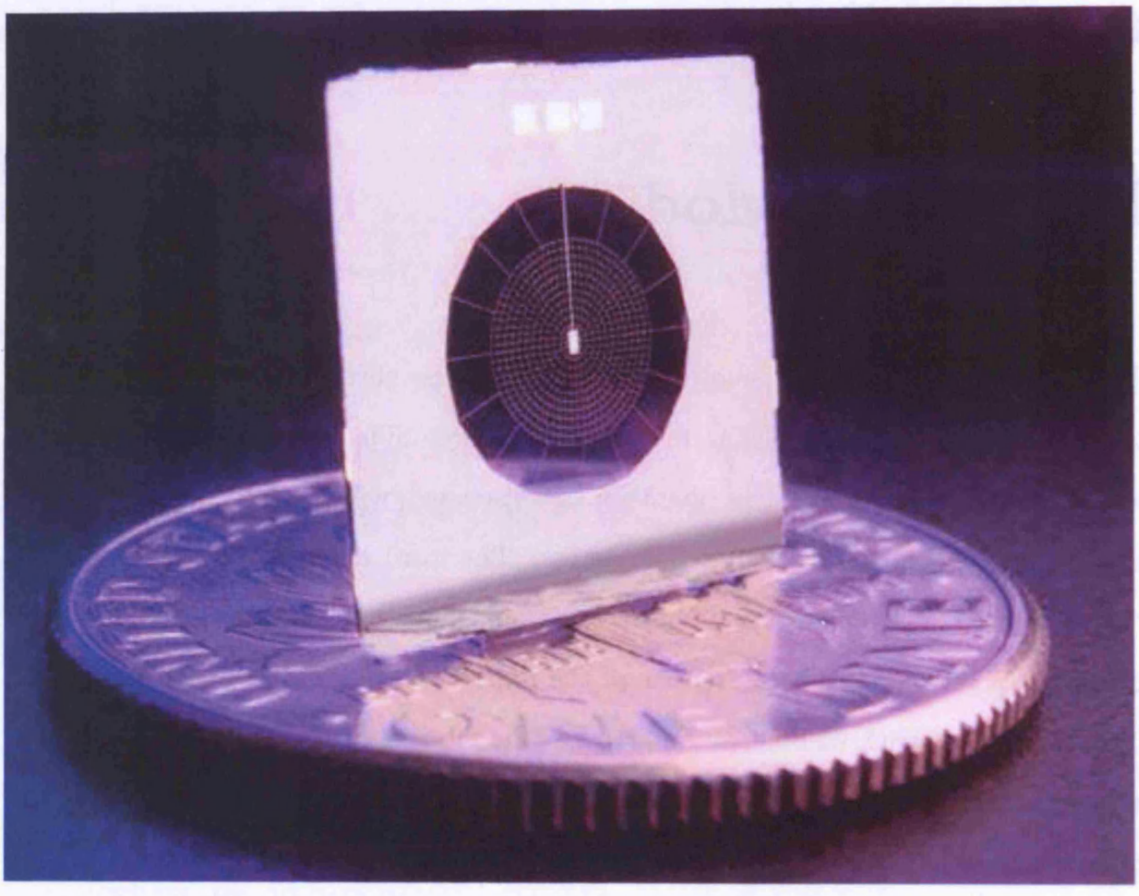

Figure 2.1: A "spider web" composite bolometer. The thermometer sits in the center of the absorber mesh. The mesh is connected to the heat sink via a web of thin legs. The legs are engineered to be as thin as possible so as to make the thermal conductance as small as possible.(Image taken from NASA's Web site [21])

the same temperature. In operation, the power from the source incident on the absorber raises the absorber's and the thermistor's equilibrium temperature. If the rate of change of the thermistor's resistance with temperature (dR/dT) is positive, a voltage bias is used for reading out. If dR/dT is negative, a current bias is used. A semiconductor bolometer, such as the nuetron transmutation doped (NTD) germanium used in Planck and Hershel bolometers [29], would have a negative value for dR/dT. A bias current (I_b) is sent through the thermistor causing a voltage drop across the thermistor; measuring the voltage will give us the resistance value of the thermistor via Ohm's law: $V(T) = I_b R(T)$. This value enables us to determine the source signal. In order to get a reading, we must compare the source signal with the off source signal. The bolometer would be oriented to a point away from the source, an empty spot in the sky. This gives us the off source signal, or the signal the thermistor registers when pointed at "nothing." Subtracting the off source signal from the source signal gives a properly calibrated measure of the power emanating from the source. A schematic of the absorption process in a generic bolometer is shown in Figure 2.2.

A composite bolometer is an example of this kind of bolometer. It consists of an absorber material connected to a thermometer (a resistor) of a dissimilar material. The bolometer is connected to its heat sink via thin legs that minimize the bolometer's thermal conductance G, see Figure 2.1. The average value of G for a leg (neglecting other contributions) would be determined by its cross-sectional area A, its length l , and its thermal conductivity κ [22]:

$$\overline{G}_{leg} = \frac{A\kappa}{l}. \tag{2.1}$$

A low thermal conductance is desirable because we detect radiation by measuring the temperature difference between the absorber at equilibrium and the heat sink.

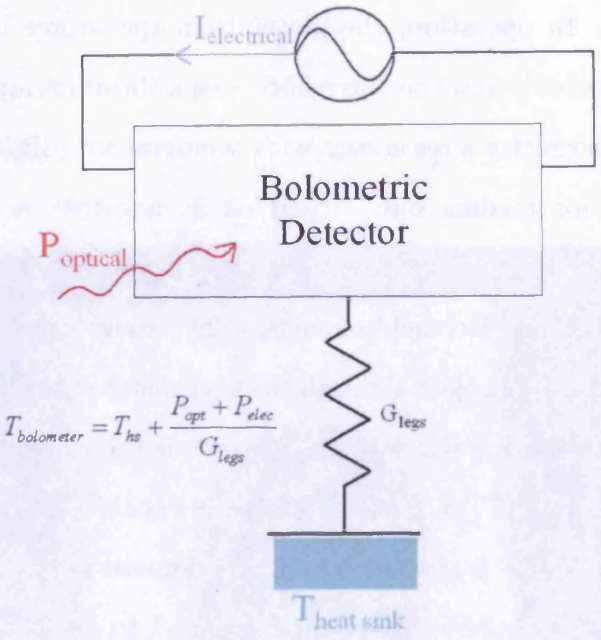

Figure 2.2: Schematic of generic bolometer operation.

The magnitude of the difference will tell us how many Watts of radiative power are hitting the absorber. A source of radiation incident on the absorber will bring the absorber to an equilibrium temperature; this will in turn warm the resistor. For small changes in temperature T (linear response regime) the resistance R changes as

$$R(T) = R(T_0) + \delta T \left(\frac{dR}{dT}\right), \tag{2.2}$$

wher T_0 is the thermistor's average operating temperature, determined by the average optical and electrical power dissipated in the thermistor and absorber. A useful parameter for bolometer discussion is α,

$$\alpha = \frac{1}{R}\left(\frac{dR}{dT}\right), \tag{2.3}$$

Thermal Property	Electrical equivalent
Conductance (G)	Inverse Resistance (1/R)
Temperature (T)	Voltage (V)
Power (P)	Current (I)
Heat Capacity (C)	Capacitance (C)

Table 2.1: Thermal Properties and Their Electrical Equivalents

whose value is specific to the thermometer and is evaluated at the the operating temperature. Again, a semiconductor bolometer would have a negative value for dR/dT. The value of the resistance will indicate the temperature of the bolometer, and the temperature of the bolometer will give the rate of absorption from the source. This can be understood in terms of an "electrical model" of thermal devices. We typically talk about the thermal properties of bolometers, Table 2.1 presents electrical "analogs" of all the relevant thermal properties of bolometers. We will use this to draw "circuit diagrams" that represent the processes involved in thermal detection.

We are interested in looking at the current state of the bolometer and figuring out what the incoming optical power must be to induce that state. In the electrical analogies, power is represented as current, so we are interested in finding the current flowing into the system. Ohm tells us that

$$I = \frac{V}{R}. \tag{2.4}$$

In our analogy, I is the sum of the optical power and the electrical power that we must put in to read the resistance,

$$I \rightarrow P_{optical} + P_{electrical}. \tag{2.5}$$

R is going to be the inverse of the thermal conductance G of the legs,

$$R \rightarrow \frac{1}{G_{legs}}. \tag{2.6}$$

Finally, V is going to be the difference in temperature between the heat sink and the bolometer,

$$\Delta V \rightarrow T_{bolometer} - T_{heatsink}. \tag{2.7}$$

The heat sink temperature is not going to be zero, so the power absorbed is only enough to raise the temperature from that of the heat sink to an equilibrium value, $T_{bolometer}$. This gives

$$P_{opt} = (T_{bolometer} - T_{heatsink})G_{legs} - P_{elec}. \tag{2.8}$$

This is the steady-state condition of a bolometer. The general equation, allowing for power that changes with time, is

$$C\frac{dT}{dt} = P_{opt} + P_{elec} - G_{legs}(T_{bolometer} - T_{heatsink}). \tag{2.9}$$

where C is the heat capacity. Obtaining the heat capacity and thermal conductance enable us to calculate the thermal time constant of the bolometer:

$$\tau = \frac{C}{G}. \tag{2.10}$$

This time constant describes the thermal decay time of the absorber. In order to see the origin of the thermal time constant (Equation 2.10) we can use the electrical analogs to redraw the bolometer schematic in terms of circuit symbols, see Figure 2.3. In a circuit, the time constant would be equal to RC (C for capacitance); Table 2.1 shows that the thermal equivalent is C/G (with C now representing the heat

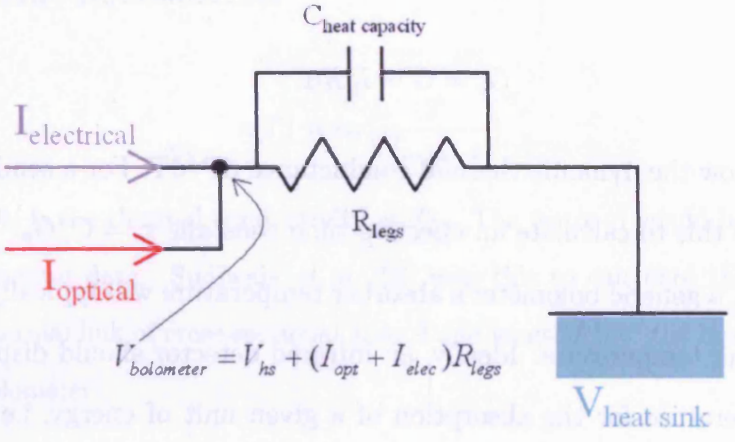

Figure 2.3: Electrical analog for generic bolometer operation. Note that the capacitance (heat capacity) does not come into the equation. This is because it's unchanging during bolometer operation, so it acts like a charged capacitor and the "current" completely bypasses it.

capacity). A problem is immediately evident: we need the thermal conductance to be small in order to have a sensitive bolometer, but the smaller we make it, the longer the time constant becomes. Hence, we can have sensitivity or speed, but not both.

The measured time constant is usually different from τ. This is due to electrothermal feedback: the temperature rise due to an increase in radiant power is affected by the fact that R changes with temperature. Rearranging Equation 2.8 illustrates this,

$$\Delta T = \frac{P_{opt} + P_{elec}}{G_{legs}} \rightarrow \Delta T = \frac{P_{opt} + I_b^2 R(T)}{G_{legs}}. \tag{2.11}$$

The thermal conductance is defined as the rate of change of power with respect to temperature. For a current-biased bolometer, a resistance which changes with temperature would give rise to an effective thermal conductance G_e equal to [22]

$$G_e = G - I_b^2 R\alpha, \tag{2.12}$$

where G is now the dynamic thermal conductance dP/dT. For a semiconductor, $G_e > G$. We use this to calculate an effective time constant $\tau_e = C/G_e$.

In operation, a generic bolometer's absorber temperature will typically be higher than its heat sink temperature. Ideally, an infrared detector should display a large change in temperature for the absorption of a given unit of energy, i.e. it should have a small heat capacity, and so is generally engineered to have such a property. As the heat capacity increases with temperature (Equation 3.66), it is desirable to have a low detector temperature.

Once the thermometer gives us the bolometer temperature, we have all the information we need to determine the optical power detected from the source. How the resistance of the thermometer changes with temperature determines the responsivity of the bolometer. Responsivity is a term which describes a detector's ability to convert input power into signal, specifically it is the change in voltage drop per watt of absorbed power. Its units will depend what sort of signal it puts out, but in general

$$Responsivity = \frac{dSignal}{dPower}. \tag{2.13}$$

In the case of a bolometer [22]:

$$Responsivity = \frac{I_b R\alpha}{G_e(1 + i\omega_s \tau_e)}, \tag{2.14}$$

where ω_s is the frequency at which the incident radiant power is modulated.

Mather [24] makes the assumption that thermal conductivity of the system varies with temperature according to a power law:

$$\kappa(T) = \kappa_0 \left(\frac{T}{T_{heatsink}} \right)^{\beta}, \tag{2.15}$$

where k_0 is the thermal conductivity at T_{hs}. The factor β would be determined by experimental data. Sudiwala *et al.* [23] uses this to calculate the power flow across a thermal link of cross-sectional area A and length l (i.e. the heat conducting leg of a bolometer),

$$P_{leg} = \frac{\int_{T_{hs}}^{T} \kappa(T) dt}{\int_0^l \frac{1}{A} dx}, \tag{2.16}$$

which gives us

$$P_{leg} = \frac{A\kappa_0 T_{hs}}{l(\beta+1)} (\Phi^{\beta+1} - 1), \tag{2.17}$$

where $\Phi = T/T_{hs}$. From $P_{leg} = G\Delta T$, we get the thermal conductance in terms of a temperature ratio:

$$G(\Phi) = \frac{G_0}{\beta+1} \left(\frac{\Phi^{\beta+1} - 1}{\Phi - 1} \right), \tag{2.18}$$

where G_0 is $G(\Phi)$ at the limit where $T \rightarrow T_{hs}$. We can then reexpress Equation 2.8 as

$$P_{elec}(\Phi) = \frac{G_0 T_{hs}}{\beta+1} (\Phi^{\beta+1} - 1) - P_{opt}. \tag{2.19}$$

Thermal bolometers are characterized by their load curves, their voltage-current characteristics. These can be from the results of incrementing $R(T)$ and $P_{elec}(\Phi)$ from $T_{heatsink}$ to a maximum temperature. The values of voltage and current are then found via $P = I^2R$, i.e.

$$V = \sqrt{P(T/T_{hs})R(T)}$$

and (2.20)

$$I = \sqrt{\frac{P(T/T_{hs})}{R(T)}}.$$

The reader is encouraged to look at the works of Mather [24], Sudiwala [23], Richards [22], and Clark-Jones [25] for further and more in-depth discussion of bolometer theory.

2.2 Noise and NEP

The following section touches very briefly on the origins of the equations for noise and NEP. For a more detailed discussion, the reader is encourage to read the text by van der Ziel [26] and the papers by Kuzmin *et al.* [27, 28], and Richards [22] from which this section was derived. There will be a level of naturally occurring noise in the bolometer below which measurement will require averaging the signal over as long an amount of time as possible. This noise is due to a combination of Johnson, phonon, photon, and equipment noise. Noise and its resulting noise equivalent power (NEP) must be considered when making any detector. We calculate the sensitivity of the bolometer by finding its total NEP, which is the ratio of the noise spectral density, the noise power per unit of bandwidth, to the responsivity. Specifically, the NEP is defined as the incident signal power required to obtain a signal equal to the noise in a 1 Hz bandwidth:

$$NoiseEquivalentPower = \frac{NoiseSpectralDensity}{Responsivity}. \quad (2.21)$$

The NEP relates the uncertainty in the detected power to the integration time via

$$dPower = \frac{NEP}{\sqrt{2t_{integration}}}, \tag{2.22}$$

so it has units of $(Watts/\sqrt{Hz})$, regardless of the nature of detection. For a bolometer, the NEP equation would be [29]

$$NEP^2_{total} = NEP^2_{phonon} + NEP^2_{Johnson} + NEP^2_{photon}$$

$$\downarrow \tag{2.23}$$

$$NEP^2_{total} = 4k_BT^2G + \frac{4k_BTR}{S^2} + 2Q(h\nu_o + \eta\epsilon_b k_B T_b).$$

The relevant temperature is that of the bolometer (absorber). R is the bolometer resitance; S, the responsivity; Q, the absorbed incident power; μ_o, the central frequency; η, the overall transmission of the system, ϵ_b, the emissivity of the background; and T_b, the temperature of the background. The lower the temperature, the lower the NEP, the greater the sensitivity, i.e. the lower the signal it can detect.

2.2.1 Johnson Noise

Also known as Johnson-Nyquist noise. This is noise due to random electron fluctuations in a medium; the only way to be rid of it would be to have the system at absolute zero temperature. In a circuit, these fluctuations will give rise to a voltage and, hence, a current that will be there regardless of the optical input. The magnitude of the noise contribution will depend on the resistance of the absorber and its temperature. In order to derive the Johnson noise, it helps to envision a closed circuit consisting of a noiseless resistor of the absorber's resistance and an

impedance-matched terminator connected to a heat sink at 0K. Connecting these entities would be transmission lines of the same impedance as the absorber. The current due to the electron fluctuation is flowing through the resistor, so it's radiating power I^2R. The magnitude of this power, with $d\nu$ centered at ν, will be the power radiated

$$P_\nu = \frac{2h\nu d\nu}{exp(\frac{h\nu}{kT}) - 1} \tag{2.24}$$

A Taylor series expansion will show that this goes to $k_BTd\nu$ when $h\nu \ll kT$, (the noise frequency will be $\sim 10 - 20Hz$) so the power radiated will be k_BTB, where B the bandwidth in question. The terminator impedance will also be radiating. As it is heat sunk to 0K, it will simply radiate the same power as the absorber resistor. As these sources are incoherent, they will add so that the power is $2k_BTB$. This will be the power for each polarization. As we will not be blocking any polarizations, we will have two dimensions, so we multiply by two to get $4k_BTB$. We are interested in how the electrons' fluctuations will affect the voltage. If we multiply the power by resistance, we will get the square of the voltage.

$$V^2_{Power} = 4k_BT_eBR_{2DEG} \tag{2.25}$$

To find (square of) the value of the Johnson noise, we divide Equation 2.25 by the bandwidth, obtaining units of $V/\sqrt{Hz}$. The Johnson noise contribution to the total NEP^2 is obtained by dividing by the square of the responsivity (Equation 2.21) to get the familiar $4k_BTR/S^2$.

2.2.2 Shot Noise

Shot noise arises from the flow of quantized units of energy. Electrical and thermal currents are made up of electrons and phonons, respectively. The flow of these energy units will not be consistent: for a given steady electrical or thermal current, randomly arriving electrons or phonons passing by a given point will be observed. This randomness will give rise to what is called shot noise in the system.

To derive the equation for shot noise, we must look at current flow from the quantum perspective. (Electrical current will be used for the derivation, but the theory covers thermal current as well.) The seemingly continuous flow in a system is actually a random progression of charge carriers. We will call these current pulses. If we were sitting at a point on a wire watching the current go by, the overall current will be the sum total of the current pulses we see pass by. We will mark the contribution of each pulse as it passes our point, the current would only exists in those finite times during which a current pulse is flying by. We can use the Dirac delta function to describe the overall current as a function of time.

$$I(t) = \sum_j q\delta(t - t_j), \tag{2.26}$$

where t_j is the random arrival time of the charge q. In order to evaluate the duration of a current pulse, we use the autocorrelation function:

$$R_I(t') = \lim_{T\to\infty} \int_{-T/2}^{T/2} I(t)I(t + t')dt. \tag{2.27}$$

From this, we can get the noise spectrum through the Wiener-Khintchine theorem [26], which states that the noise spectrum is the Fourier transform of the autocorrelation function:

$$S_I(f) = 2\int_{-\infty}^{\infty} R_I(t')e^{-i2\pi ft'}dt', \tag{2.28}$$

where $S_I(f)$ is the one-sided power spectral density and f is the frequency of the noise. $S_I(f)$ will be the mean-square current fluctuation in a unity bandwidth($\bar{i}^2/\Delta f$). For the final shot noise expression, we plug in the current equation (Equation 2.26 into Equation 2.27),

$$R_I(t') = \lim_{T\to\infty} \sum_k \sum_{k'} \int_{-T/2}^{T/2} \delta(t - t_k)\delta(t - t_{k'} + t')dt$$

$$\downarrow \tag{2.29}$$

$$R_I(t') = \lim_{T\to\infty} \sum_k \sum_{k'} \delta(t - t_{k'} + t').$$

To simplify, we average such that the contributions from the instances where $t_k \neq t'_k$ vanish from the Fourier transform that gets us the power spectral density, i.e. $R_I(t') = q\bar{I}\delta(t')$. The Fourier transform of a delta function gives one, so plugging Equation 2.29 into Equation 2.28 gives

$$S_I(f) = 2q\bar{I}, \tag{2.30}$$

the equation for the shot noise. Note that it is independent of frequency, meaning it is "white" noise. Also, it is a function of the average current. In an AC system, the average current will be zero, so shot noise is exclusively a DC occurrence. To get the contribution of the shot noise to the total NEP, we divide by the responsivity:

$$NEP_{shot}^2 = \frac{2q\bar{I}}{S^2} \tag{2.31}$$

2.2.3 Phonon Noise

Fluctuations in the energy of a bolometer will give rise to the phonon noise. This noise is caused by phonons passing through the thermal conductance of the device. Phonons are quantized units of energy equalling kT_e (for a 2DEG), the phonon noise can therefore be described by shot noise equations. In order to describe it, we will again use the electrical analogs in Table 4.1. The unit of charge q in Equation 2.30 will be kT_e. Current is given by the product of inverse resistance and voltage. We see that the thermal equivalents of these values are thermal conductance G and power P. Therefore phonon NEP is given by

$$NEP^2_{phonon} = 2k_B T_e G P, \tag{2.32}$$

but we recall that $G = dP/dT$, so we can simplify by revaluating P in terms of G and T:

$$NEP^2_{phonon} = 2k_B T_e^2 G. \tag{2.33}$$

The final adjustment is to the coefficient. As when we were considering Johnson noise, we will imagine this system radiating into terminated free space. The resulting radiation will be incoherent, the intensity will therefore add linearly, so the proper value for NEP^2_{phonon} will be twice the value given in Equation 2.33,

$$NEP^2_{phonon} = 4k_B T_e^2 G. \tag{2.34}$$

2.2.4 Photon Noise

Photon noise can again be described by shot noise arguments due to the particle nature of light. This noise is a quality of the radiation source, there's nothing we can

do to lessen it. The NEP_{photon} in Equation 2.23 is an approximation that assumes that the incoming radiation has a very narrow bandwidth around a central frequency ν_o. This is a fair assumption on our part due to the fact that we generally use filters to block out unwanted wavelengths.

2.2.5 Other Noise

In addition to all of the above, there will be noise due to signal amplification as well as the inherent noise of the equipment used during operation. Nearly all electronic systems are subject to low frequency 1/f or flicker noise. All of these must be factored in to the total NEP of the device in order to accurately assess the sensitivity of the detector.

2.3 Hot Electron Bolometers

A hot electron bolometer (HEB) uses the intrinsic heat capacity and thermal conductance of its absorber to determine its performance. Radiation from the source is generally coupled to the absorber through superconducting antenna. An incoming photon is absorbed by an electron in the absorber which transfers it to other electrons in the system at a rate determined by τ_{ee}, the electron-electron scattering time. The electons' energy is transferred to the lattice via electron-phonon interaction, the rate at which this occurs being τ_{ep}, which is much longer than τ_{ee}. The resultant temperature rise changes the electrical properties of the absorber. The earliest HEBs used metal film absorbers. Nahum and Martins developed an x-ray detecting HEB [30] which used a normal metal-insulator-superconductor (NIS) junctions to measure the change in temperature of the absorber, it was proposed that the same idea could be used for FIR wavelengths [31, 32, 33]. A working detector

based on these theories was developed by Chouvaev *et al* [34]. Yngvesson [35] has proposed using a 2DEG as the detector element of an antenna-coupled hot electron bolometer.

HEBs using a superconductor as the absorber have been developed [36, 37, 38]. Superconducting HEBs make use of the electron gas in a superconductor. Below the transition temperature, Cooper pairs form in the superconductor enabling current to flow without resistance, meaning the potential drop across the superconductor disappears. The superconductive state is achieved after a single Cooper pair is formed; once that pair is there, the normal electrons still in the system have no potential to drive them and so cannot contribute to the current. At the transition temperature, Cooper pairs are present about fifty per cent of the time, meaning that pairs are breaking and reforming. Superconductive HEBs operate right at the transition temperature of the superconductive metal they're made from (niobium is very common). A bias current is used to make sure they do not slip into the superconductive state. An incoming photon will hit the superconducting HEB and impart so much energy to the electrons that they become too "hot" and fly apart. Even a partly-formed Cooper pair will have considerably lower loss characteristics than a lone electron, so the result will be a sharp jump in the resistance. This sharpness can be seen in Figure 2.4, the transition curve of niobium. That plot shows that niobium has very large α at the transition region; it would have a correspondingly large responsivity.

Early semiconductor HEBs used for millimeter astronomy were made of InSb. They operated in the 90-140 GHz range [39, 40].

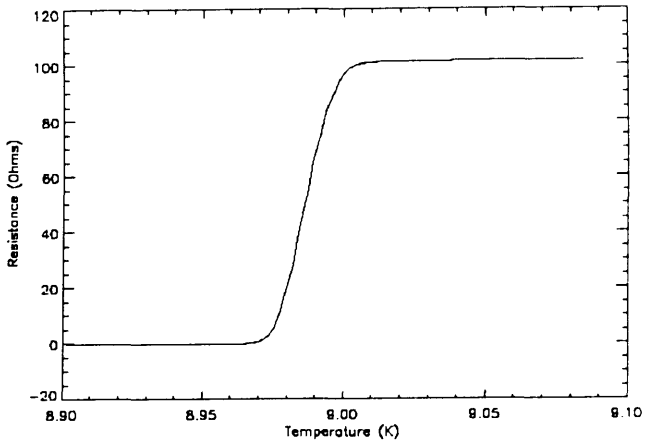

Figure 2.4: Niobium transition curve of sample measuring 5×25 μm^2 from test at Cardiff University. Niobium is often used for constructing superconducting HEBs.

2.4 Cold Electron Bolometers

A cold electron bolometer (CEB) works by removing the photoexcited electrons from the absorber system before they can share their energy with the lattice. Proposed by Kuzmin *et al* [28], a CEB makes use of a superconductor-insulator-normal metal-insulator-superconductor (SINIS) structure [41, 27]. A schematic is shown in Figure 2.5 The absorber is cooled to 300-350 mK to ensure that most of the electrons in the normal metal are at or below the Fermi level. These electrons are trapped by the presence of the energy gaps in the superconducting contacts; there are no available states into which the unexcited electrons can tunnel. An incoming photon excites an electron in the system to an energy above that of the superconductor's energy gap. Rather than allow this electron to distribute its energy to the phonons in the system, a bias voltage sweeps the electron to the barrier and encourages tunneling into the superconducting contact. The process is illustrated in Figure 2.6.

This flow of hot electrons out of the normal metal would constitute a current

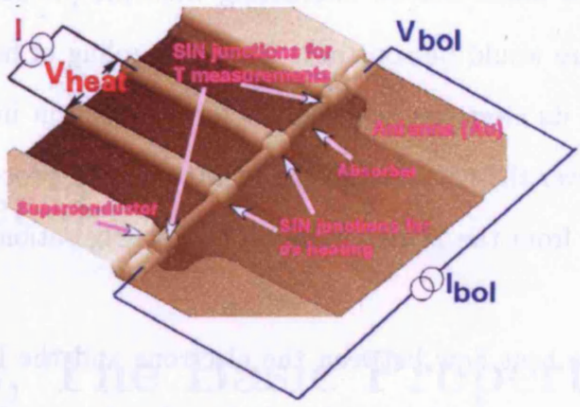

Figure 2.5: Schematic of Kuzmin's CEB made with a normal metal absorber. (Taken from Agulo *et al* [42])

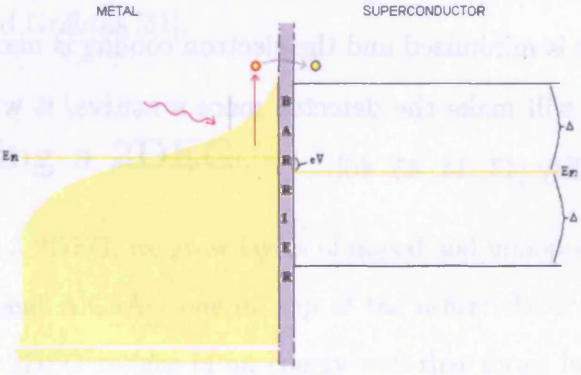

Figure 2.6: CEB made from SINIS structure. The low operating temperature keeps the normal metal's electrons below the Fermi level. An incoming photon allows an individual electron to get above the superconductor energy gap and tunnel into the superconducting contact where it registers as a photocurrent.

whose magnitude would describe the rate of energy absorption from the source. Because the hot electrons would not be interacting with the phonons in the metal, the metal's temperature would be constant. This decoupling of heat flow between the normal metal and its electrons would allow for a condition in which the electron temperature is lower than the metal's temperature. The process by which hot electrons are removed from the 2DEG is called microrefrigeration (it's also called nanorefrigeration).

There will be some heat flow between the electrons and the lattice, but most of the hot electrons tunnel out of the system before they have a chance to interact with the lattice or with other electrons. The overall effect of the tunneling is to cool the electron gas to an equilibrium temperature; the magnitude of this cooling is determined by the bias voltage. A CEB, like any other bolometer, is an equilibrium device; the input power must equal the output power. A CEB will have the sum of its electron-phonon power and it cooling (tunneling) power equal to the optical input power. Adjusting the bias voltage optimizes the tunneling rate such that the electron-phonon power is minimized and the electron cooling is maximized. A lower absorber temperature will make the detector more sensitive, it will also lower the 2DEG's electron mobility [43, 44, 45, 46].

Chapter 3

2DEGs, The Basic Properties

What follows is a discussion on the fabrication and properties of a 2DEG. First basic construction of the semiconductor stack that gives rise to a 2DEG will be addressed, with the exact material data for the fabrication chapter. Then the electrical, thermal, and magnetic properties of 2DEGs will be discussed. Many of the discussions presented are derived from the texts by Kittel [47], Ashcroft and Mermin [48], Liboff [49], Sze [50], and Griffiths [51].

3.1 Making a 2DEG

In order to make a 2DEG, we grow layers of doped and undoped semiconductor (in our case, GaAs and AlGaAs) one on top of the other; the order is illustrated in Figure 3.2. The 2DEG resides in an energy well that forms in the system due to band bending that occurs in semiconductors with different band gaps when brought into contact with one another. Whenever this union occurs, the Fermi levels of the touching parties must equalize. We will look at a metal/semiconductor interface first (discussion derived from text in Bube [53], Fraser [54], and Gavryushin [55]). A metal's Fermi sea can simply readjust, but the equilibration process in semiconductor

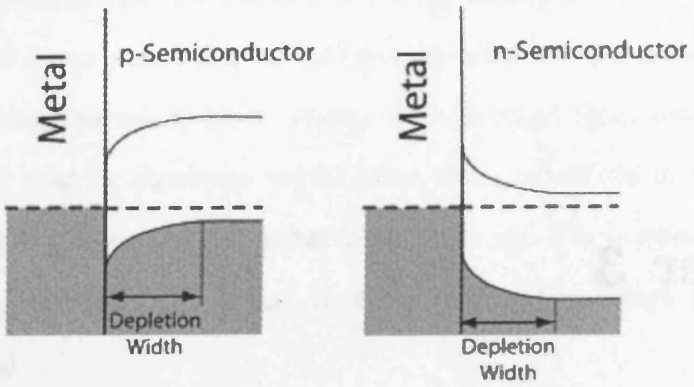

Figure 3.1: Illustration of band bending in metal-semiconductor junctions. In the case of contact between metal and an n-type semiconductor, a Schottky energy barrier is formed. (Image taken from Rockett [52])

is achieved via a migration of charge carriers into the junction region. The charges flow freely until the Fermi levels equalize. In the immediate area of the junction a depletion region will form where the mobile carrier densities are zero. The width of the depletion region is dependent on the material properties of the semiconductor and the voltage applied across the junction. The energy bands of the semiconductor will bend depending on how the semiconductor is doped. In the p-doped case, the conduction and valence bands will be pulled downwards. The nature of this junction is ohmic. Current will flow easily through this junction because of the attractive Coulombic forces between the holes in the semiconductor and the electrons in the metal. In the case of an n-doped semiconductor, the Coulombic forces are repulsive, leading to an energy barrier at the metal-semiconductor interface, or a Schottky barrier. This has the effect of bending the conduction and valence bands upwards. Both cases are illustrated in Fig 3.1.

In the ideal case of a metal/n-doped semiconductor junction, the barrier height ($q\Phi_{Barrier}$) is determined by the work function of the metal and the electron affinity of the semiconductor. The former is the amount of energy required to take an

electron from the Fermi level of the metal to the vacuum level (effectively infinity), the latter is the amount of energy required to remove an electron from the conduction band edge of the semiconductor to the vacuum level. In the n-type case, the equation reads

$$q\Phi_{n-typeBarrier} = q(\Phi_{metal} - \chi_{semiconductor}), \tag{3.1}$$

where q is the electron's charge, Φ_{metal} is the metal's work function, and $\chi_{semiconductor}$ is the semiconductor's electron affinity. In the ideal metal/p-doped semiconductor junction, where the bands are bent downwards, the equation is

$$q\Phi_{p-typeBarrier} = E_{BandGap} - q(\Phi_{metal} - \chi_{semiconductor}), \tag{3.2}$$

where $E_{BandGap}$ is the band gap energy of the semiconductor in question.

In reality, distortions of the semiconductor's crystal lattice can cause the barrier height to be different than the equations predict. The distortions lead to energy states in the semiconductor's energy gap that can act as either donors or acceptors. In the case of n-doped GaAs, Equation 3.1 generally underestimates barrier height. The surface states in GaAs dominate the barrier formation, leading to about same height(70-80 meV) regardless of the work function of the metal in contact.

Equations 3.1 and 3.2 are easily adapted to semiconductor/semiconductor junctions. For these equations, we will call the semiconductor in which the barrier forms Semiconductor 1 and the contacting semiconductor Semiconductor 2. If Semiconductor 1 is an n-type, then

$$q\Phi_{n-typeBarrier} = q(\chi_{semiconductor2} - \chi_{semiconductor1}). \tag{3.3}$$

If Semiconductor 1 is p-type,

$$q\Phi_{p-typeBarrier} = E_{BandGap} - q(\chi_{semiconductor2} - \chi_{semiconductor1}). \quad (3.4)$$

The bands of semiconductors put into contact with each other will bend up or down depending upon their charge concentrations relative to each other. A schematic of a 2DEG structure is shown in Fig. 3.2 and a representative energy level diagram is shown in Fig. 3.3 (top to bottom on the former = left to right on the latter). Each layer will have its own Fermi level; band bending will occur as they equilibrate. For a 2DEG HEB, the contacts would be metal, so a Schottky barrier forms between the contact and the undoped GaAs cap layer. The next layer is made of n-doped AlGaAs; electrons from this layer will flow into the GaAs layer in order to equilibrate their Fermi levels. The bands on the n-doped side of the GaAs/n+ AlGaAs interface will bend upwards, forming Schottky barriers, while the bands on the relatively positive GaAs side will bend downwards. This mismatched bending forms an energy well at the interfaces, but one whose bottom is well above the Fermi level. The next layer is of undoped AlGaAs which is called the spacer layer. The spacer layer limits the amount of electrons that are available for the 2DEG. The wider the spacer layer, the lower the 2DEG electron density. The spacer is what allows us to tune this property of the 2DEG.

The final layer before the substrate is an undoped GaAs "buffer" layer. Undoped AlGaAs has a higher Fermi level than GaAs, so we will see an energy well form on the GaAs side of the interface just as we did at the cap layer/n+ AlGaAs interface, but this well will have its base below the Fermi level. If we give the system a burst of energy, from an LED, for example, the electrons in the n+ AlGaAs layer will absorb enough energy to surmount the barrier between them and the buffer layer. Once over, they will fall into the energy well there. They will be confined to this well unless they absorb photons of sufficient energy to liberate them. The electrons

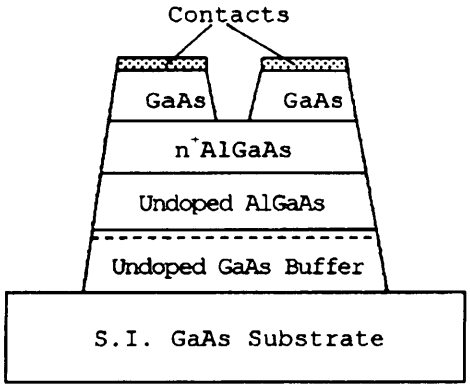

Figure 3.2: Sketch of 2DEG producing semiconductor stack. The 2DEG's location is indicated by the dotted line. (Adapted from image in Yngvesson [35]) Note: This figure is not to scale.

in this well comprise the 2DEG. You can think of the well as confining electrons in the z direction. In the x and the y directions, there is a continuum of energy states in which the electrons can reside; the result is a two-dimensional metal or a 2DEG.

3.2 Contacts

Note in Figure 3.2 the space between the contacts and the 2DEG. In order to read out, we will have to make low-resistance ohmic contact to the 2DEG. Good contacts are essential to the functionality of a 2DEG detector and very difficult to fabricate; they were the main focus of our efforts. Doping methods involve sharply increasing the electron density in the regions of the heterostructure immediately below the contacts, forming a low resistance path from 2DEG to the contact.

3.2.1 Diffusion Doping

Diffusion doping is the oldest and most widely used doping method. It involves placing alloys over the contact areas and annealing the detector. These alloys contain

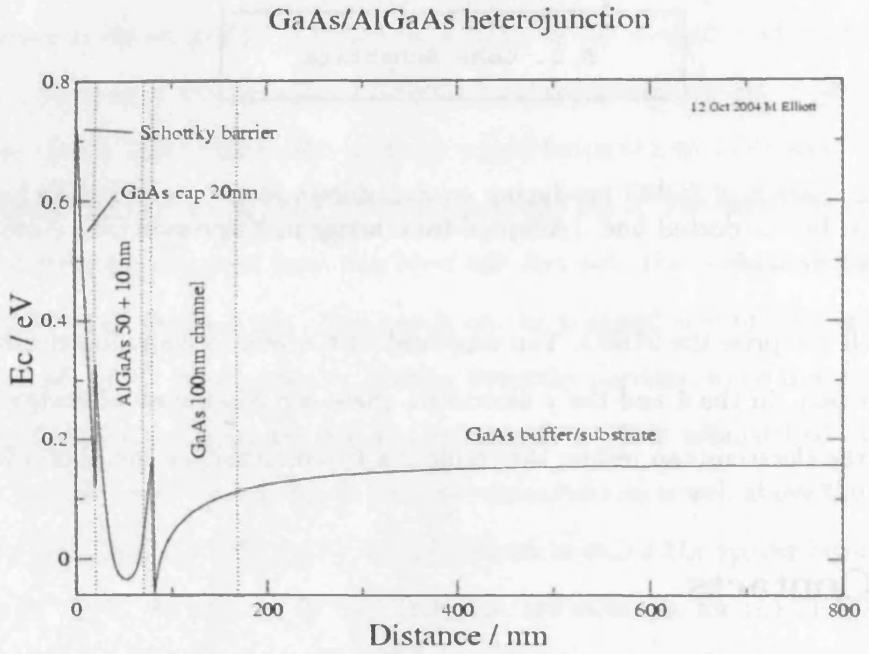

Figure 3.3: Schematic of conduction band of semiconductor stack, energy vs. layer thickness. Zero nm denotes the contact/cap layer junction and positive progression is downwards through the stack. The vertical dotted lines represent layer boundaries. The Fermi level is at 0 eV. Plot from computer model designed by Dr. Martin Elliott at Cardiff University.

elements that will easily diffuse into the heterostructure and act as donor or acceptor atoms. In the case of GaAs, a III-V semiconductor, we want alloys of Group IV or Group VI elements. These elements will serve as donors when diffused into the heterostructure, making an n-type contact to the 2DEG. For long term durability, these contacts must be passivated to avoid degradation [56].

Our contacts used AuGe with a nickel layer [57]. The gold counteracted the tendency of germanium to bead up during the annealing process, making for a rough surface on the contact pad.

3.3 Electrical Properties

3.3.1 DC Case

The electrons in a 2DEG are simply electrons confined to a plane. At any given time, the electrons are moving around with energies equal to k_BT ($1/2\ k_BT$ for each degree of freedom). The electrons will collide with each other, scattering off of each other. The time since their last collision and before their next is the mean-free or scattering time:

$$\tau_s = \frac{m^*\mu}{e}, \tag{3.5}$$

where μ is the mobility of the electrons and m^* is the effective mass (which is introduced because we made our 2DEG structures from semiconductors). The mobility of the electrons is of paramount importance in determining the fitness of the 2DEG for detector use. Rearranging Equation 3.5 gives

$$\mu = \frac{e\tau_s}{m^*}. \tag{3.6}$$

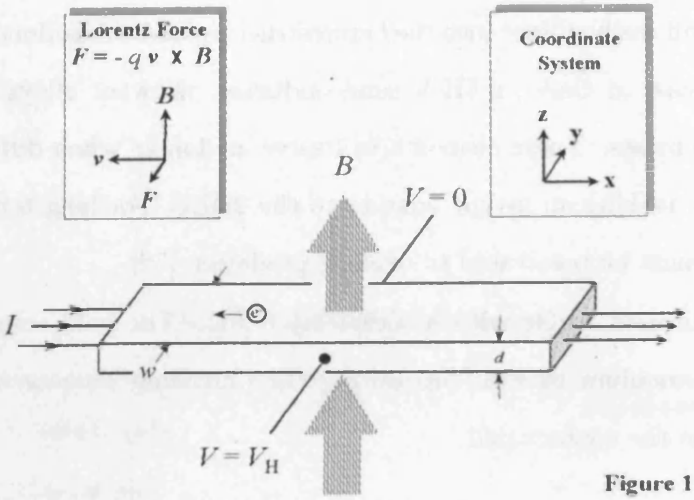

Figure 3.4: Schematic of Hall effect showing direction of Lorentz force. (Image taken from NIST [58])

In general, this equation describes the relationship between the mobility and the time constant of electrons in a semiconductor and can also be used for 2DEGs. There are different time constants for different electron interactions, hence there will be different mobilities. Equation 3.6 refers to the Hall mobility. We find the Hall mobility by using the Hall effect: the phenomenon in which a current carrying medium (CCM) is subjected to a magnetic field that is nonparallel to the current direction. A voltage arises that is mutually perpendicular to the current direction the component of the magnetic field that is perpendicular to the current direction. See Figure 3.4.

The reason this voltage arises is because the magnetic field will exert a force on the moving electrons in the current, pushing them towards the edge of the CCM as they move along:

$$\mathbf{F}_{\text{magnetic}} = q\mathbf{v} \times \mathbf{B} = I\boldsymbol{l} \times \mathbf{B}, \tag{3.7}$$

where $\mathbf{v}$ is the electron velocity, $\mathbf{B}$ is the magnetic field, $\mathbf{I}$ is the current, and l is the length of wire subject to the influence of the magnetic field. This is the familiar Lorentz force. Assuming a magnetic field completely perpendicular to the current, a transverse electric (Hall) field will be produced such that (assuming a magnetic field in the z direction)

$$\mathbf{F_{magnetic}} = IlB\hat{\mathbf{j}} = q\mathbf{E_{Hall}}. \tag{3.8}$$

This electric Hall field will give us the Hall voltage. Assuming a consant $\mathbf{E_{Hall}}$ and using the fact that $V = \int Edr$, we can call the transverse measure of the CCM w and say that

$$\mathbf{V_{Hall}} = \mathbf{E_{Hall}}w. \tag{3.9}$$

With the Hall voltage, we can get the charge density of the CCM via

$$n_e = \frac{IB}{qV_H}, \tag{3.10}$$

and use this to get the mobility from the following equation,

$$\mu = \frac{1}{qn_e\rho_s}, \tag{3.11}$$

where ρ_s is the sheet resistance of the CCM. Note: Equation 3.10 is not the most accurate measure of the charge density. A more precise measurement can be obtained from observing Shubnikov de Haas oscillations of the 2DEG's resistivity [59, 60], to be discussed later.

Ohm's law states that

$$\mathbf{j} = \sigma \mathbf{E}, \tag{3.12}$$

where $\mathbf{j}$ is the current density and σ is the conductivity. Current density can also be represented in the form of drift velocity,

$$\mathbf{j} = -n_e q \mathbf{v_d}, \tag{3.13}$$

where $\mathbf{v_d}$ is the drift velocity, which is the average velocity of the electrons when electron-electron and electron-lattice collisions are taken into consideration. We would obtain it from the Lorentz force:

$$\mathbf{v_d} = \int_{-\tau_s}^{\tau_s} \frac{\mathbf{F_L}}{m^*} dt = \int_{-\tau_s}^{\tau_s} \frac{q(\mathbf{E} + \mathbf{v_d} \times \mathbf{B})}{m^*}. \tag{3.14}$$

As we have an electric field, we have to add a $q\mathbf{E}$ term to the Lorentz force in order to be complete. The limits of plus and minus τ_s would amount to the time the electron travels between collisions (assuming electron-impurity collisions are more frequent than electron-phonon collisions). An electron's average travel time, therefore, will last $2\tau_s$. With a constant Lorentz force, the drift velocity becomes

$$\mathbf{v_d} = q(\mathbf{E} + \mathbf{v_d} \times \mathbf{B}) \frac{\tau_s}{m^*}. \tag{3.15}$$

As Equation 3.6 shows, the mobility is directly proportional to the scattering time, so it will decrease with rising electron temperature. Mobility can also be represented as a function of drift velocity,

$$\mu = \frac{|v_d|}{E}. \tag{3.16}$$

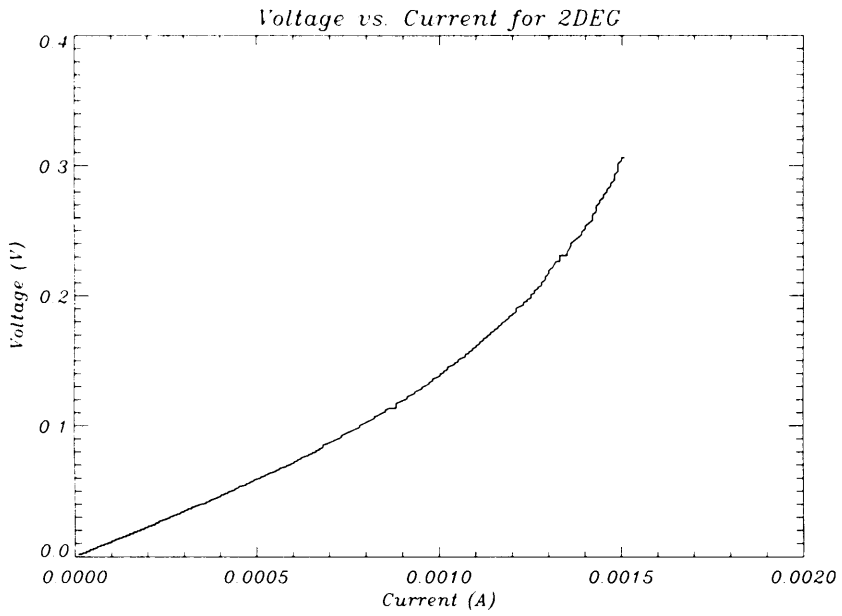

Figure 3.5: A graph of measured voltage vs. applied current for a 2DEG structure. As the current through the 2DEG increases, the electrons get warmer, decreasing their mobility value. This leads to the increasing resistance evident in the increasing slope. Warming the 2DEG increases its resistance, just as in a metal. Despite originating in a semiconductor stack, 2DEGs behave like (two-dimensional) metals.

Combining Equations 3.12 and 3.13 in the case of no magnetic field and rearranging, we obtain

$$v_d = -\frac{\sigma E}{n_e e}. \tag{3.17}$$

This allows us to write

$$\mu = \frac{\sigma}{n_e e} = \frac{1}{\rho n_e e}, \tag{3.18}$$

as the resistivity is just the reciprocal of the conductivity. Solving Equation 3.18 for ρ, we can obtain resistance in terms of mobility:

$$R = \frac{\rho l}{A} = \frac{l}{\mu n_e e A}. \tag{3.19}$$

So, as the mobility decreases, the resistance increases. Figure 3.5, an IV curve of a 2DEG, demonstrates this phenomena.

We can combine Equations 3.13 and 3.15 to get the current density in terms of the electric and magnetic fields:

$$\mathbf{j} = n_e e^2(\mathbf{E} + \mathbf{v_d} \times \mathbf{B})\frac{2\tau_s}{m^*}. \tag{3.20}$$

As we are working with 2DEGs, we will put this equation in 2D vector terms. Assuming that the electric and magnetic field are perfectly perpendicular, we get

$$\begin{pmatrix} j_x \\ j_y \end{pmatrix} = \frac{n_e e^2 \tau_s}{m^*} \begin{pmatrix} E_x + v_{dy} B \\ \\ E_y - v_{dx} B \end{pmatrix} = \frac{n_e e^2 \tau_s}{m^*} \begin{pmatrix} E_x + \frac{j_y B}{ne} \\ \\ E_y - \frac{j_x B}{ne} \end{pmatrix}. \tag{3.21}$$

This leads to the following relations:

$$\sigma_0 E_x = \omega_c \tau_s j_y + j_x \quad \text{and} \quad \sigma_0 E_y = -\omega_c \tau_s j_x + j_y, \tag{3.22}$$

where σ_0 is the conductance, defined as

$$\sigma_0 = \frac{n_e e^2 \tau_s}{m^*} = n_e e \mu, \tag{3.23}$$

and ω_c is the cyclotron frequency, defined as

$$\omega_c = \frac{eB}{m^*}. \tag{3.24}$$

Because this is a two-dimensional system, the conductivity will have the form of a 2×2 matrix,

$$(\sigma) = \begin{pmatrix} \sigma_{xx} & \sigma_{xy} \\ \\ \sigma_{yx} & \sigma_{yy} \end{pmatrix}. \tag{3.25}$$

We obtain the elements of the matrix by applying Ohm's law in two dimensions:

$$\begin{pmatrix} j_x \\ \\ j_y \end{pmatrix} = \begin{pmatrix} \sigma_{xx} & \sigma_{xy} \\ \\ \sigma_{yx} & \sigma_{yy} \end{pmatrix} \begin{pmatrix} E_x \\ \\ E_y \end{pmatrix}, \tag{3.26}$$

giving us

$$j_x = \sigma_{xx} E_x + \sigma_{xy} E_y \quad \text{and} \quad j_y = \sigma_{yy} E_y + \sigma_{yx} E_x. \tag{3.27}$$

By assuming the electric field to be acting only in one axis at a time we obtain,

$$j_x = \sigma_{xx} E_x = \sigma_{xy} E_y \quad \text{and} \quad j_y = \sigma_{yy} E_y = \sigma_{yx} E_x. \tag{3.28}$$

Using the same assumption, we combine Equations 3.22 and 3.28 and solve for the various σ values:

$$\sigma_{xx} = \sigma_{yy} = \frac{\sigma_0}{1+(\omega_c\tau_s)^2} \quad \text{and} \quad \sigma_{xy} = -\sigma_{yx} = -\frac{\sigma_0\omega_c\tau_s}{1+(\omega_c\tau_s)^2}. \tag{3.29}$$

Resistivity is the reciprocal of conductivity, so the resistivity matrix will be the inverse of the conductivity matrix:

$$(\rho) = (\sigma)^{-1} = \frac{1}{\sigma_{xx}\sigma_{yy} - \sigma_{xy}\sigma_{yx}} \begin{pmatrix} \sigma_{yy} & -\sigma_{xy} \\ -\sigma_{yx} & \sigma_{xx} \end{pmatrix} = \begin{pmatrix} \frac{1}{\sigma_0} & \frac{\omega_c\tau_s}{\sigma_0} \\ -\frac{\omega_c\tau_s}{\sigma_0} & \frac{1}{\sigma_0} \end{pmatrix}. \tag{3.30}$$

We apply our current in the x direction only, so j_y is zero. We measure the voltage across the x and y axes and calculate the electric fields through the relation $\mathbf{E} = \Delta\mathbf{V}$. This will get us values for σ_0 and τ_s. In order to get the electron density within the 2DEG, we take readings from the integer quantum Hall effect (IQHE).

3.3.2 AC Case

If the applied field is AC, the drift velocity will change with time. We can rewrite the Lorentz force (acting on an electron) in terms of the AC drift velocity:

$$\mathbf{F_{ACLorentz}} = m^* \left(\frac{d\mathbf{v_d}}{dt} + \frac{\mathbf{v_d}}{\tau_s} \right) - (e\mathbf{v_d} \times \mathbf{B}) = -e\mathbf{E_{ACL}} \tag{3.31}$$

The $\mathbf{E_{ACL}}$ is from the fact that $\mathbf{F}$=q$\mathbf{E}$. Assuming a magnetic field in the positive z direction, a 2D $\mathbf{v_d}$ that has positive x and y components, and an$\mathbf{E_{ACL}}$ that has positive x and y components of equal magnitude. From this we get

$$(F_x)$$
$$m^* \dot{v}_{d_x} + \frac{m^*}{\tau_s} v_{d_x} + eBv_{d_y} = -eE_{ACL_x}$$

and (3.32)

$$(F_y)$$
$$m^* \dot{v}_{dy} + \frac{m^*}{\tau_s} v_{d_y} - eBv_{d_x} = -eE_{ACL_y}.$$

Rearranging gives us

$$(F_x)$$
$$m^* \dot{v}_{d_x} = -eE_{ACL_x} + eBv_{dy} - \frac{m^*}{\tau_s} v_{d_x}$$

and (3.33)

$$(F_y)$$
$$m^* \dot{v}_{dy} = -eE_{ACL_y} - eBv_{dx} - \frac{m^*}{\tau_s} v_{d_y}.$$

Let's call

$$v_{d_x} = v_1 e^{i\omega t}, \quad v_{d_y} = v_2 e^{i\omega t}, \quad \text{and} \quad E_{ACL_{x/y}} = E_0 e^{i\omega t}, \tag{3.34}$$

where ω is the frequency of oscillation and E_o is a constant. To figure out what v_1 and v_2 are we can apply the electric field in one direction and combine F_x and F_y. Applying the field in the x direction gives us

$$(F_x)$$
$$i\omega m^* v_1 = -eE_o + eBv_2 - \frac{m^*}{\tau_s} v_1$$

and (3.35)

$$(F_y)$$
$$i\omega m^* v_2 = -eBv_1 - \frac{m^*}{\tau_s} v_2.$$

Solving for v_1 and v_2 gets

$$v_1 = \frac{-eE_0\tau_s}{m^*}\left(i\omega\tau_s + \frac{(\omega_c\tau_s)^2}{1+i\omega\tau_s} + 1\right)^{-1} \quad \text{and} \quad v_2 = -\frac{\omega_c\tau_s}{1+i\omega\tau_s} v_1. \tag{3.36}$$

Now we can find the AC conductivities. Recalling that $\mathbf{j} = -ne\mathbf{v_d}$ we can state that

$$j_x = \sigma_{xx} E_{ACL_x} = -nev_{d_x} \quad \text{and} \quad j_y = \sigma_{xy} E_{ACL_x} = -nev_{d_y}. \tag{3.37}$$

which leads us to

$$\sigma_{xx} = \frac{ne^2\tau_s}{m^*}\left(i\omega\tau_s + \frac{(\omega_c\tau_s)^2}{1+i\omega\tau_s} + 1\right)^{-1}$$
and (3.38)
$$\sigma_{xy} = \frac{\omega_c\tau_s ne^2\tau_s}{(1+i\omega\tau_s)m^*}\left(i\omega\tau_s + \frac{(\omega_c\tau_s)^2}{1+i\omega\tau_s} + 1\right)^{-1}.$$

Repeating the above steps, but setting the electric field in the y direction, gives $\sigma_{yy} = \sigma_{xx}$ and $\sigma_{yx} = -\sigma_{xy}$. As in the DC case, finding the inverse of the conductivity matrix gets us the values for the resistivity:

$$(\rho) = \begin{pmatrix} \frac{(1+i\omega\tau_s)^2}{\sigma_0((1+i\omega\tau_s)^2+(\omega_c\tau_s)^2)} & \frac{\omega_c\tau_s(1+i\omega\tau_s)}{\sigma_0((1+i\omega\tau_s)^2+(\omega_c\tau_s)^2))} \\ -\frac{\omega_c\tau_s(1+i\omega\tau_s)}{\sigma_0((1+i\omega\tau_s)^2+(\omega_c\tau_s)^2)} & \frac{(1+i\omega\tau_s)^2}{\sigma_0((1+i\omega\tau_s)^2+(\omega_c\tau_s)^2)} \end{pmatrix}. \quad (3.39)$$

The impedance of a 2DEG in the AC regime contains a real and an imaginary term:

$$Z_{2DEG} = R + i\omega L_k = R(1 + i\omega\tau_m) \quad (3.40)$$

where R is the low frequency resistance, L_k is the kinetic inductance, and τ_m is the momentum relaxation time.

3.4 Thermal Properties:

The thermal properties of electrons in the 2DEG are determined by the density of states and the electrons' interaction with the surrounding medium. The distribution function describes the probability of finding an electron in, at, or below a given energy. For electrons (and fermions in general), we use the Fermi-Dirac distribution:

$$f(\epsilon) = \frac{1}{\exp\left(\frac{\epsilon-\mu}{k_B T}\right) + 1}. \quad (3.41)$$

It is a function of both energy and temperature. The quantity μ is the chemical potential and is determined by the (electron) temperature of the system. As T approaches zero, μ will approach ϵ_F, the Fermi energy. At T=0, we would fully expect all electrons to be at or below the Fermi energy. For non-zero temperatures, the chemical potential is a value that ensures calculations using the distribution function yield the correct number N of particles in the system.

As to the number of particles in a system, we need to know the density of states

(g_ϵ) of the system, which describes the number of states at a given energy. For a 2DEG, this is $2m^*/\pi\hbar^2$. Note that it's independent of energy. This means that all energy levels are equally degenerate: there are $2m^*/\pi\hbar^2$ spaces for electrons at each energy level. Degeneracy means that there are multiple states that exist at the same energy level. If it were not for degeneracy, we could simply count the number of electrons in a system and divide that number by two (as only two electrons can coexist on a given energy level), the resulting number would be the ordinal number of the highest energy level at 0K; which would be the Fermi level. We can only do this for systems with no degeneracy, such as a quantum dot, which is zero-dimensional. We need the density of states of the system to determine the number of electrons at or below a given energy level E:

$$N_e = \int g(\epsilon) f(\epsilon) d\epsilon. \tag{3.42}$$

If we integrate from 0 to infinity, we will get the total number of electrons in the system, assuming we've chosen our μ correctly. Note: The density of states calculation used above is for a *perfectly* two-dimensional system. In actuality, our 2DEG will have some finite depth; assume this is in the z direction. This does not mean we will have multiple energy states associated with the z-component. We will, in fact, only have one. Call the z depth a and the x and y dimensions equal to L. In operation, a $\ll$ L. The z wave vector will be

$$k_z = \frac{n\pi}{a}, \text{ with n=1,2,3,...,} \tag{3.43}$$

where n is a quantum number. Quantum numbers are introduced because the z energy levels will have the form of those of a particle in a box (see Fig. 3.6). The energy levels would be described by

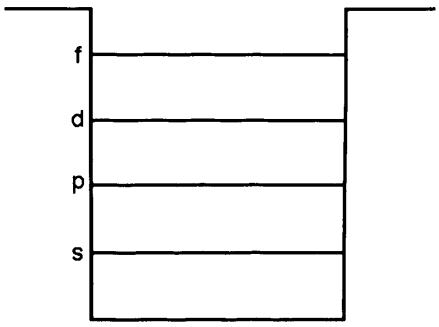

Figure 3.6: Representation of energy levels in a zero- dimensional system, better known as a particle in a box. These would be the "extra" energy z energy levels available to electrons in a 2DEG, but the large energy spacing will only allow occupation of the ground state.

$$E_z = \frac{\hbar^2 k_z^2}{2m^*}. \tag{3.44}$$

For a small a, the spacing on the energy levels will be enormous, too high for the electrons in the 2DEG to go anywhere but the lowest energy level. Each z energy level would contain all of the xy energy states; if we could get to E_{z2} our density of states would double; at E_{z3}, we'd have triple the states of E_{z1}. But, again, we can only remove one to the lowest order energy level in z, so we just have those xy energy states that come with it.

To calculate the electron-phonon time constant (Equation 2.10) requires figuring out the thermal conductance and heat capacity of the 2DEG. The thermal conductance is the rate of change of the power with respect to temperature,

$$G = \frac{dP}{dT_e}, \tag{3.45}$$

and is given by the equation

$$G = 5\Sigma(T_l^4 - T_e^4)A, \tag{3.46}$$

where T_e is the electron temperature, and A is the (planar) area of the 2DEG, and Σ is the material specific electron-phonon coupling constant [61, 62].

The Fermi energy equation is dependent on the dimension of the system, the most useful to us being the two and three-dimensional cases. In both, the relationship between Fermi energy ϵ_F and Fermi wave vector k_F is represented by

$$\epsilon_F = \frac{\hbar^2 k_F^2}{2m^*}, \tag{3.47}$$

but the representation of k_F differs in 2D and 3D:

$$\begin{array}{cc} 2D & 3D \\ k_{F2D} = \sqrt{2\pi n_e} & k_{F3D} = \sqrt[3]{3\pi^2 n_e}. \end{array} \tag{3.48}$$

where n_e is the dimensionally appropriate electron density. (Note how the 2D and 3D densities describe a circle and a sphere, respectively, with k_F as the radius. The factor of 2 is due to electron spin.) The number of electrons in either system can be found by

$$N_0 = \frac{\delta n_e}{\delta \sigma_F}. \tag{3.49}$$

In general, the heat capacity of a substance is the rate of change of its energy density (u) with respect to temperature.

$$C = \left(\frac{\delta u}{\delta T}\right). \tag{3.50}$$

The energy density is the amount of internal energy (U) per unit volume in a 3D system and the amount per unit area in a 2D system. In both systems

$$U = 2\sum_{k} \epsilon(\mathbf{k}) f(\epsilon(\mathbf{k})). \tag{3.51}$$

In k space, the unit volume will be $\Delta\mathbf{k}8\pi^3$ and the unit area will be $\Delta\mathbf{k}4\pi^2$. We use these values to calculate the 3D and 2D energy densities:

$$\begin{aligned} u_{2D} &= \frac{U}{\Delta\mathbf{k}4\pi^2} = \frac{1}{2\pi^2\Delta\mathbf{k}} \sum_{k} \epsilon(\mathbf{k}) f(\epsilon(\mathbf{k})); \\ u_{3D} &= \frac{U}{\Delta\mathbf{k}8\pi^3} = \frac{1}{4\pi^3\Delta\mathbf{k}} \sum_{k} \epsilon(\mathbf{k}) f(\epsilon(\mathbf{k})). \end{aligned} \tag{3.52}$$

In the limit as $\Delta\mathbf{k} \rightarrow \infty$, we can use the following relations:

$$\begin{aligned} &2D \\ &\lim_{\Delta k \rightarrow \infty} \frac{1}{2\pi^2\Delta\mathbf{k}} \sum_{k} F(\epsilon(\mathbf{k})) = \int \frac{d\mathbf{k}}{2\pi^2} F(\epsilon(\mathbf{k})) \\ &3D \\ &\lim_{\Delta k \rightarrow \infty} \frac{1}{4\pi^3\Delta\mathbf{k}} \sum_{k} F(\epsilon(\mathbf{k})) = \int \frac{d\mathbf{k}}{8\pi^3} F(\epsilon(\mathbf{k})), \end{aligned} \tag{3.53}$$

where $F(\epsilon)$ represents a generic function of ϵ. This enables us to represent the 2D and 3D energy densities:

$$\begin{aligned} u_{2D} &= \int \frac{d\mathbf{k}}{2\pi^2} \epsilon(k) f(\epsilon(k)); \\ u_{3D} &= \int \frac{d\mathbf{k}}{4\pi^3} \epsilon(k) f(\epsilon(k)). \end{aligned} \tag{3.54}$$

We use the relationship between energy ϵ and wave vector k (Equation 3.47) to get the above equations in the following form,

$$\int_{-\infty}^{\infty} G(\epsilon) F(\epsilon) d\epsilon, \tag{3.55}$$

where $G(\epsilon)$ is the density of levels. In order to make this conversion, we have to express the vector $\mathbf{k}$ in terms of spherical coordinates; in the 2D case,

$$\int \frac{d\mathbf{k}}{2\pi^2} F(\epsilon(k)) = \int_0^{2\pi} \int_0^{\infty} \frac{k}{2\pi^2} F(\epsilon(k)) dk d\theta = \int_0^{\infty} \frac{k}{\pi} F(\epsilon(k)) dk; \tag{3.56}$$

and in the 3D case,

$$\int \frac{d\mathbf{k}}{4\pi^3} F(\epsilon(k)) = \int_0^{2\pi} \int_0^{\pi} \int_0^{\infty} \frac{k^2}{4\pi^3} F(\epsilon(k)) \sin\phi dk d\phi d\theta = \int_0^{\infty} \frac{k^2}{\pi^2} F(\epsilon(k)) dk. \tag{3.57}$$

Using the wave vector energy relation, we can replace k and dk with energy (ϵ) terms, giving us

$$\begin{array}{cc} 2D & 3D \\ \int_0^{\infty} \frac{m^*}{\pi\hbar^2} F(\epsilon) d\epsilon & \int_0^{\infty} \frac{1}{\pi^4\hbar^3} \sqrt{2m^{*3}\epsilon} F(\epsilon) d\epsilon. \end{array} \tag{3.58}$$

Checking the form of Equation 3.55, we can pull the 2D and 3D densities of levels out of these integrals:

$$G(\epsilon)_{2D} = \frac{m^*}{\pi\hbar^2} \qquad G(\epsilon)_{3D} = \frac{1}{\pi^4\hbar^3} \sqrt{2m^{*3}\epsilon} \ . \tag{3.59}$$

These are the number of levels in each system. To get the density of *states*, we have to take into consideration how many spaces there are for electrons at each level. As electrons are fermions, there are two, so we multiply by two to get the 2D and 3D densities of state:

$$g(\epsilon)_{2D} = \frac{2m^*}{\pi\hbar^2} \qquad g(\epsilon)_{3D} = \frac{2}{\pi^4\hbar^3} \sqrt{2m^{*3}\epsilon} \ . \tag{3.60}$$

Note, again, that the 2D density of states is independent of energy. Recall that

a real 2DEG system would have a finite z depth, leading to an increase in the system's degeneracy. A quick reordering of the 3D density of states shows how that z-component shows up:

$$g(\epsilon)_{3D} = \frac{2m^*}{\pi\hbar^2}\left(\frac{1}{\pi^3\hbar^2}\sqrt{2m^{*3}\epsilon}\right). \tag{3.61}$$

So the third dimensional component amounts to the multiplicative factor in the parentheses. In the case of our system, we will be running at very low temperatures, so low that we can assume we are operating at the Fermi energy. If we replace ϵ with ϵ_F in Eq. 3.61, we get a constant density of states for the 3D system as well. We can put this in terms of the electron density(n_e) via Equations 3.47 and 3.48 so that

$$g(\epsilon)_{3D} = \frac{2m^*}{\pi^4\hbar^2}\sqrt{\left(\frac{3n_e}{4\pi}\right)^{2/3}}. \tag{3.62}$$

In order to get the energy densities of the systems, we make use of the Sommerfeld approximation

$$u = \int_{\infty}^{-\infty} \epsilon g(\epsilon) f(\epsilon) d\epsilon = \int_0^{\epsilon_F} \epsilon g(\epsilon) d\epsilon + \frac{\pi^2}{6}(k_B T)^2[\epsilon_F g'(\epsilon_F) + g(\epsilon_F)] + O(T^4). \tag{3.63}$$

We are operating at a very low temperature, so the electrons are going to be residing near the Fermi level, which is why the Fermi energy is used as a limit. The $O(T^4)$ represents some fourth-order values that will be too small to be a consequential contributor of value for C. For integration, we only have to worry about terms having temperature in them (see Equation 3.50) so separate calculations for the 2D and 3D case are unnecessary. Furthermore, the density of levels is constant, so the $g'(\epsilon_F)$ goes to zero, therefore

$$u = \frac{\pi^2}{6}(k_B T)^2 g(\epsilon_F). \tag{3.64}$$

Differentiating with respect to temperature gives us

$$C = \frac{(\pi k_B)^2 g(\epsilon_F)}{3} T \tag{3.65}$$

for both cases. Evaluating heat capacities, using the densities of levels for the 2D and 3D case:

$$\begin{array}{cc} 2D & 3D \\ C_a = \frac{2\pi m^* k_B^2 T}{3\hbar^2} & C_v = \frac{2\pi k_B^2 T}{3\pi^3 \hbar^3}\sqrt{2m^{*3}\epsilon_F}. \end{array} \tag{3.66}$$

The units of each of these would be heat capacity per unit area (2D) and heat capacity per unit volume (3D). Putting the 3D heat capacity in terms of n_e, we get

$$C_v = \frac{2m^* k_B^2 T}{3\pi^2 \hbar^2}\sqrt{\left(\frac{3n_e}{4\pi}\right)^{2/3}}. \tag{3.67}$$

We can now combine Equations 3.66 and 3.46 to get the electron-phonon time constant for the 2D state:

$$\tau_{ep(2D)} = \frac{2\pi k_B^2 m^* T_e}{15\Sigma(T_l^4 - T_e^4)\hbar^2}. \tag{3.68}$$

The rate of travel of a photoexcited electron in our 2DEG will be determined by the diffusion time

$$\tau_d = \frac{L^2}{\pi^2 D} \tag{3.69}$$

where L is the length of travel of the electron and D is the diffusivity of the 2DEG. The diffusivity describes the random motion that an electron undergoes in

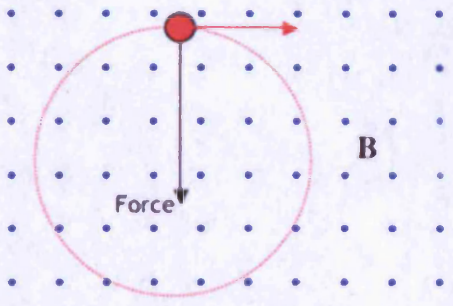

Figure 3.7: The path of an electron in a uniform magnetic field due to Lorentz force. (Image taken from Thieman et al [63].)

traversing a CCM. The value for D can be related to the mobility through the Einstein relation:

$$D = \frac{k_B T \mu}{e}. \tag{3.70}$$

When designing our detector, we would want to make sure that the excited electrons reach the contacts (to be read out) before they lose their energy to the lattice, i.e. we want $\tau_d < \tau_{ep}$. Knowing the properties of our 2DEG, we would choose a maximum contact separation L such that our diffusion time is less than our electron-phonon recombination time.

3.5 Magnetic Properties:

If we inject an electron into a magnetic (B) field, the electron will feel a force that is mutually perpendicular to the B field and the electron's motion. This force is described by the Lorentz equation and will result in a centripetal acceleration that will cause the electron to travel in a circular path, as shown in Fig. 3.7. For the sake of this argument, let's assume that the B field is in the positive z direction, resulting in circular motion in the xy plane. This means that the vector potential

of the field is

$$\mathbf{A} = (-\mathbf{yB}, \mathbf{0}, \mathbf{0}). \tag{3.71}$$

The B field being the curl of **A**. The Hamiltonian describing the motion is therefore

$$H = \frac{1}{2m^*}(\mathbf{p} - \mathbf{eA})^2. \tag{3.72}$$

where **p** is the momentum vector. We use the time-independent Schrodinger equation to describe the energy of this electron:

$$\hat{H} = \frac{1}{2m^*}[(\hat{p_x} + eyB)^2 + \hat{p_y}^2 + \hat{p_z}^2]\Phi = E\Phi. \tag{3.73}$$

where E is the energy and Φ is the eigenfunction. We know that both $\hat{p_y}$ and $\hat{p_z}$ commute with $\hat{H}$ because the Hamiltonian normally commutes with the momentum operator and there are no x or z terms in the Hamiltonian. The eigenfunction of the momentum operator is of the form $e^{ik_g g}$, a standing wave, and there's nothing to indicate that there's anything else going on in the x or z direction, but the y term in the Hamiltonian means that the eigenfunction is going to need a unique y-component. For the moment, let's call that unique component f(y), giving us an eigenfunction of

$$\Phi = e^{i(k_x x + k_z z)} f(y). \tag{3.74}$$

Operating will give us

$$\frac{1}{2m^*}[(\hbar k_x + eyB)^2 + \hat{p_y}^2 + (\hbar k_z)^2]e^{i(k_x x + k_z z)}f(y) = Ee^{i(k_x x + k_z z)}f(y). \tag{3.75}$$

Simplifying,

$$\frac{1}{2m^*}[(\hbar k_x + eyB)^2 + \hat{p_y}^2]f(y) = \left[E - \frac{(\hbar k_Z)^2}{2m^*}\right] \tag{3.76}$$

The z-component of the kinetic energy has been moved over because a z-oriented B field will have no effect on motion parallel to the z-axis it only effects xy-plane motion.

$$\begin{gathered}\left[\frac{(eB)^2}{2m^*}\left(\frac{\hbar k_x}{eB} + y\right)^2 + \frac{\hat{p_y^2}}{2m^*}\right] = \left[E - (\frac{(\hbar k_z)^2}{2m^*})f(y)\right] \\ \downarrow \\ \left[\frac{\hat{p_y^2}}{2m^*} + \frac{K}{2}(y - y_0)^2\right] = \left[E - (\frac{(\hbar k_z)^2}{2m^*})f(y)\right]\end{gathered} \tag{3.77}$$

where $K = (eB)^2/m^*$ and $y_0 = -\hbar k_x/eB$. The left-hand side of this equation has the form of the Hamiltonian of a simple harmonic oscillator (SHO). That makes perfect sense, looking at the electron's motion along the y-axis, it would be observed undergoing steady harmonic oscillation. As this is an SHO equation, we can get the natural frequency of oscillation, from the "spring constant" K:

$$\omega_c^2 = \frac{K}{m^*} = \left(\frac{eB}{m^*}\right)^2. \tag{3.78}$$

And this will be the cyclotron frequency, it indicates the natural frequency an electron will exhibit when executing circular motion due to movement in given (perpendicular to the electron's path) B field. The nth order wave function of an SHO is a Hermite polynomial,

$$\Phi_n = A_n \mathcal{H}(\zeta) e^{-(\zeta^2/2)}, \tag{3.79}$$

leading to the following equation for energy levels for a charged particle in a B field:

$$E_n = \hbar\omega_c \left(n + \frac{1}{2}\right) + \frac{(\hbar k_z)^2}{2m^*} \tag{3.80}$$

These are the Landau levels. Subtraction shows that the spacing between adjacent Landau levels is $\Delta E = \hbar\omega_c$. The term from the z-component of the kinetic energy gives us the following eigenfunction for our system (i.e. the f(y) put in as a place holder earlier),

$$f_n = A_n \mathcal{H}_n \left[\sqrt{\frac{m^*\omega_c}{\hbar}}(y - y_0)\right] \exp\left[-\frac{1}{2}\frac{m^*\omega_c}{\hbar}(y - y_0)^2\right]. \tag{3.81}$$

which, finally, gives us the following wave function for a charged particle in a B field:

$$\Phi_n = A_n \mathcal{H}_n \left[\sqrt{\frac{m^*\omega_c}{\hbar}}(y - y_0)\right] \exp\left[-\frac{1}{2}\frac{m^*\omega_c}{\hbar}(y - y_0)^2 + i(k_x x + k_z z)\right]. \tag{3.82}$$

Having established the energy level equation for Landau levels, the next step is to determine their degeneracy. First of all, what does degeneracy mean for a Landau level? Let's assume that we are conducting our experiment in a large (wrt y_0) box with a volume of L^3. The wave function seems to be degenerate in k_x, judging from the presence of k_x in y_0, so we will represent k_x in terms of our new space:

$$k_x = \frac{2\pi n_x}{L}, \tag{3.83}$$

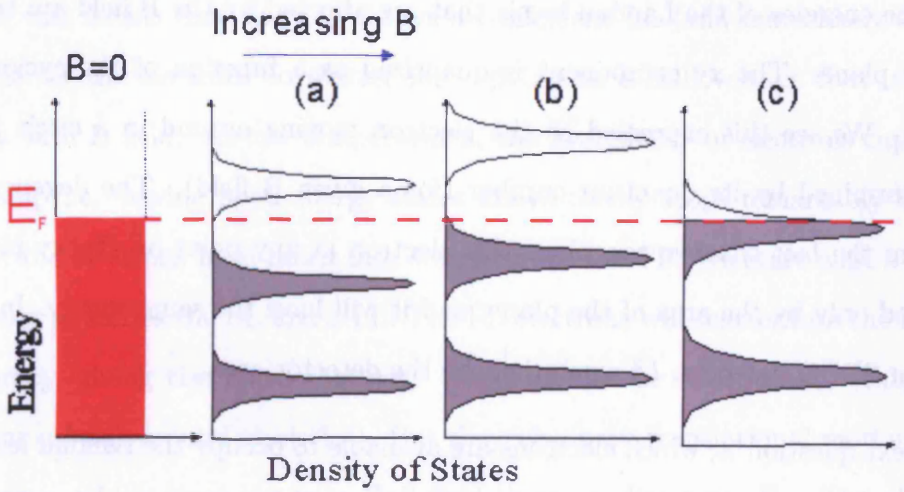

Figure 3.8: A representation of the Landau energy states of the 2DEG shifting with increasing magnetic field. The system depicted is one in which a low temperature has put all the electrons in the 2DEG at or below the Fermi energy (E_f). When the Fermi level is between states, electron scattering in the xx direction is impossible, amounting to an xx resistivity value of zero. (Image taken from one in Leadly [64])

where n_x is the quantum number. The x wave vector has this form to ensure that the wave function, which will be of the form $\sin k_x x$, goes to zero at the extents of the system. With this constraint, we rewrite y_0 as,

$$y_0 = -\frac{2\pi\hbar n_x}{eBL}. \tag{3.84}$$

The quantity y_0 is the value of the center of the circular path that the electron will take in a B field. In our experiment, its maximum possible value would be L (we assume that the area of the electron's circular path is small in comparison to L^2). We can solve Eq. 3.84 for the maximum value,

$$n_x = -\frac{2\pi\hbar}{eBL^2}. \tag{3.85}$$

The absolute value of this quantity represents the degeneracy of the Landau

levels. The energies of the Landau levels that are affected by the B field are those in the xy plane. The xy component is quantized as a function of the cyclotron frequency. We see this expressed as the electron moving around in a circle at a speed determined by its quantum number (for a given B field). The degeneracy arises from the fact that we can place this electron at any point on the xy plane, constrained only by the area of the plane, and it will have the same energy. In the case of our 2DEG detector, L^2 would just be the detector area.

The next question is, which electrons are available to occupy the Landau levels? We are operating at a very low temperature, so we can make the assumption that all the electrons are at or below the Fermi level; therefore it is only those electrons at the Fermi level that are free to scatter (having nothing "above" them to get in their way). The only way they can scatter is if there is some energy state to scatter into, i.e. a Landau level to occupy. For this to occur, the energies of the Fermi level (FL) and Landau levels (LL) must match (within the limits of Heisenberg uncertainty). Bringing the LL into coincidence with the FL is simply a matter of choosing the right B field. At a low B field, the FL will match with a higher order LL. If we increase the B-field steadily, the lower order LLs will ascend in their energy value, passing by the Fermi level as they go. The electrons in the FL will scatter at those specific values of the B field that bring the LLs into coincidence. An artist's rendition of this phenomenon serves as Fig. 3.8.

Recalling Ohm's law in two dimensions (Eq. 3.27), let's assume a low temperature 2DEG system with a current in the positive x direction and a B field in the positive z direction (so keep an eye on j_x). These conditions will lead to a Hall voltage being established perpendicular to the current's axis (Equation 3.8). The B field will also give rise to LLs in the 2DEG. At high (77K and above) temperatures, electrons in the 2DEG occupy a continuum of partially filled levels above

the FL; this means that there is always a coincident LL (and more likely several) available for the electrons to scatter into, giving us a Hall voltage that increases linearly with B field. At low temperatures, the availability of electrons capable of scattering (i.e. having open energy states above them) drops remarkably because most of the electrons have fallen into states under the FL. We start with a B field value that equalizes the FL and a LL. The FL electrons will scatter into the Landau degeneracy, giving rise to conductivity values in the xx direction,σ_{xx} (this is the electrons moving around in circles). But they also have translational motion in the x direction, which gives rise to a Hall field in the y direction, E_y. The electrons are being pulled in the xy direction; their scattering along that line gives us the σ_{xy} value. Now let's increase the B field until there is not a LL that matches the FL. There are no states for the FL electrons to scatter into; no scattering in the xx direction means no resistivity in that direction (i.e. infinite conductivity) and, hence, no electric field in that direction. Interestingly, this does not mean no current in the x direction. Looking at the Equation 3.27 again, we see that current can flow in the x direction even when E_x is zero. We will continue to have the Hall field E_y and electrons scattering in the xy direction, but those electrons got in when the LL and the FL were coincident. The resistivity in the xy direction (ρ_{xy} the reciprocal of σ_{xy}) will remain constant until we bring another LL into coincidence and pluck some more electrons from the FL.

At each point of FL/LL coincidence, the Hall resistivity will jump by a quantized increment, $\frac{h}{ne^2}$, where n is a positive non-zero integer. This is the integer quantum Hall effect (IQHE). A plot of ρ_{xy} vs. B-field will show the resistivity increasing in IQHE steps at those points of FL/LL coincidence. At these same values of B, a graph of ρ_{xx} vs. B will show sharp peaks where there is suddenly xx resistivity. The width of these peaks would be directly proportional to the width of the LLs. The

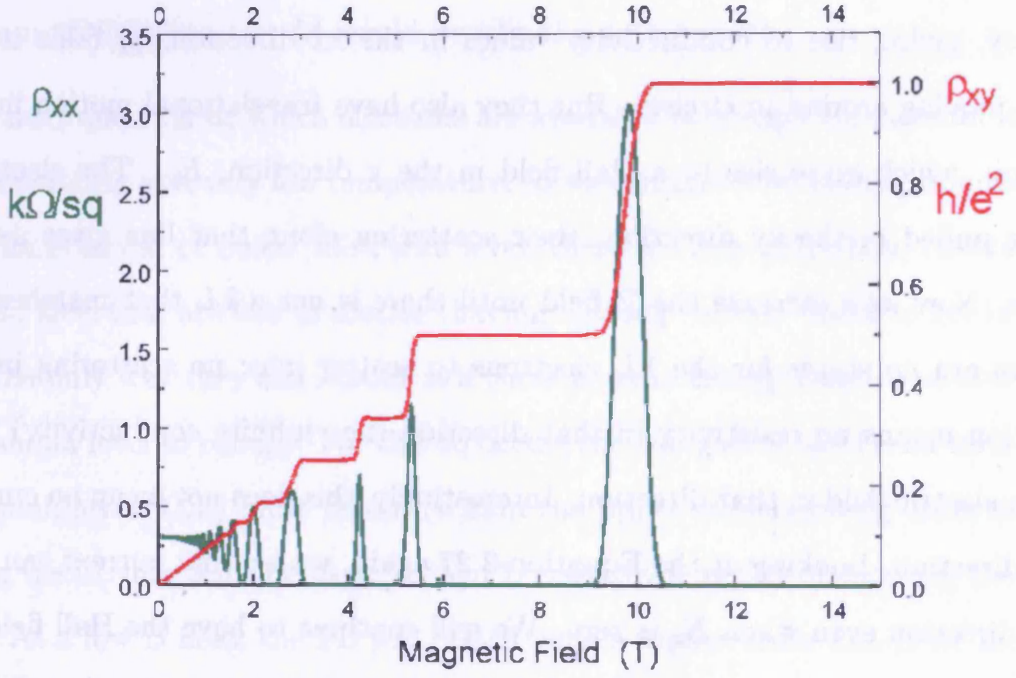

Figure 3.9: Graph showing 2DEG xx and xy resistivites (ρ_{xx} and ρ_{xy}) as a function of magnetic field. The integer quantum Hall effect is evident in ρ_{xy}, while Shubnikov de Haas oscillations are evident in ρ_{xx}. Only the Hall resistance is evident in the plot of ρ_{xy}. The IQHE is only seen in 2DEGs at less than 4.2K; we can assume that any resistivity not due IQHE is negligible. (Image adapted from one in Leadly [64])

value of the resistivity will depend upon the qualities of the 2DEG. These are called Shubnikov de Haas (SdH) oscillations. Plots of both phenomenon are shown in Fig. 3.9.

In the SdH effect, the oscillation of the value of ρ_{xx} will be periodic if plotted vs. the reciprocal of the B field. These oscillations provide a very accurate measure for the electron density in a 2DEG sample via the following equation:

$$n_e = \frac{e}{\pi\hbar\left(\Delta\frac{1}{B}\right)} \tag{3.86}$$

where $\Delta(1/B) = 1/B_n - 1/B_{n+1}$ and each value of $1/B$ is from a peak or trough on the graph of ρ_{xx} vs. $1/B$. Eq. 3.86 is a far more accurate measure of charge density than Eq. 3.10 and can therefore be used to get a more accurate measure the electron mobility value (Eq. 3.11).

We can find the electron temperature by fitting the oscillation curves. The SdH effect is well described theoretically by the "Lifshitz-Kosevich" formula in which the oscillatory part of the resistance can be expressed as a Fourier-like expansion [65, 66, 67],

$$\begin{aligned}\frac{\Delta\rho_{xx}(T_e,B)}{\rho_0} = & \sum_r A_r X_r \exp(-Krm^*T_D/B) \\ & \times \cos(2\pi rF/B + \phi_r)\end{aligned} \tag{3.87}$$

where ρ_0 is the zero-field resistance, F is the SdH frequency, related to the 2D electron density n_s by $F = (h/2e)n_s$. The terms A_r and ϕ_r are amplitude and phase factors for each harmonic number r. The relative electron effective mass m^* is 0.067 for the GaAs-based 2DEGs examined here, and $T_D = \hbar/2\pi k_B\tau_s$ is the so-called Dingle temperature and is related to the scattering lifetime τ_q of electrons in the quantized Landau levels. The Dingle temperature can be determined through the fit

of the curve and from it, τ_q. Having τ_q allows us to determine the quantum mobility using the form Equation 3.6 and replacing τ_s with τ_q. The fundamental constant $K = 2\pi^2 k_B m_0/\hbar e = 14.693\ \mathrm{TK}^{-1}$

Central to our experiments is the thermal damping factor

$$X_r = \frac{Krm^* T_e/B}{\sinh(Krm^* T_e/B)} \tag{3.88}$$

arising from the Fermi-Dirac distribution of states around the Fermi level, and which contains all the temperature dependence of the SdH effect. From this factor, by examining the SdH effect as power is dissipated in the sample, it is possible to calculate the electron temperature T_e, if all other quantities in Equation 3.87 are known.

The broadening of the LL can be described by the quantum mobility, μ_q. We get this value by employing Equation 3.6 with the time constant, τ_q, determined from the Heisenberg uncertainty principle:

$$\Delta E \Delta t \leq \hbar \rightarrow \hbar \Delta\omega \tau_q = \hbar \rightarrow \tau_q = (2\pi\Delta\nu)^{-1}, \tag{3.89}$$

where $\Delta\nu$ is the uncertainty in frequency of the LL.

Chapter 4

2DEG Detectors

A 2DEG acts like an ultra thin metal film of exceptional conductivity. Through doping and choice of semiconductor material, the electrical and thermal properties of the electrons can be controlled, and knowing the properties of the electrons allows us to model them. Detectors that are made from superconducting or normal metal films can be made with 2DEGs with the benefit being that we can tailor the 2DEG properties to maximize detector sensitivity. This chaper will discuss the design and theory of operation of 2DEG HEBs and CEBs.

4.1 A 2DEG HEB

Yngvesson proposed a 2DEG HEB [35]. A 2DEG HEB would function much like a superconducting HEB bolometer. Incoming radiation warms the electron gas, decreasing the time between electron-impurity collisions (the scattering time), and increasing the overall resistance of the 2DEG. The electrons give up their energy to the lattice via electron-phonon interactions; in equilibrium, there would be a steady heat flow from the 2DEG to the lattice. The equation governing the 2DEG/lattice system would be

$$P_{opt} = (T_{bolometer} - T_{heatsink})G_{ep}. \tag{4.1}$$

Therefore, the 2DEG would be hotter than the heat sink by $\Delta T = \frac{P_{opt}}{G_{ep}}$. The lattice would be connected to a heat sink through a high thermal conductance interface, in order to maintain a low lattice temperature. The incoming power from the radiation source determines the equilibrium resistance of the 2DEG.

A 2DEG HEB has several advantages over a superconducting HEB. Firstly, the effective mass of electrons in semiconductors is usually at least ten times lower than electron mass in metals. The electrical conductivity per electron in a 2DEG is on the order of 10^5 times higher than in a metal. 2DEG electrons will therefore have a lower resistance than metallic electrons so less material is needed to impedance match the 2DEG to the source. A 2DEG will also have smaller values of heat capacity and thermal conductance than a metal, making τ_{ep} smaller. Table 4.1 compares the properties of niobium at its transition temperature and a GaAs based 2DEG. While the responsivity of a superconducting HEB would be better, a 2DEG HEB would be faster. You could also tune the properties of the 2DEG through semiconductor choice and doping. If we could make a 2DEG absorber with a superconducting thermometer, we would have the best of both worlds.

A transition edge sensor (TES) primarily consists of a thin film of superconducting metal cooled to just below its transition temperature which acts as the absorber. It is basically a superconducting HEB. Antenna-coupled radiation raises the temperature of the superconductor causing it to leave the superconducting state. A device of this type is described by Prober [68]. The transition from superconducting to normal state is usually on the order of millikelvins [69]. This means a dramatic change in resistance for even small rises in temperature. This change would be measured through the voltage across a bias resistor in parallel with the absorber [70]. A

Material (at 9K)	effective mass (kg)	heat capacity (J/K)	thermal conductance (W/K)	time constant (s)
Niobium	9.11×10^{-31}	1.58×10^{-10}	2.0×10^{-1}	7.93×10^{-10}
GaAs 2DEG	6.1×10^{-32}	1.97×10^{-14}	5.91×10^{-4}	3.34×10^{-11}

Table 4.1: Comparison of properties of niobium and a GaAs 2DEG for use in an HEB. We are assuming a detector area of 1 mm^2 (and in the case of the niobium a thickness of 25 nm). The temperature of 9K was chosen because it would be the approximate operating temperature of a niobium HEB. For niobium, the heat capacity is found from $C = \gamma TV$, where $\gamma = 700 \frac{J}{K^2 m^3}$, and the thermal conductance is found from $G = 4AT^3V$ [38], where $A = 8.2 \times 10^9 \frac{W}{K^4 m^3}$ [72]. In both equations, T is temperature in degrees Kelvin and V is volume in m^3. 2DEG properties calculated from equations found in Chapter 3.

2DEG could improve the function of a TES by acting as the absorber. Again, the heat capacity of the 2DEG is lower than in a metal so the electrons in the 2DEG will get hotter upon the absorption of radiation. The 2DEG would be coupled to the superconducting film and the two systems will come into equilibrium. The film will in turn experience a larger rise in temperature than it would alone making it more sensitive to the absorbed radiation. The electron density in a 2DEG is considerably less than that of a metal, so the film would have to be of a size that would about equalize the number of electrons in the two systems to ensure an appreciable rise in temperature of the film. So the size of the superconducting film in a 2DEG TES would be smaller than in a regular one. While the low electron density in the 2DEG is advantageous for sensitivity, the corresponding high inductance and plasma frequency in the GHz (Burke, *et al.* [71]) makes electromagnetic coupling and absorption difficult.

4.2 A 2DEG CEB

A 2DEG CEB would function differently from a 2DEG HEB in that the temperature of the electrons is measured by two voltage biased superconductor-insulator-normal metal (SIN) junctions. In order to make a CEB, we take the 2DEG structure described in the HEB section and use a superconducting (at the operating temperature) metal as the contact. This is good because, for a 2DEG, τ_{ep} is proportional to $1/T^3$; a lower absorber temperature means a more sensitive (albeit slower) detector.

The structure of a 2DEG CEB is identical to that of a 2DEG HEB except for the contacts. For a 2DEG HEB, the contacts are ohmic; for a 2DEG CEB, we have superconducting tunnel junction contacts. Our 2DEG structures contain layers of n-doped semiconductor. When an n-type semiconductor is brought into contact with a metal, a Schottky energy barrier is formed on the semiconductor side of the interface. With a normal metal contact, the electrons in the 2DEG can tunnel through the Schottky barrier whether they be hot or cool, escaping into the electrical leads and contributing to dark noise. This probability is increased with higher bias voltage. In the case of a superconducting contact, the only way they can tunnel out of the 2DEG is by absorbing enough energy to make it over the energy gap. Figure 4.1 illustrates the concept. The results of a program (Appendix A) simulating the cooling effect's dependence on the bias voltage can be seen in Figure 4.2. Simulated IV curves of the 2DEG at various electron temperatures can be seen in Figure 4.3.

In a 2DEG CEB, the tunneling current is proportional to the power emanating from the source. Figure 4.4 shows an electronic model for a CEB. Unlike the other bolometers, a CEB does not need a current to be put into it to read out, it produces a current that will travel across our leads. In the following equation, the output power will be electrical. The electron temperature is lower than the lattice temperature; this means there will be heat flow from the lattice to the 2DEG. This is an

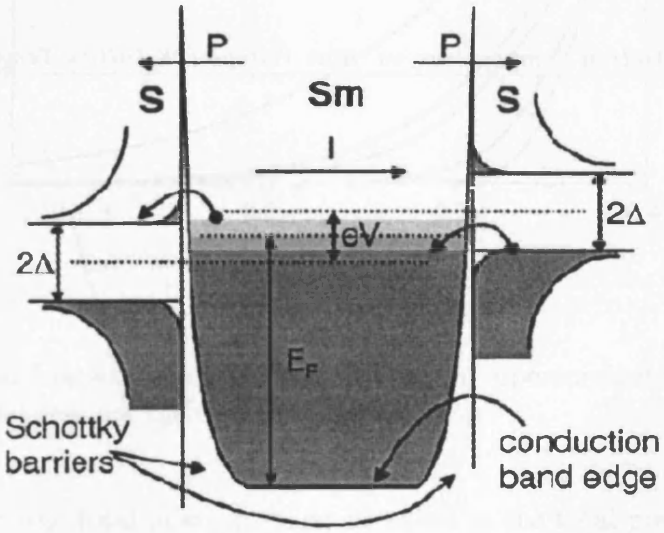

Figure 4.1: Illustration of heavily n-doped semiconductor interacting with superconducting contacts under a leftward voltage bias V. The semiconductor region is labeled Sm, while the superconducting regions are labeled S. Note the formation of Schottky barries at the Sm-S interfaces. The gray areas denote occupied, single-particle electron states. Single electrons are evident in superconductors' conduction bands because the illustration assumes a non-zero temperature, allowing non-paired electrons to exist above the Fermi level in the superconductor. P represents heat flow, I represents current. (Image taken from Savin *et al* [73]

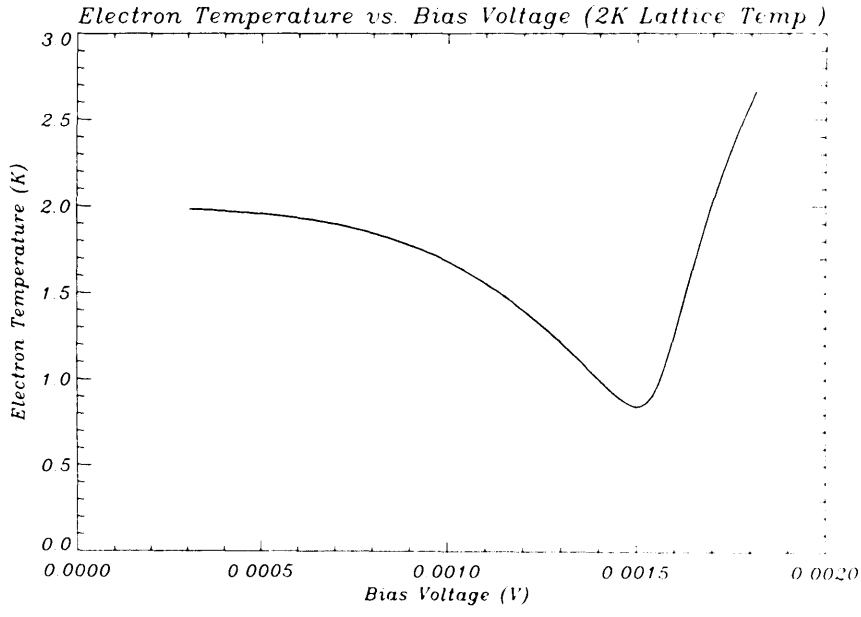

Figure 4.2: Graph showing cooling effect of tunneling current in a 2DEG CEB. In this simulation, produced by an IDL program, the lattice temperature is 2 K and the optical power is 1 picowatt.

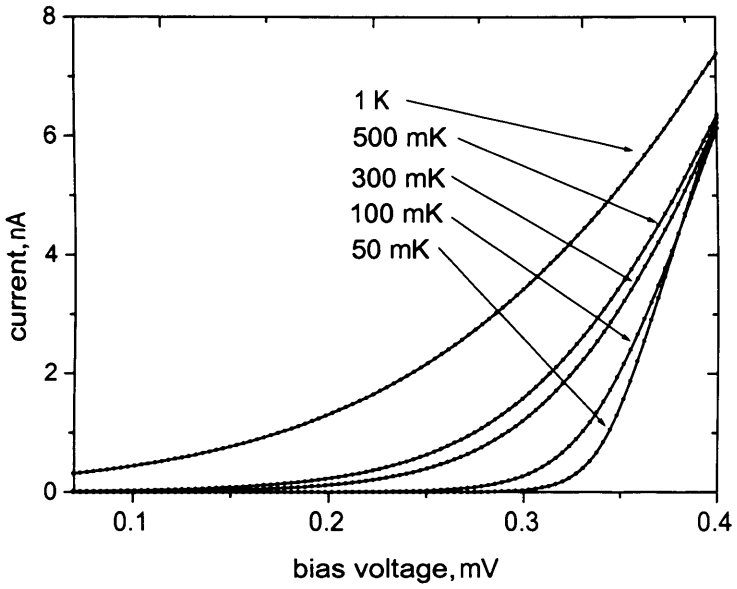

Figure 4.3: IDL simulated IV curves for 2DEG with superconducting tunnel contacts. The temperatures are the electron temperatures.

equilibrium device, the total power in must be equal to the total power out, so

$$P_{output} = P_{optical} + P_{thermal} \tag{4.2}$$

$P_{thermal}$ represents the rate of heat flow from the lattice to the 2DEG. To represent that we use Table 2.1 and Ohm's law:

$$P_{thermal} \rightarrow I_{thermal} = \frac{V}{R} \tag{4.3}$$

We know from the standard bolometer section that V is analogous to the difference between the electron and lattice temperatures. Heat flowing from the lattice to the electrons that holds them, so R will be the reciprocal of the electron-phonon thermal conductance,

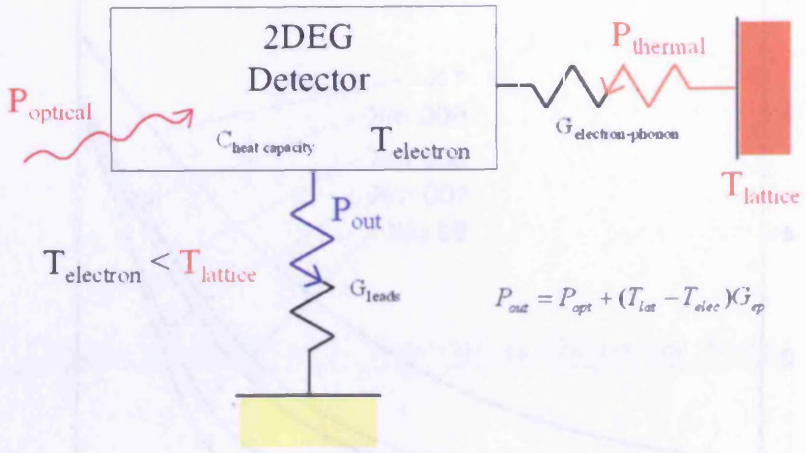

Figure 4.4: Schematic of 2DEG CEB in operation.

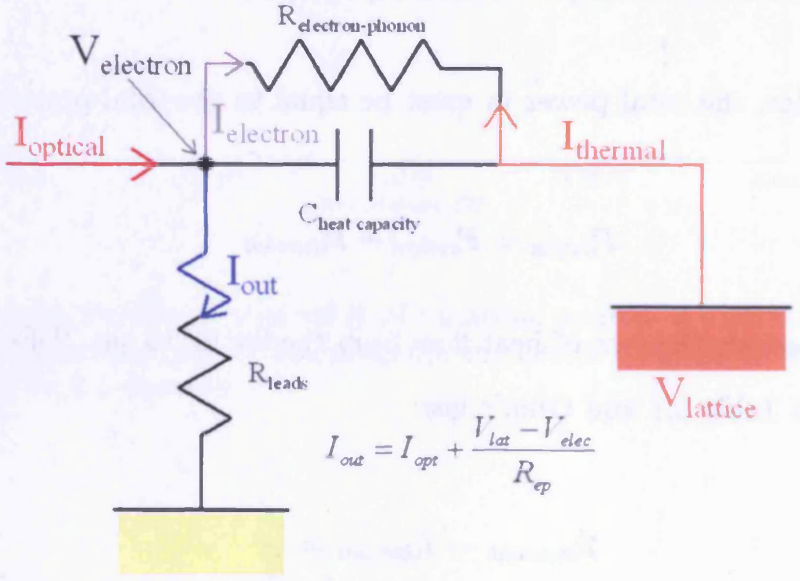

Figure 4.5: Electrical analog for a 2DEG CEB in operation. As in the generic bolometer analogy, the heat capacity does not come into play because it's unchanging and therefore neither taking or giving "current."

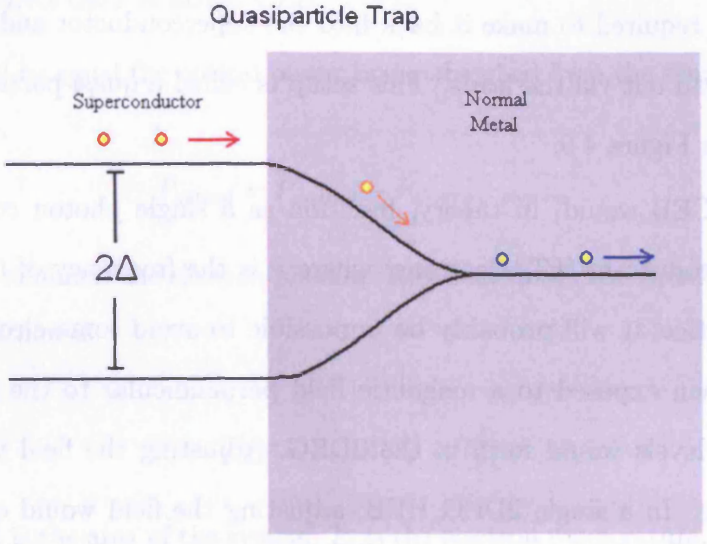

Figure 4.6: A conceptual drawing of a quasi-particle trap in operation. Hot electrons fall into the lower energy levels available in the metal, cooling in the process.

$$I_{thermal} = (T_{lattice} - T_{electron})G_{electron-phonon}. \tag{4.4}$$

Rearrangement of Equation 4.2, gives us an equation for determining optical power,

$$P_{optical} = P_{output} - (T_{lattice} - T_{electron})G_{electron-phonon}. \tag{4.5}$$

While the bias voltage will make a "forward" current favorable, there is still the possibility of hot electrons back-tunneling into the 2DEG so that the tunneling current registers as smaller than it ought to be. In order to prevent this, we put a layer of normal metal on top of the superconducting contact. The transition edge from the top of the energy gap in the superconductor into the continuum of the metal is a smooth one. Hot electrons in the superconductor with fall into the metal's Fermi sea, giving up their heat to the electrons in the metal. Once so cooled, they do not

have the energy required to make it back into the superconductor and are trapped until they are read out via the leads. This setup is called a quasi-particle trap [74]; it's illustrated in Figure 4.6.

The 2DEG CEB would, in theory, function as a single photon counter: each photon would produce $h\nu/kT_e$ electrons, where ν is the frequency of the incoming photon. In practice, it will probably be impossible to avoid some electron-phonon interaction. When exposed to a magnetic field perpendicular to the plane of the 2DEG, Landau levels would form in the 2DEG. Adjusting the field would adjust the level spacing. In a single 2DEG HEB, adjusting the field would constrain the absorption spectrum of the 2DEG HEB. Only photons matching the Landau energy spacing (within Heisenberg limits) would be able to excite the 2DEG. Furthermore, only photons able to impart energies greater than Δ would be detected. A string of 2DEG HEBs, each with a different magnetic field acting on them tuned to a specific wavelength would then constitute a 2DEG spectrometer. Kawano, *et al.* [75] have fabricated and tested frequency selective bolometers consisting of 2DEG hall probes placed in a magnetic field.

4.3 Reading Out a 2DEG CEB:

In operation, infrared photon energy will be channeled into the 2DEG via an antenna. Ideally, all this energy would go into raising the electrons to a high enough energy state to tunnel out of the 2DEG and into the superconductor, but in practice some of the energy will go into heating the 2DEG lattice, creating phonons. Within the detector, then, there will be power flowing into the electrons and into the lattice. We are draining off the power going into the electrons via the tunneling current, which is cooling the 2DEG. The sum of these two power flows within the

detector will be equal the optical power being absorbed from the source,

$$P_{optical} = P_{cooling} + P_{electron-phonon}. \tag{4.6}$$

We will minimize the electron-phonon (EP) heat flow. The equation describing the EP heat flow is

$$P_{EP} = \Sigma_{2D} A(T_e^5 - T_p^5), \tag{4.7}$$

where A is the area of the system, T_e is the electron temperature, and T_p is the phonon temperature. Σ is given by the following equation(Wellstood *et al* [62])

$$\Sigma_{2D/3D} = \frac{k_B^5 g_{2D/3D}(\epsilon_F)\Gamma(5)\zeta(5)}{9\pi\rho\hbar^4 v_s^4 v_F}, \tag{4.8}$$

where $\Gamma(n)$ is the gamma function, $\zeta(n)$ is the Riemann zeta function, ϵ_F is the Fermi energy, ρ is mass density, v_s is the longitudinal speed of sound in the material, and v_F is the Fermi velocity, which is obtained from the kinetic energy equation,

$$v_F = \sqrt{\frac{2\epsilon_F}{m}}. \tag{4.9}$$

Σ can be represented as

$$\Sigma = 0.524\alpha^*\gamma, \tag{4.10}$$

where

$$\alpha^* = \frac{4\zeta(3)k_B^3\epsilon_F^2}{3\pi\rho\hbar^4 v_s^4 v_F} \quad \text{and} \quad \gamma = \frac{C_{a/v}}{T_e}. \tag{4.11}$$

Σ is most often found by experiment and then used to calculate other quantities,

such as the thermal conductance (Equation 3.46). Σ can be used to find τ_{ep} via

$$\frac{1}{\tau_{ep}} = \frac{\Sigma_{2D/3D} T_e^4}{0.524 C_{a/v}} \tag{4.12}$$

As the EP heat flow equation shows, minimizing EP heat flow is a matter of equalizing the electron and phonon temperatures. The cooling power describes the tunnelling rate from the 2DEG to the SC. We model it using Fermi's golden rule [76], which gives the probability of electronic transitions in systems in which the transition probability is constant in time. We use it here to describe the readout mechanism in our detector, a tunneling process. Again, the photoexcited electrons in the 2DEG will only register as photocurrent if they tunnel through the barrier between the 2DEG and the superconductor (SC) readouts. These electrons must be at an energy higher than that of the superconductor's band gap energy (Δ) in order to tunnel because there are no available states to tunnel into within the band gap. The probability of this occurrence is given by the following equation:

$$P_{12} = \frac{2\pi}{\hbar} |M_{12}|^2 \delta(E_2 - E_1). \tag{4.13}$$

The numbers represent two different states in the two media: 1 represents the initial state in the 2DEG; 2, the final state in the SC. The δ-function is 1 if $E_2 = E_1$ and zero otherwise. The electron is not going to gain or lose any energy in jumping through the barrier, so the energy levels on either side have to be equal. At the heart of this equation is the interaction matrix element M_{12}. The initial and final states of the electron can be represented by wave functions; both of which will have non-zero probability fields extending into the finite barrier region. We assume that the barrier is thin enough that these probability fields overlap (if they did not, there would be no tunnelling). The overlap of these wave functions within the barrier is described

by the interaction matrix element, which will depend inversely on the thickness of the barrier (as the thinner the barrier, the greater the interaction between states 1 and 2). In this instance,

$$|M_{12}|^2 = \alpha_m \rho_1 \rho_2. \tag{4.14}$$

Where the ρ_1 and ρ_2 represent the states in each medium and α_m is a factor describing the coupling strength between the states. The latter can be represented as a function of the normal resistance, R_N:

$$\alpha_m = \frac{h}{e^2 R_N} \tag{4.15}$$

In the case of a 2DEG CEB, the "normal" resistance will be the result of electrons tunneling through the Schottky barriers between the 2DEG and the superconducting contacts. The tunneling resistivity for a Schottky barrier is given by [77]

$$\rho_T = \frac{k_B^2}{q^2 A^* \Phi_B} \exp\left(-\frac{\Phi_B 4\pi}{h}\sqrt{\frac{\epsilon_s m^* \epsilon_0}{N_e}}\right), \tag{4.16}$$

where A^* is Richardson's constant [78], ϵ_s is the dielectric constant, N_e is the 3D electron density, and Φ_B is barrier height of the semiconductor. To calculate the rate of transfer through the barrier , we must integrate over all electronic energy states.

$$Rate = \frac{2}{\hbar}\int |M_{12}|^2 \delta(E_2 - E_1) = \frac{\alpha_m}{\hbar}\int \rho_1 \rho_2 \delta(E_2 - E_1) dE_1 dE_2 = \frac{\alpha_m}{\hbar}\int \rho_1 \rho_2 dE \tag{4.17}$$

We replaced E_1 and E_2 with E to represent an energy level present in both media. The bit to fill in now is the two ρs. The electrons will be tunnelling from the

2DEG into the superconductor so we are concerned with the number of electrons in the 2DEG and the number of available states in the superconductor. We get the number of electrons in the 2DEG by integrating the Fermi-Dirac distribution over energy (Eq. 3.42). The density of states of a 2DEG is a constant (Eq. 3.60), so it can be incorporated into R_N. On the superconductor side, we assume that all the states are empty and waiting for electron population. The ρ for the superconductor will therefore be its density of states, so

$$\rho_1 = \frac{1}{exp\left(\frac{E-eV}{k_B T_e}\right)+1} \quad \text{and} \quad \rho_2 = \frac{E-\epsilon_{F2}}{\sqrt{(E-\epsilon_{F2})^2-\Delta^2}}. \tag{4.18}$$

where ϵ_{F2} is the difference in the Fermi levels. We are interested in energies above the Δ of the superconductor, so our limits of integration will be from Δ to infinity. We will assume that the Fermi levels have equalized, so ϵ_{F2} is zero:

$$Rate = \frac{\alpha_m}{\hbar}\int_{\Delta}^{\infty} \frac{1}{exp\left(\frac{E-eV}{k_B T_e}\right)+1} \frac{E}{\sqrt{E^2-\Delta^2}} dE. \tag{4.19}$$

We now have an expression for the rate of transfer from the 2DEG into the superconductor through a barrier. To get the tunnelling current, we simply multiply by the unit of charge e [79]:

$$I_T = \frac{e\alpha_m}{\hbar}\int_{\Delta}^{\infty} \frac{1}{exp\left(\frac{E-eV}{k_B T_e}\right)+1} \frac{E}{\sqrt{E^2-\Delta^2}} dE. \tag{4.20}$$

We get the power transferal rate by tacking on the energy transferred by each electron $(E - eV)$:

$$P_T = \frac{e\alpha_m}{\hbar}\int_{\Delta}^{\infty} \frac{E-eV}{exp\left(\frac{E-eV}{k_B T_e}\right)+1} \frac{E}{\sqrt{E^2-\Delta^2}} dE. \tag{4.21}$$

P_T would be the cooling power $P_{cooling}$ in Equation 4.6. We wrote a program

in IDL that would calculate I_T, P_T, and P_EP under the constraint imposed by Equation 4.6 (the text of the code is contained in Appendix'A). The following values were made adjustable: the superconductor Δ; the lattice temperature (used as a parameter in determining T_e); R_N; $P_{optical}$; the 2DEG area; α_m; the emissivity of the background, ϵ_b; the central frequency of the 2DEG, μ_o; the transmission of the system,η; and n_e. In order to calculate Σ, results from Appleyard, *et al* [1] were used. They used the following equation for the electron-phonon power flow:

$$P_{EP} = (\dot{Q}(T_e) - \dot{Q}(T_l))n_e A, \tag{4.22}$$

where $\dot{Q}$ is the power transfer per electron and $\dot{Q} \propto T^5$ at our operating temperatures [1, 80]. We can calculate G via

$$G = \frac{d\dot{Q}}{dT} n_e A. \tag{4.23}$$

Combining this equation with Equation 3.46, we get

$$\Sigma = \frac{\dot{Q} n_e}{T^5}. \tag{4.24}$$

Appleyard *et al* found a value of $\dot{Q} \approx (61 \pm 10)T^5$eV/s for their GaAs samples. The T^5 term will cancel making Σ constant for the 2DEG, as in a metal.

The program operates by making an array of bias voltages and electron temperatures. For each bias voltage, a value is obtained for I_T, P_T, and P_{EP} for each electron temperature. Of these results, only those corresponding to values T_e that satisfy Equation 4.6are kept; in this way, we get an accurate measure of the electron temperature of the system. Through a plot of T_e vs. bias voltage, we can see which values of the bias will most effectively lead to cooling of the 2DEG. The derivative of the Fermi-Dirac distribution (Equation 3.41) with respect to T_e was included:

$$\frac{df(\epsilon)}{dT_e} = \frac{exp\left(\frac{E-eV}{k_BT_e}\right)}{k_BT_e^2\left(exp\left(\frac{E-eV}{k_BT_e}\right)+1\right)^{-2}} \tag{4.25}$$

This allowed me to calculate $\frac{dI_T}{dT_e}$, $\frac{dP_T}{dT_e}$, and $\frac{dP_{EP}}{dT_e}$, which allowed me to calculate the responsivity via Equation 2.13:

$$\frac{dI_T}{dP_{optical}} = \frac{\frac{dI_T}{dT_e}}{\frac{dP_T}{dT_e}+\frac{dP_{EP}}{dT_e}}. \tag{4.26}$$

The responsivity allows me to calculate the total NEP via Equation 2.23.

4.4 Simulations

Using the program we simulated the effects of changing the operating parameters of the detector. We used aluminum contacts and, unless otherwise specified, the lattice temperature was 300 mK, the normal resistance was 10 $k\Omega$, the optical power was 1×10^{-16} Watts, the detector area was $1000\mu m^2$, $n_e = 1.8 \times 10^{15}m^{-2}$, and $\dot{Q}$ =1×10^{-17}Watts/K^5. We looked at how the electron temperature and the NEP varied as a function of the bias voltage. Because our concern was the 2DEG's performance, we chose the low optical power and only looked at the NEP contributions from the phonon, shot, and Johnson noise.

4.4.1 Lattice Temperature Variation

Increasing lattice temperature adversely affects the ability of the tunnel junction to cool the 2DEG and the NEP rises as a result (Figure 4.7). The 2DEG is decoupled from the lattice, but not completely. Equation 4.7 describes the heat flow between the lattice based phonons and the 2DEG. As the lattice temperature rises so does T_p and with it the magnitude of P_{EP}. The only way to drain this heat from the

system is through the cooling power (P_T). The cooling power is a function of the bias voltage and the superconductor's material properties (Equation 4.21) and has a peak value. If the lattice temperature and hence T_p get too high, the cooling power peak value will be insufficient to drain enough heat from the 2DEG to lower its temperature below that of the lattice. The temperature dependent phonon and Johnson noise will rise as a result, leading to the increase in total NEP.

4.4.2 Normal Resistance Variation

As the normal resistance goes up, again, the detector's cooling ability and NEP suffer (Figure 4.8). The tunneling current (and, therefore, the cooling power) is inversely proportional to the normal resistance (see Equation 4.20); as the normal resistance goes up, the ability of the tunnel junction to draw heat out of the system decreases. This keeps energy in the system longer and gives it time to warm the 2DEG. The cooling power keeps going down as the normal resistance goes up until it has no effect at all. The increase in the Johnson noise contribution is exacerbated by its direct dependence on the electron temperature and its inverse dependence, thorough the responsivity, on the normal resistance. (Equations 2.23 and 4.26) while the phonon noise would increase due to its square dependence on the electron temperature. The shot noise is reduced due to its direct dependence on I_T (Equation 2.30), but Johnson and phonon noise are far greater contributors to the total NEP.

4.4.3 Absorber Area Variation

As the area goes up, the cooling ability suffers and the NEP with it (Figure 4.9). The increase in area is causing an increase in P_{EP} rate due to an increased thermal conductance (Equation 3.46) so more of the photon's energy is going into the 2DEG as a whole, warming it up. The cooling power, on the other hand, is not being affected,

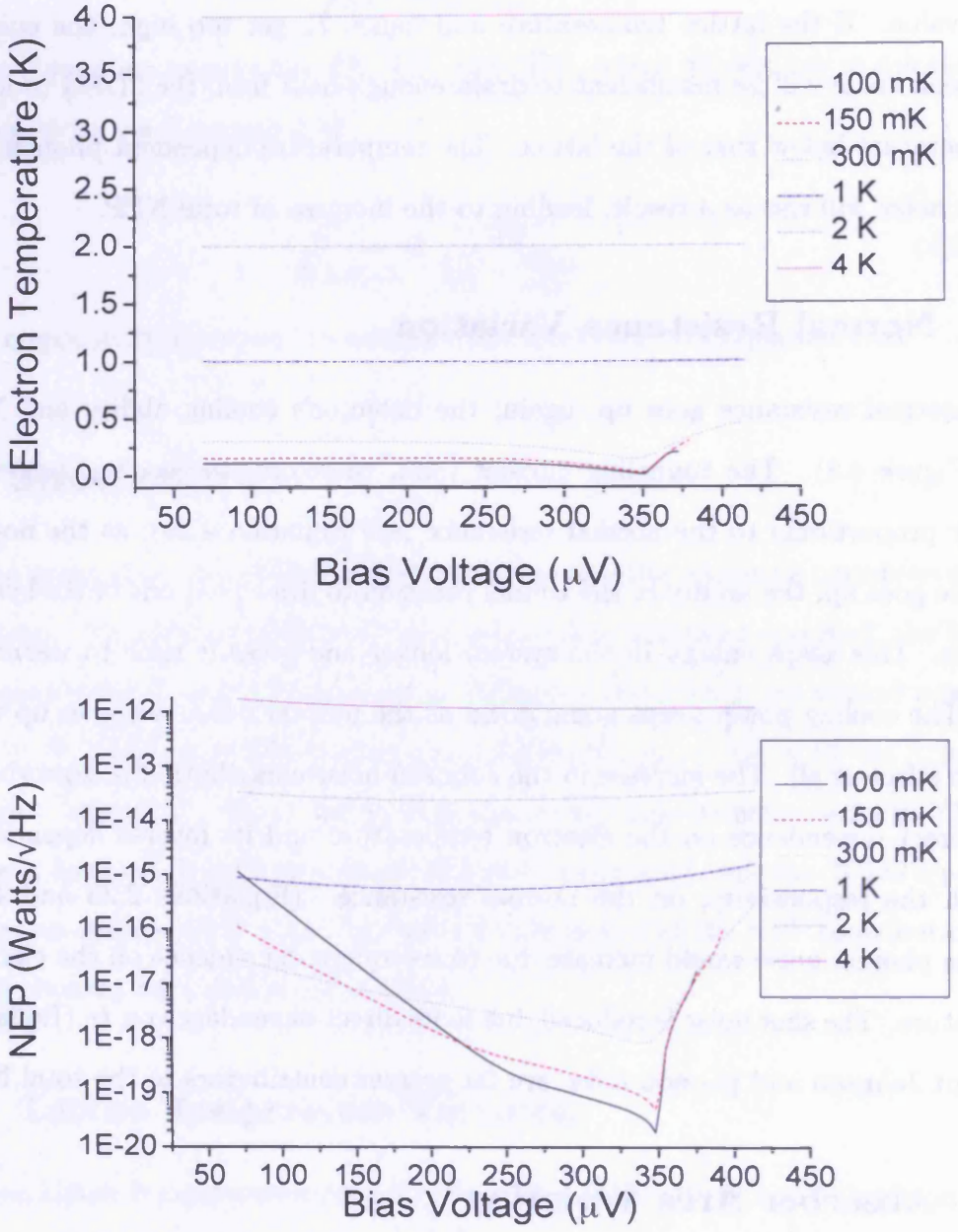

Figure 4.7: Effects of lattice temperature variation on electron temperature and NEP.

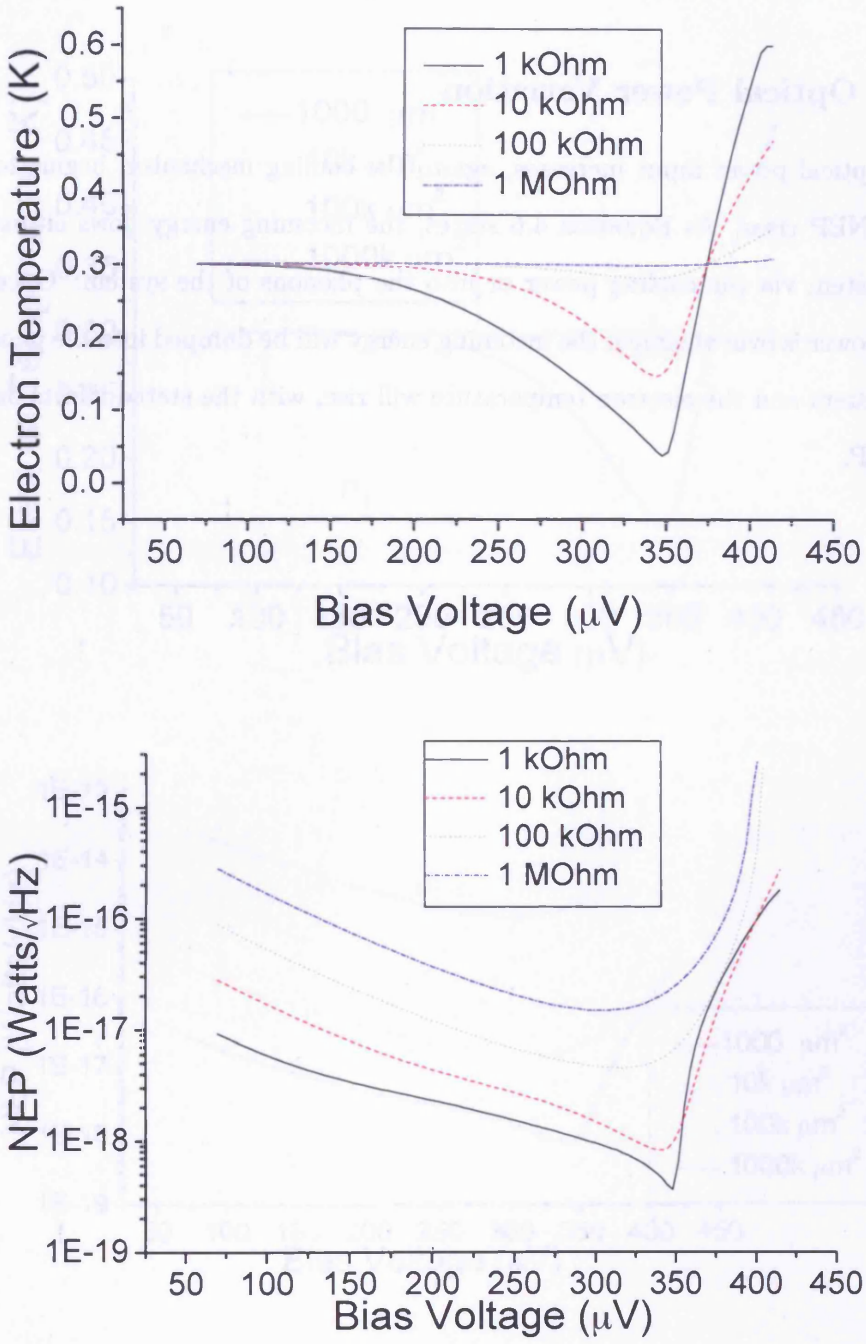

Figure 4.8: Effects of normal resistance variation on electron temperature and NEP.

so we eventually get to a point where the cooling mechanism is overwhelmed.

4.4.4 Optical Power Variation

As the optical power input increases, again, the cooling mechanism begins to fail and the NEP rises. As Equation 4.6 states, the incoming energy flows either out of the system via the cooling power or into the phonons of the system. Once the cooling power is overwhelmed, the incoming energy will be dumped into the phonons of the system and the electron temperature will rise, with the stated effects on the total NEP.

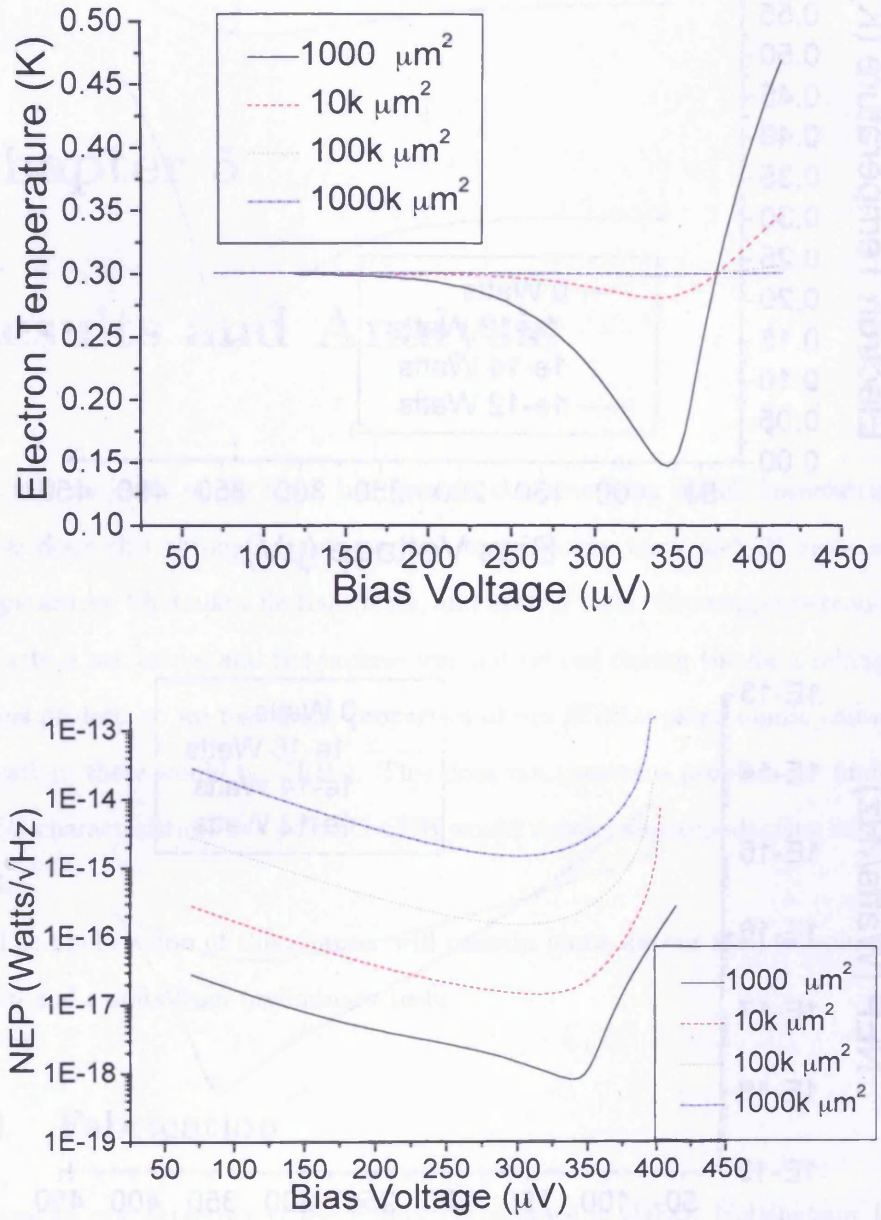

Figure 4.9: Effects of absorber area variation on electron temperature and NEP.

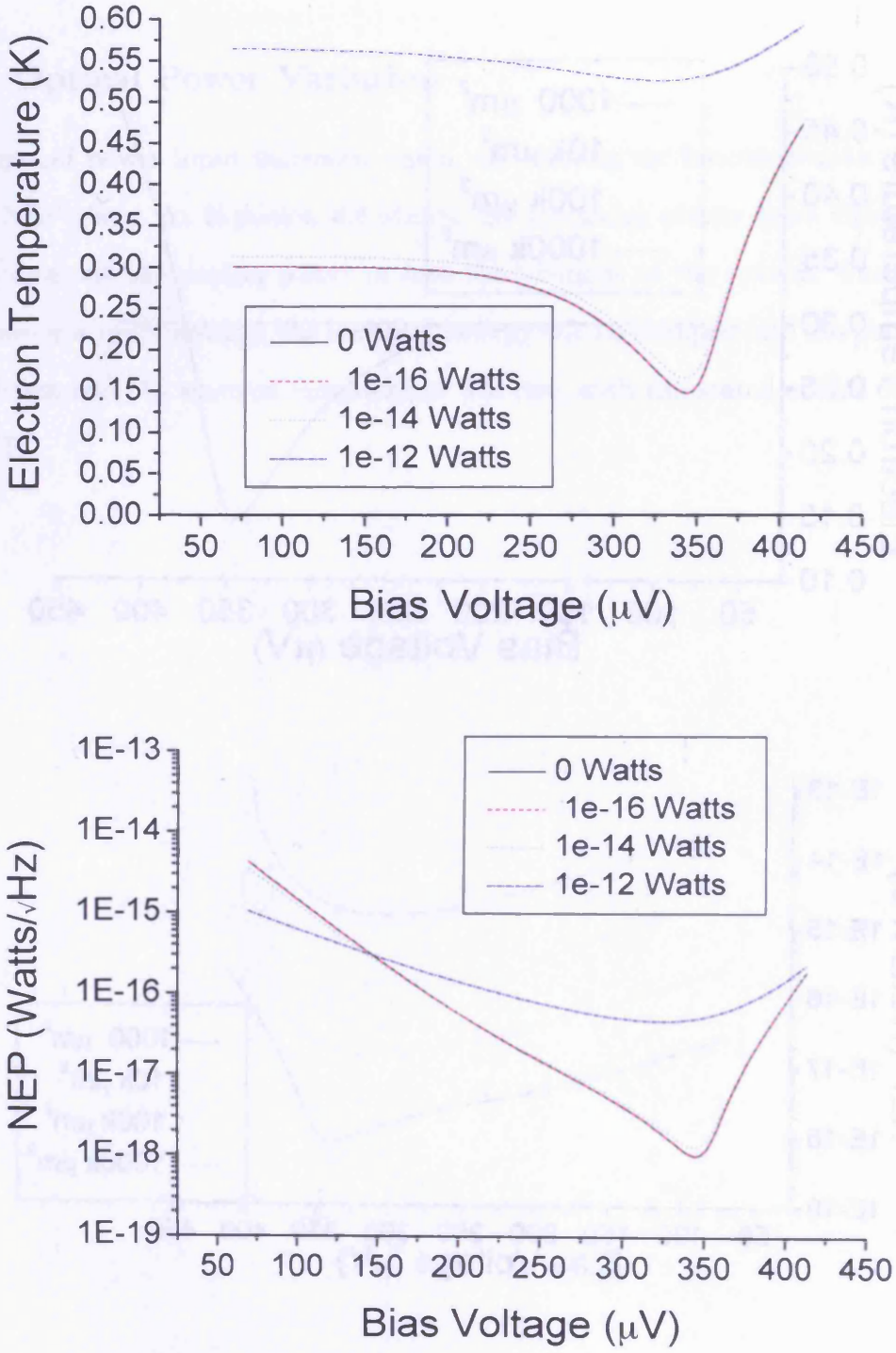

Figure 4.10: Effects of optical power variation on electron temperature and NEP.

Chapter 5

Results and Analysis

The vast majority of our work has been in characterizing 2DEG heterostructures. We've done this through resistance vs. temperature tests and IV tests at fixed temperatures, Shubnikov de Haas tests, and optical tests. Growing superconducting contacts is not trivial and the process was not refined during the data taking phase of this project, so we tested the properties of our 2DEGs using ohmic contacts (in operation, these would be HEBs). This does not present a problem for finding the 2DEG characteristics, but a 2DEG CEB would require superconducting contacts to work.

The final section of this chapter will contain plans for our final sample configuration and results from preliminary tests.

5.1 Fabrication

Central to our detectors is the ability to produce a 2DEG. Nottingham University was pursuing the growth of 2DEG heterostructures in order to studying their properties. They gave us a portion of one of their wafers for our initial tests. The structures were grown by molecular beam epitaxy (MBE) using a Gen-II system on 2

inch semi-insulating substrates. All the growths were performed at a substrate temperature of 630°C. The growth rate of GaAs and AlAs was one monolayer per second and half a monolayer per second, respectively, as measured by the reflection high-energy electron diffraction (RHEED) technique. The As/(Ga,Al) beam equivalent pressure ratio determined by an ionization gauge was 12. The samples were rotated during growth to improve uniformity. The wafer was grown on a semi-insulating GaAs substrate. The layer order from the substrate up was as follows: 2 micron GaAs buffer layer, 400Å $Al_{0.33}Ga_{0.67}As$ undoped spacer layer, 400Å $1.3 \times 10^{18} cm^{-3}$ silicon-doped (modulation doped) $Al_{0.33}Ga_{0.67}As$ layer, and a 170Å GaAs capping layer.

Sheffield University also has an MBE facility. We wanted to see how difficult it would be to grow a decent 2DEG heterostructure in a system not optimized for that purpose. Ease of fabrication would be an issue for mass production. At our request, they grew us two wafers. The first was grown on a GaAs substrate and the layer order was 1 micron GaAs buffer layer, 200Å $Al_{0.33}Ga_{0.67}As$ undoped spacer layer, 200Å $2.5 \times 10^{17} cm^{-3}$ silicon-doped $Al-0.33Ga_{0.67}As$ layer, and a 200Å GaAs capping layer. The second wafer was grown to the doping and thickness specifications of the Nottingham wafer. We do not have the specifics of their growth process save for a growth temperature of 620°C and a growth rate of 1 $\mu m/hr$.

We designed a variety of mesa structures for our tests. Most were eight-terminal Hall bars of varying dimensions, but we included a meander structure as well. A sketch of the Hall bar and meander designs is shown in Figure 5.1. The Hall bar configuration allowed for 4-wire measurements of a detector in simulated operation. All of our tests involved placing a voltage across the longitudinal direction of our Hall bars via the longitudinal contacts, simulating a photocurrent. We measured the voltage drop across the 2DEG itself via the transverse contacts, theoretically

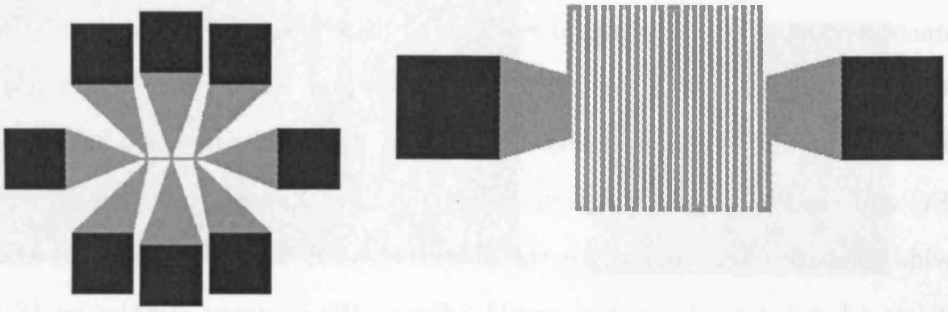

$20 \times 500\mu\mathbf{m}^2$ $20 \times 24,480\mu\mathbf{m}^2$

Figure 5.1: Sketches of Hall bar and meander configurations and dimensions. Dimensions correspond to just the Hall bars and does not include contact areas.

eliminating the contribution of the transverse contacts' resistance. The tests for which data is presented were performed at cryogenic temperatures ranging from 77 K to 450 mK. In all tests, we monitored the current through the system via a bias resistor at room temperature which was in series with the 2DEG.

Our choice of Hall bar dimensions for our experimental samples focused on ease of fabrication and comparison of size-related properties rather than on optimal detector performance. The Hall bar measured $20 \times 500\mu\text{m}^2$ and the meander measured $20 \times 24,480\mu\text{m}^2$ arranged in a mm^2 "footprint."

The meander structure was created for optical tests; we wanted to see how well the 2DEG would directly absorb photons. To that end, the footprint of the meander structure was on par with the wavelengths of THz photons we are interested in. The path of the meander is such that the impedance was matched to free space. This was a wholly experimental configuration as our meander design can never be used for a CEB: it's length means that a photoexcited electron would invariably undergo heat exchange with a phonon before reaching a readout contact (so it could be an

HEB).

The mesas were created via standard photolitohography wet etch. The ohmic contacts were applied in a thermal evaporation chamber. We evaporated 100 nm of $Ge_{12}Au_{88}$ followed by 28 nm Ni and then 300 nm Au. We then annealed at 400°C for 1 min. The AuGe was used to provide an ohmic connection between the 2DEG and the contact via diffusion during the annealing process. The Ni would provide good electrical contact for the mounting wires while the Au would ensure that wires bonded to the surface would adhere. We mounted samples on 16 pin connectors (Figure 5.2) and TO 8 headers(Figure 5.9) and connected the sample contacts to the pins via wire bonding. Our initial Hall bar designs had the contact pads connected to the mesas by rectangular strips. These had a lot of contact resistance and made testing difficult when we lost one or both of the longitudinal contacts. We eventually adopted graduated connectors shown in Figure 5.1 which minimized the contact resistance.

5.2 R vs.T and IV tests

For R vs. T tests, we made a dip probe by mounting a 16-pin socket on the end of a wooden rod. We soldered 0.2 mm diameter copper wire to each pin on the socket and ran the copper wire to a D-connector. We housed this assembly in a stainless steel tube and mounted a box on the warm end to hold the D-connector (see Figure 5.2). For determination of the temperature, we mounted a BC diode on the socket as close to the sample as possible. For these tests, we assumed that the electron temperature was equal to the lattice temperature. For testing, we simply lowered the mounted sample into a nearly empty helium dewar. We ran a constant current of $\sim$10 nA (current calculated by measuring voltage across a bias resistor)

Figure 5.2: Dip probe used for resistance vs. temperature tests. This probe had a sixteen-pin socket for the sample mounts. The smaller image shows picture of one of our mounted Hall bars. The object mounted to the right of the Hall bar is a diode thermometer.

across the longitudinal contacts and recorded temperature and voltage data as we slowly lowered the sample. A low current was necessary to minimize the heating of the sample. To check for symmetry of the resistance vs. temperature curve, we changed the current direction and continued to take data as we removed the sample. This was an important preliminary test because it proved whether or not we had a 2DEG. A poorly manufactured heterostructure would display the R vs. T curve of a semiconductor rather than a metal. Both the Nottingham and Sheffield samples displayed R vs. T behavior in keeping with that of a metal, as shown in Figure 5.2. For temperatures below 4.2 K, we used a cryostat capable of reaching temperatures of 300 mK. We did lower temperature tests primarily for resistance values to use in our IV tests.

We performed IV tests at fixed temperatures in the same cryostat in which we conducted our <4.2K R vs. T measurements. We measured the voltage across the 2DEG via a 4-wire measurement of the Hall bar in the cryostat; we placed a thermometer near the sample to determine the ambient temperature. We applied the

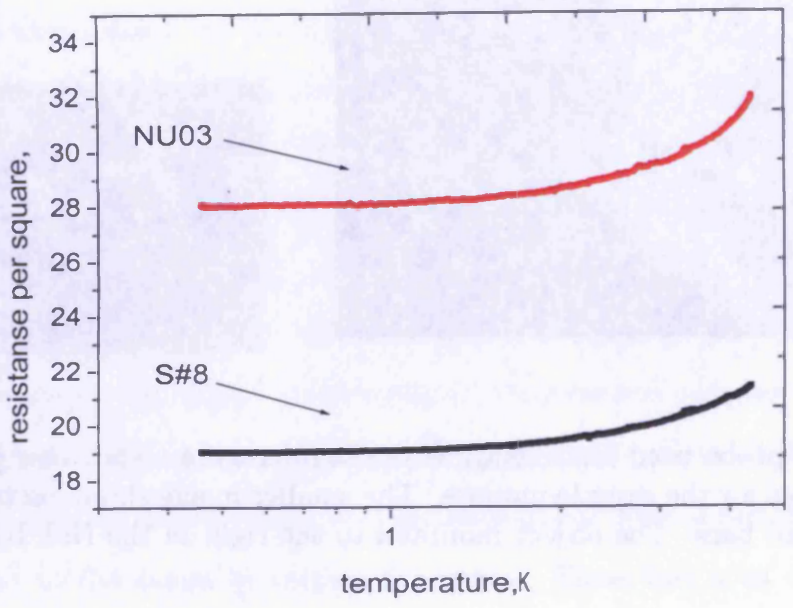

a.

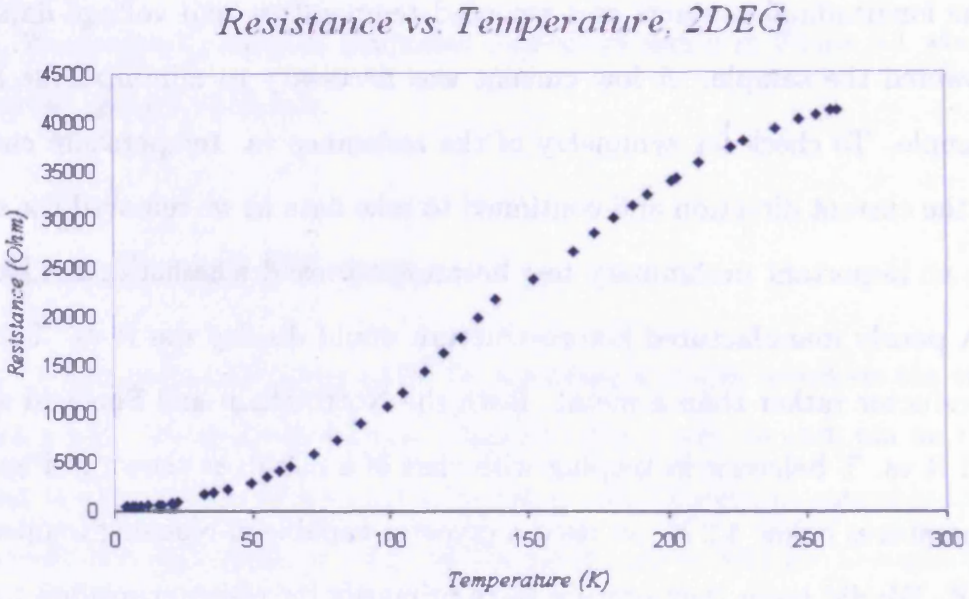

b.

Figure 5.3: a. R vs. T tests for two dimensionally identical hall bars, one made with the Nottingham material (NU03) and the other with the Sheffield material. The resistance of both samples rises with temperature, as in a metal, proving that the 2DEG is present in both heterostructures. b. R vs. T for NU03 sample being warmed to room temperature from a helium bath. The NU03 sample was the one we used for further testing due to its superior performance.

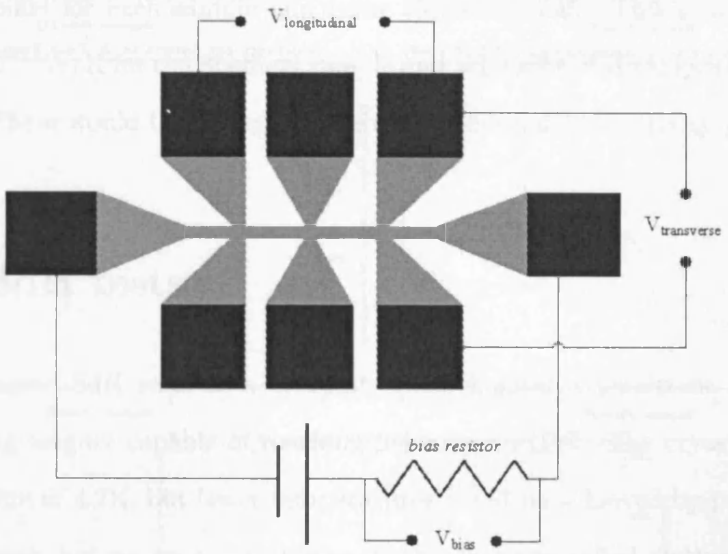

Figure 5.4: Schematic showing setup for SdH tests.

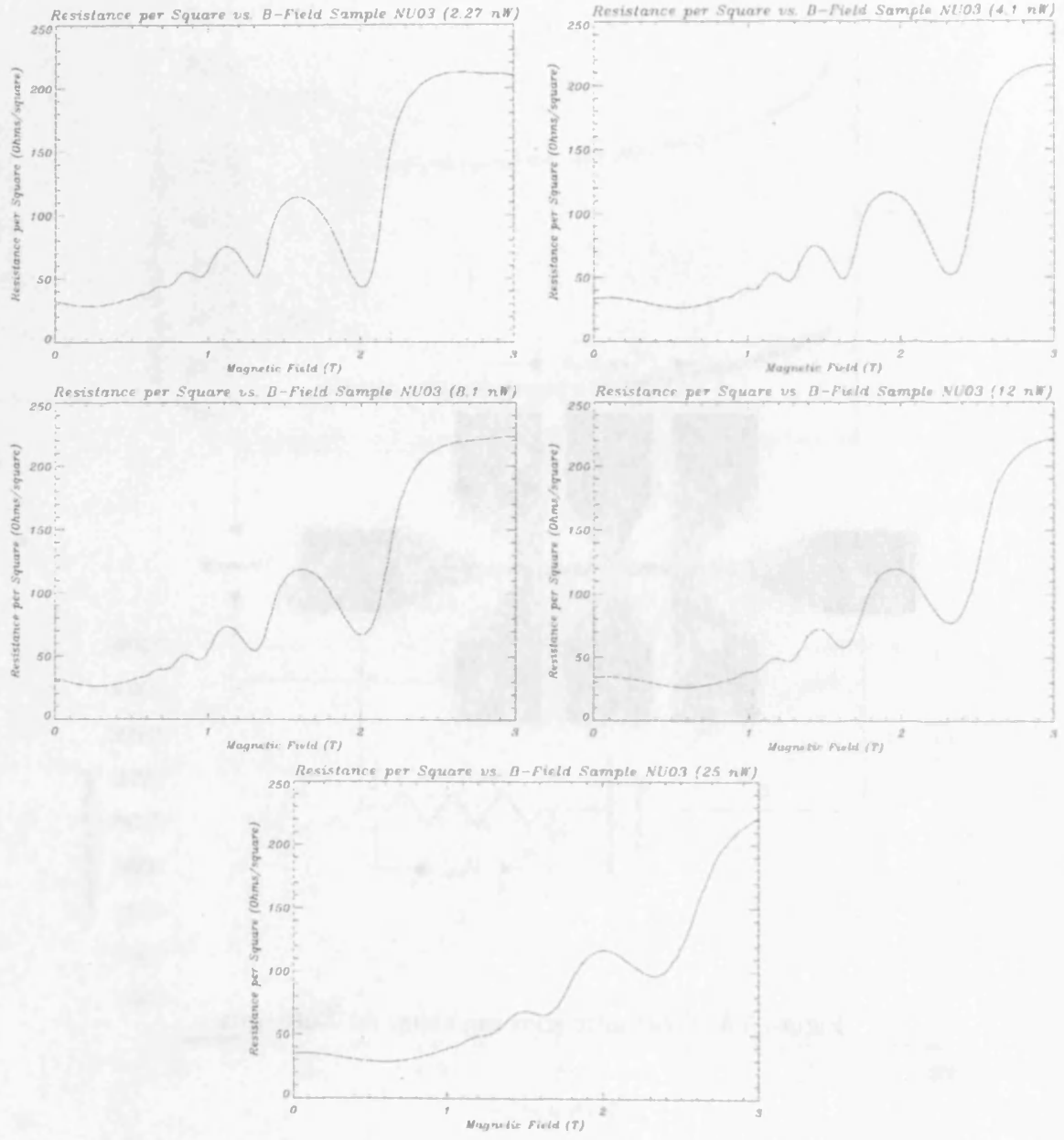

Figure 5.5: Shubnikov de Haas oscillations in Nottingham sample dissipating constant powers. Note the dampening of the oscillations at the higher power levels. This is due to the higher temperature of the 2DEG electrons.

current through applying an increasing voltage across an external, room temperature bias resistor. As the cryostat temperature dropped (to an ultimate temperature of 450 mK) we recorded voltage drop across the Hall bar and its temperature. We changed the bias voltage at different temperatures to see how the current through the 2DEG changed. From our R vs. T curves, we could determine the temperature of the 2DEG throughout the measurement. We made rudimentary calculations of the thermal conductivity by recording the power dissipation and temperatures at two points for each sample and using Equation 3.45. This gave us a value of $\approx 1.26 \times 10^{-16}$W/K for the Sheffield sample and $\approx 1.1 \times 10^{-17}$W/K for the Nottingham sample. These would be average values of the thermal conductivity per electron.

5.3 SdH tests

We performed SdH tests in a cryostat which housed a persistent current superconducting magnet capable of reaching fields up to 12 T. The cryostat had a base temperature of 4.2K, but lower temperatures could be achieved by pumping on the sample space, but we were not able to do this in a controlled method and so could not rely on the readings produced. We mounted the samples on a probe that we then inserted into the heart of the magnet space. The sample was oriented such that the plane of the 2DEG was perpendicular to the direction of the B field. We wired an external bias resistor to the longitudinal contacts on the Hall bar configuration (see schematic in Figure 5.4. We used the voltage across the bias resistor to monitor the current through the 2DEG. We used the transverse contacts to monitor the longitudinal voltage (and from it the longitudinal resistance) and to monitor the transverse Hall voltage. We mounted an optical LED and a resistive thermometer on the sample holder. The LED allowed us to shine light on the heterostructure and

observe the effect on the 2DEG. We observed a lower resistance with illumination, matching previous studies [81, 82].

Our initial round of tests involved two samples made from Nottingham material, NS01 and NS02, and a third sample made from the original Sheffield material, CS01. The Nottingham samples were manufactured there with Nottingham masks; in the case of NS02, we did the final anneal at Cardiff. We used our own mask, contact recipe, and annealing routine for the sample we made from the original Sheffield wafer. The latter sample failed to produce SdH oscillations. Our speculation was that this had to do with both the dimensions and the doping density of this sample. The lattice mismatch at the GaAs cap layer/AlGaAs doped layer gives rise to surface states in the GaAs that trap electrons. These surface states will take electrons from the doped layer until filled; the remaining electrons will comprise the 2DEG. The original Sheffield sample had a lower doping density and a thinner doped layer than the (successful) Nottingham sample. It's probable that there simply were not enough electrons left after the surface states were filled to populate the 2DEG.

The dependence of the oscillations on the temperature of the 2DEG was borne out in experiment. Increasing bias voltages warmed the 2DEG and populated LLs above the Fermi level leading to less pronounced oscillations (see Figure 5.5). After plotting against the reciprocal of the B field (Figure 5.6), we calculated the electron density of each sample using Equation 3.86 and the mobility from Equation 3.11. For the Nottingham sample, we found $n_e \approx 9.67 \times 10^{14} m^{-2}$ and $\mu \approx 376 m^2/Vs$. For the Sheffield sample, $n_e \approx 1.61 \times 10^{15} m^{-2}$ and $\mu \approx 127 m^2/Vs$.

The analysis process had two steps. First, Equation 3.87 was used to fit the SdH data (with typically 3 to 10 harmonics depending on field range) at a power dissipation rate low enough that we could assume that $Te = 4.22K$ (the temperature of the sample helium bath). This yielded 3-10 amplitudes and phases, a value for

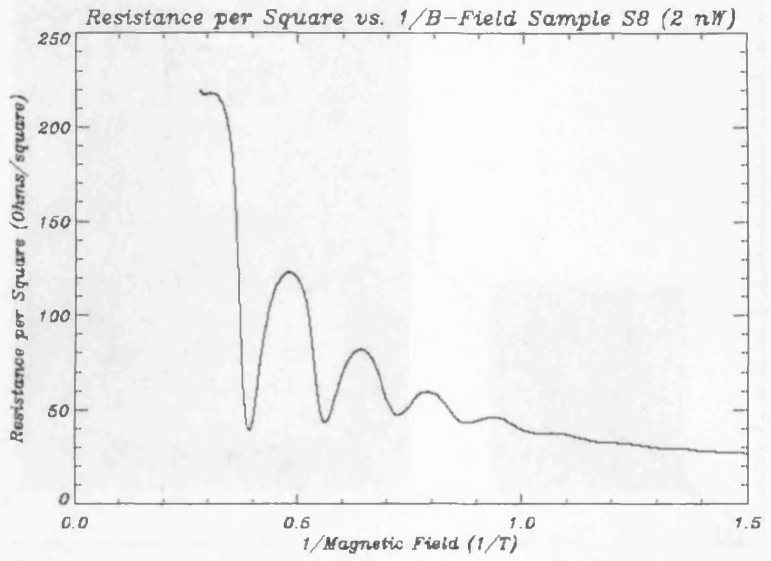

Figure 5.6: Plot of SdH oscillations vs. reciprocal of B field in Sheffield sample.

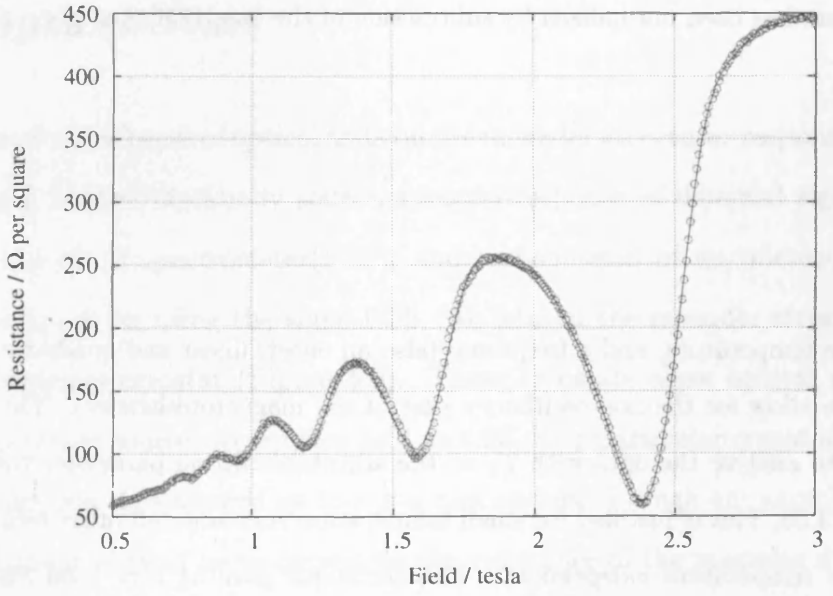

Figure 5.7: Example of fitted SdH data (from Sheffield sample; red dots enclosed in circles is original data with error; blue line is fit).

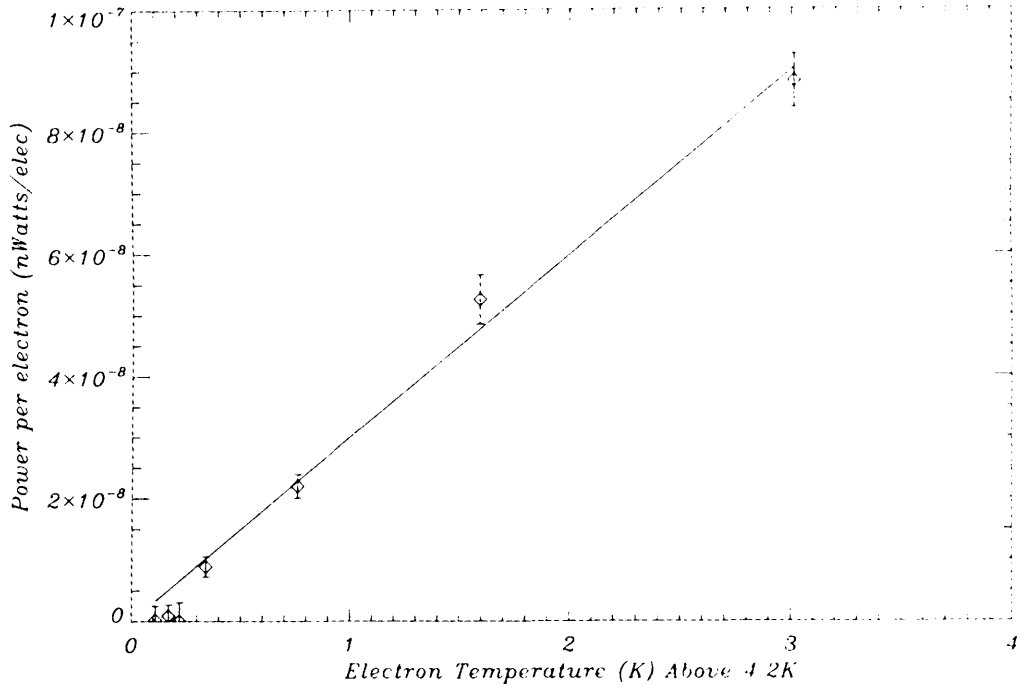

Figure 5.8: A temperature vs. power/electron plot for NU03. The reciprocals of the slope will give G per electron for the 2DEG at those power rates. Note: The temperature has been normalized by subtraction of the base temperature.

the Dingle temperature, and a frequency (also an offset, linear and quadratic term in $\rho(B)$ to allow for the non-oscillatory part of the magnetoresistance). The next step was to analyze the data with T_E as the adjustable fitting parameter through Equation 3.88, This is justified for small temperature rises since all other terms are essentially temperature independent. This technique gave us very good fits (see Figure 5.7). This allowed us to calculate the dynamic thermal conductance of the 2DEG at these settings, shown in Figure 5.8.

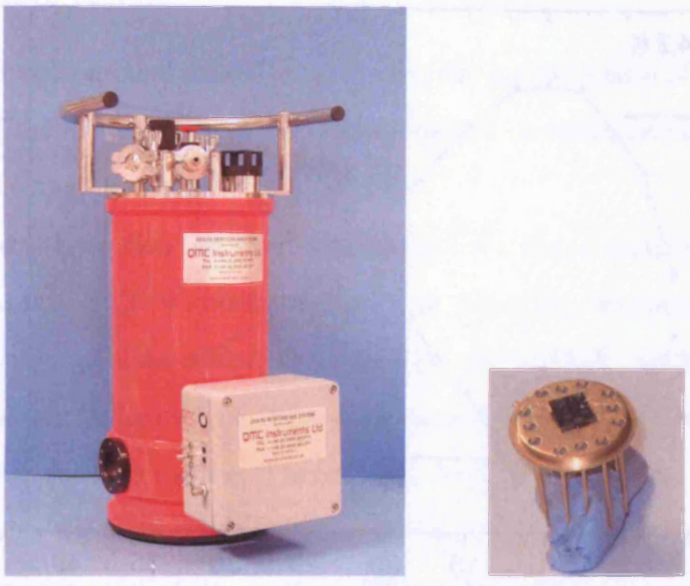

Figure 5.9: A QMC Instruments liquid helium cryostat with amplifier box. We shone radiation through the filtered window at its base. We mounted the samples on TO 8 headers (shown in smaller image) for these tests.

5.4 Optical Tests

We performed three types of optical tests on the meander structure: responsivity and noise using a filtered blackbody source, spectral response of detected signal using a Fourier transform spectrometer(FTS), and transmission of an unetched 2DEG heterostructure of an using the same FTS. We housed the meander structure in a QMC Instruments cryostat (Figure 5.9). These cryostats allow optical access by room-temperature sources to samples held at 4.2K. Our particular cryostat also had an electronics box that allowed us to run a bias current through our sample in situ. The bias current allowed us to determine the resistance of the meander during the experiment. The resulting data is shown in Figure 5.10

The blackbody source was simply a heated chamber. The resulting radiation was sent through a chopper, a propeller-like construct that, when spinning, inter-

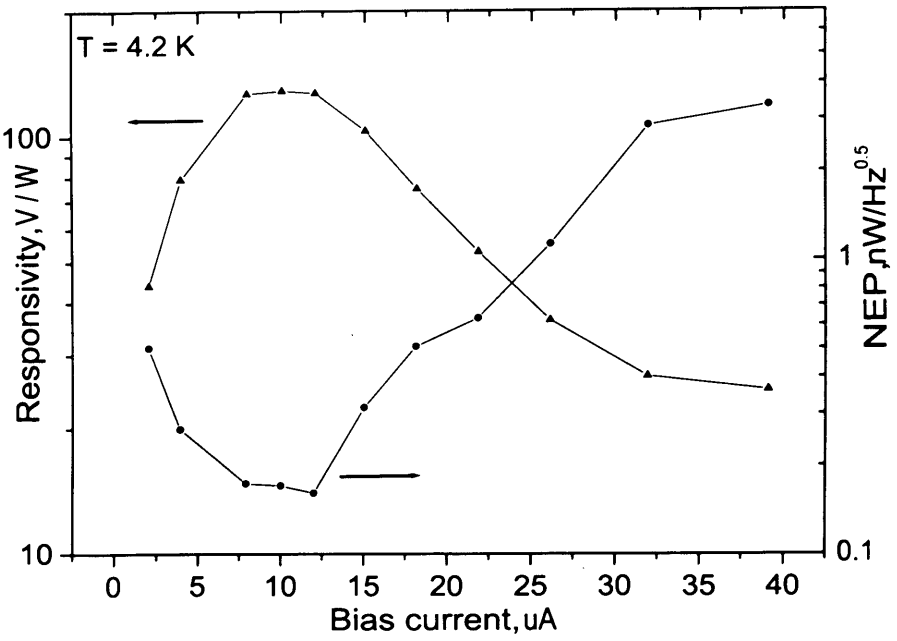

Figure 5.10: Plot of meander responsivity and NEP vs. bias current from blackbody source test.

mittently blocked the blackbody signal. This approximated a square wave. The blackbody radiation warmed the electrons in the meander and increased its resistance; we saw this as a peak in the current flowing in the meander that was centered around the rotation frequency of the chopper. The purpose of this test was to test the capability of the 2DEG to act as direct photon detector.

The FTS is a type of Michelson interferometer. The source is heated to a temperature of $\sim$ 1000°C and sends a beam of collimated radiation onto a mirror. This mirror sends the beam into a splitter, reflecting one half of the beam to a mirror perpendicular to the original beam and transmitting the other half to an in-line mirror. The two beams reflect back to the beam splitter where they combine on the side opposite the source. These two beams contain the entire bandwidth of radiation that the source is putting out. The respective path lengths determine which wavelengths will be constructively or destructively added. The FTS used one

fixed mirror and one that moved continuously during the course of the experiment. The rate of the moving mirrors' oscillation enables us to reconstruct the spectrum through a Fourier transform.

The direct absorption test involved putting a section of unetcted heterostucture in the path of the FTS. We performed this test to see whether the spectral response had more to do with the etched structure (the meander) or the 2DEG itself. The results are shown in Figure 5.11. The oscillations in the graph are due to reflection of the beam from the back surface. The reflected beam constructively and destructively interferes with the incident beam. More striking is that this graph shows 100% transmission over most of its range, a result which surprised us. A 2DEG should act like a thin metal film and should therefore not be transparent to incoming EM waves. To figure out why, we had to think of what conditions would make a metal film appear transparent. The radiation was traveling through air (approximated as free space, through the heterostructure, and then back into air. For absorption to occur, the heterostructure's impedance would have to be matched to that of free space ($\approx 377\Omega$). As there was no absorption, the question was whether the heterostructure's impedance was greater or lesser than that of free space. We were not sure of the mechanism involved in the 2DEG's interaction with the radiation, but we were able to use three different methods to model it: as a circuit; quantum mechanically; and using a plasmon approach. These approaches allowed us to think up ways to solve the absorption problem.

5.4.1 Circuit Model

The way to answer this question is to consider the situation as a circuit. What we have is two resistors in parallel, one representing free space, the other the 2DEG. An EM wave meeting the 2DEG will have a choice of paths, and EM waves always

take the path of least resistance. The wave chooses to continue along free space, so the 2DEG path must have an impedance greater than that of free space. In fact, given that there is no absorption at all, the impedance of the 2DEG must be *much* greater than that of free space. The next question is why?

In the plane of the 2DEG, along which the interaction would occur, our SdH tests showed a resistance of ~17-30 $\Omega/square$. The dimensions of the unetched heterostructure were more or less square, so the real impedance (resistance) should have been in 17-20 Ω range, but measurements of the Nottingham material's impedance during the absorption test put it at over 1000Ω. The extra impedance had to be imaginary. We had, up until this measurement, failed to take into consideration the kinetic inductance (L_k) of the 2DEG. Inductance, in general, is the property through which Faraday's Law asserts itself in a circuit. If the magnetic field through a loop (the flux, Φ_B) is changing due to a change in current, the inductance will establish an emf according to $\mathcal{E} = -LdI/dt$. We generally speak of the self inductance of a loop (L), which is dependent on the geometry of the current loop ($\Phi_B = LI$). Kinetic inductance is distinguished by being solely a property of electrons. It arises from their inherent resistance to being accelerated. It is L_k that will be the relevant inductance for a 2DEG. To derive a value for a 2DEG's kinetic inductance, we start with the total conductance (from the Drude model) [83]

$$\sigma(\omega) = \frac{n_e e^2 \tau_e}{m^*} \frac{1}{1 + i\omega\tau_e} \tag{5.1}$$

where ω is the angular frequency of the incoming radiation. The reciprocal of Equation 5.1 will be the impedance per square of the 2DEG:

$$Z_{2DEG} = \frac{m^*}{n_e e^2 \tau_e}(1 + i\omega\tau_e) \longrightarrow Z_{2DEG} = R_{2DEG} + i\omega L_k. \tag{5.2}$$

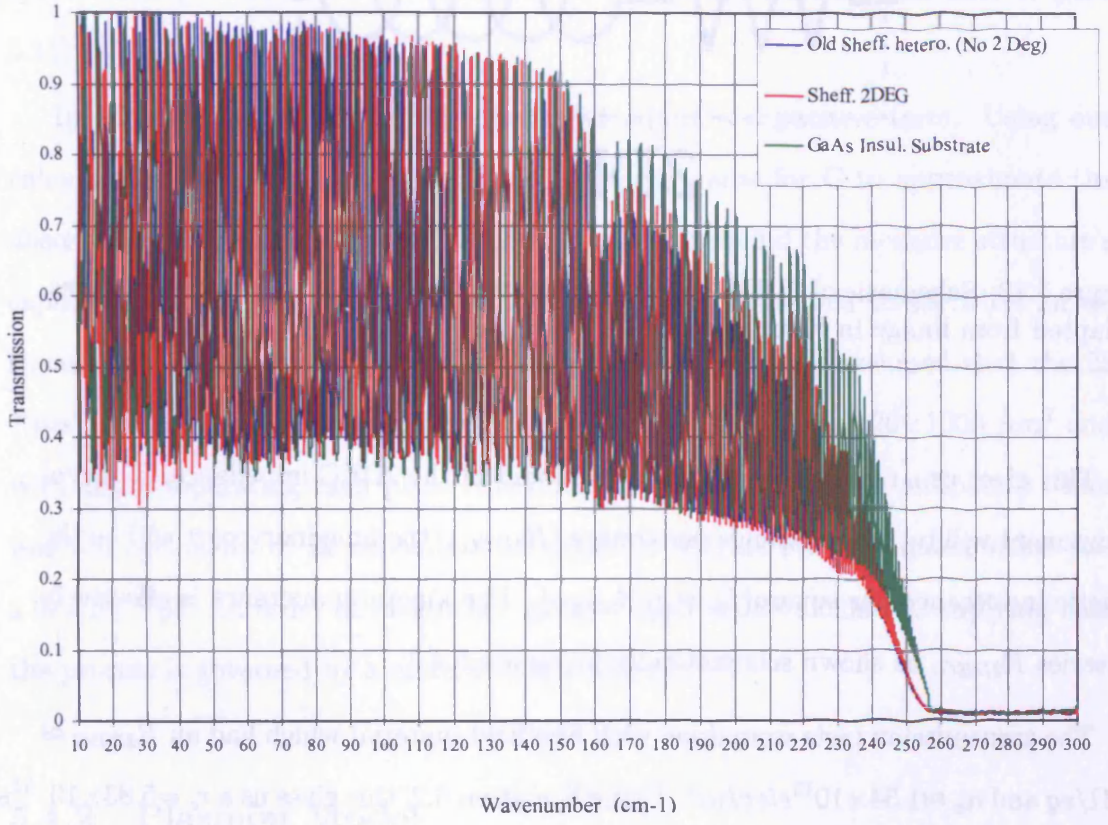

Figure 5.11: Comparison of FTS transmission through the original Sheffield heterostructure with no 2DEG, the Sheffield 2DEG heterostructure, and a GaAs insulating substrate. The fringing present is due to reflection due to the different indicies of refraction of the air, heterostructure, and substrate. Constructive and destructive interference occurs, giving rise to the variation in the transmission. The upper edge of the curve is what is relevant. Note that the transmission goes to 100% in all cases, i.e. no absorption even by the 2DEG. This is due to the high inductive impedance of the 2DEG.

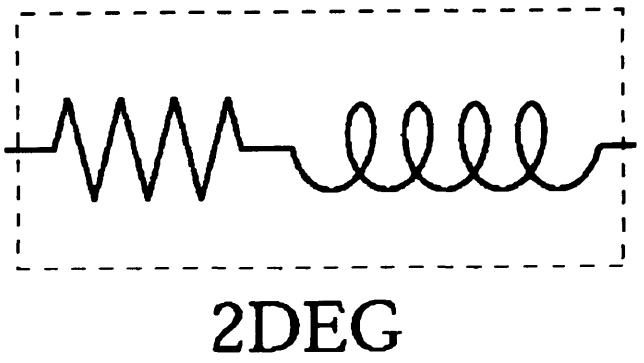

Figure 5.12: Schematic of 2DEG showing resistance and kinetic inductance in series. Adapted from image in Kang *et al.* [83]

This gives us a real and imaginary component of the 2DEG impedance. The real component will be the resistance per square (R_{2DEG}), the imaginary part will be the kinetic inductance per square($L_k = \tau_e R_{2DEG}$). The kinetic inductance is effectively in series R_{2DEG}, as shown schematically in Figure 5.4.1.

The transmission tests were done with Sheffield material which had an $R_{2DEG} \approx 30\Omega/sq$ and $n_e \approx 1.34\times10^{15} elec/m^2$. Using Equation 5.2, this gives us a $\tau_e = 5.83\times10^{-11}$s and a subsequent L_k =1.75 nH. This would give us an impedance of $\sim 11k\Omega/sq$ at a frequency of 1 THz, far too high to expect any absorption. In order to make an effective 2DEG detector, we would have to find some way to circumvent the inductive impedance.

The transmission test of the meander structure etched on the Sheffield 2DEG provided a possible solution to the inductive impedance problem. The FTS test went from 0-3THz and we observed an absorption peak at ≈1.1 THz (Figure 5.13 a.). We theorized that this absorption peak was caused by resonance due to the capacitance of the meander ($\omega = 1/\sqrt{LC}$). This capacitance would be from the

spacing between the longer lengths of the meander (see Figure 5.14).

Using ADS, a circuit simulation program, we made a circuit diagram of the path of the radiation to the meander. This diagram included the resistance of the free space leading to and from the meander as well as the contact resistance (Figure 5.15).

In addition to the 2DEG impedance, we added a capacitive term. Using our calculated values for R_{2DEG} and L_k we entered a value for C to approximate the absorption peak in the FTS test(Figure 5.13 b.). We found the meander structure's capacitance to be 1.16×10^{-5} pF. As a comparison, we decided to see what an estimate of the capacitance using $C = \epsilon_0 A/d$ would give. We assumed that the 23 "legs" of the meander corresponded to 23 plates with areas of 20×1000 μm^2 and with $40\mu m$ separating each plate (the distance from midpoint to midpoint). This was the equivalent of 22 capacitors arranged in series. The calculated value was 2.01×10^{-4} pF, an order of magnitude greater than ADS calculated, implying that the process is governed by a more intricate theory.

5.4.2 Plasmon Model

As explained in Pendry et. al [85]. A plasmon is a collective oscillation of the electron density in a given medium; similar in concept to a sound wave moving through air. This medium could be a metal or an electron gas. An incoming EM wave will cause the electron gas to oscillate. The electron gas in each system will have a characteristic frequency which will induce simple harmonic motion. This is the system's plasma frequency [48, 47]:

$$\omega_p^2 = \frac{n_e e^2}{\epsilon_0 m^*}. \tag{5.3}$$

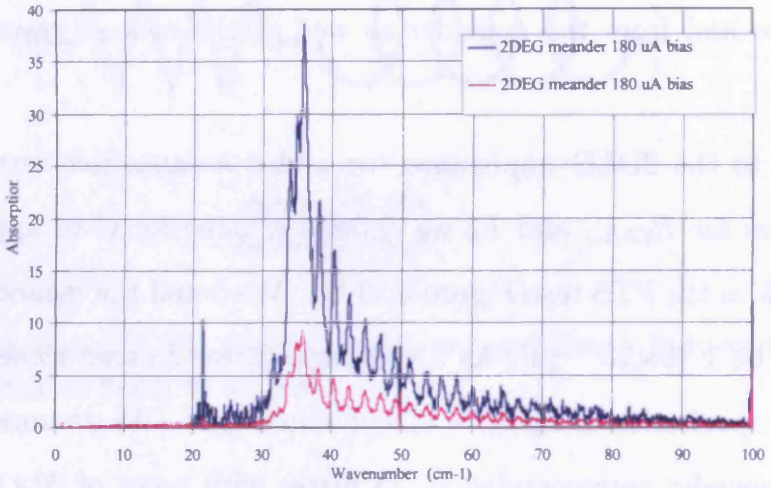

a.

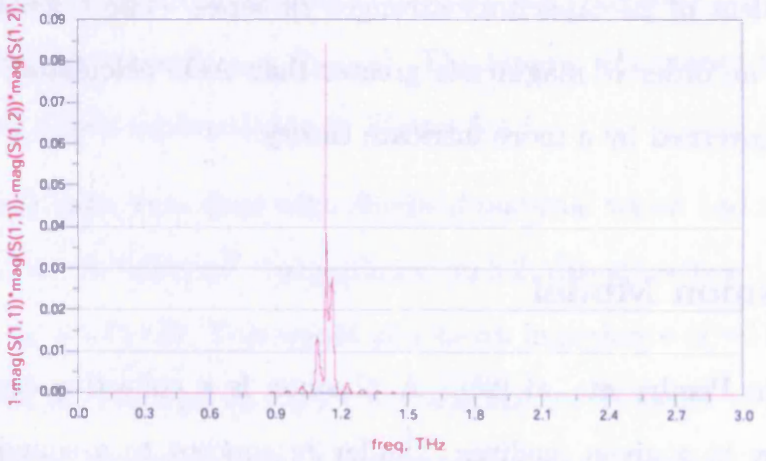

b.

Figure 5.13: The FTS test of the meander structure on the Sheffield 2DEG showed an absorption peak at $\approx 1.1THz$ (a.). We modeled the system with ADS including a value for the capacitance of the meander structure and made an absorption curve (b.), matching the absorption peak and thus determining the capacitance of the meander.

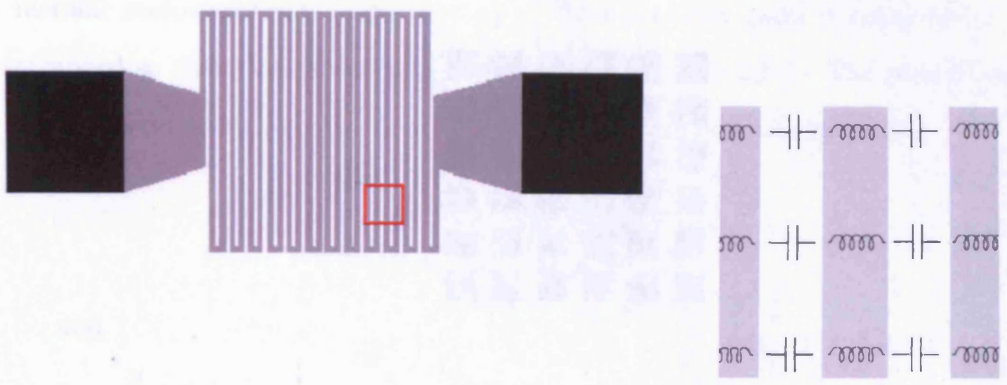

Figure 5.14: Model of meander structure showing the capacitance between straights of the meander path and the kinetic inductance of the 2DEG in the meander. These two properties will effectively make a series LC circuit.

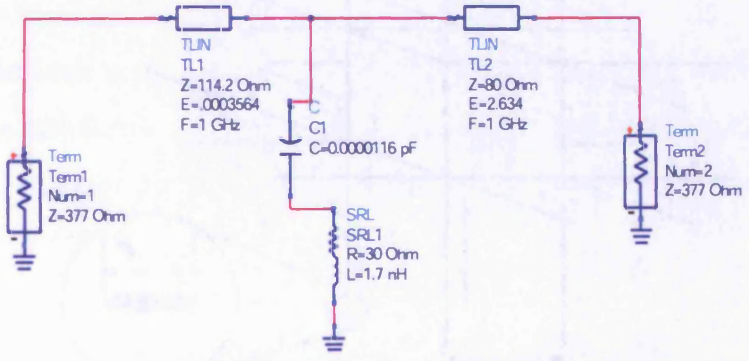

Figure 5.15: Model of the meander system using ADS. We incorporated the impedance of free space and the ohmic contacts.

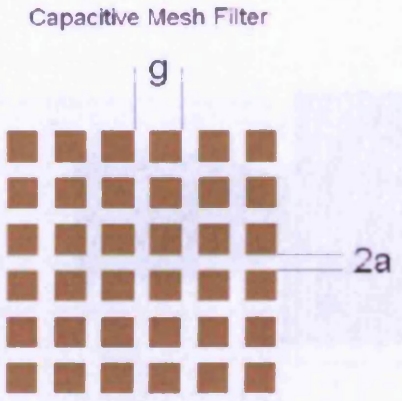

Figure 5.16: Dimensions of a capacitive mesh. (Image taken from Hooberman [84])

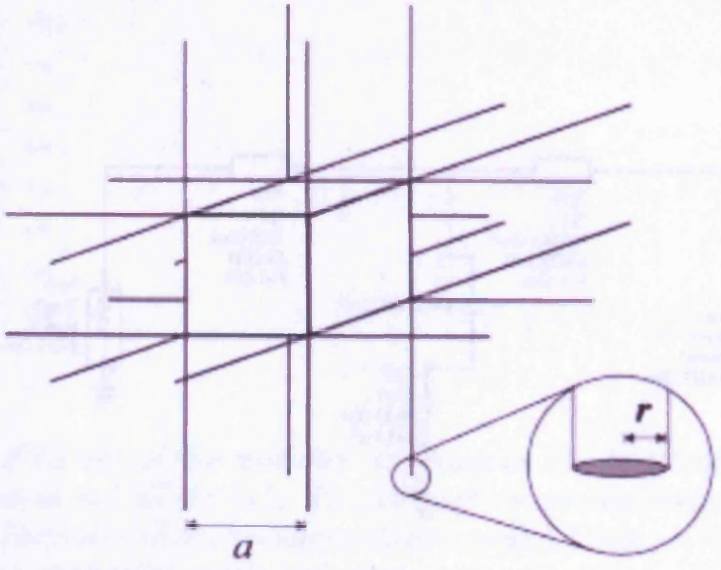

Figure 5.17: Schematic of mesostructure. Taken from Pendry et al. [85].

In order to detect THz, we will have to change the 2DEG's absorption properties. Pendry et. al [85] describes a method of generating low-frequency plasmons in metallic mesostructures. These mesostructures are thin (radii $\sim 1\mu$m) metal wires arranged so that they form a cubic lattice (see Figure 5.17). The properties of a mesostructures is a function of the wire radius r and the wire spacing a:

$$\omega_p^2 = \frac{2\pi c^2}{a^2 ln(a/r)}. \tag{5.4}$$

and

$$m^* = \frac{\mu_0 \pi r^2 e^2 n}{2\pi} ln(a/r), \tag{5.5}$$

where n is the electron density of the wire material. This model will enable us to determine by how much we would have to change the effective masses of the electrons in the 2DEG in order to achieve the absorption we want, i.e. ω_p=1 THz.

5.5 "Ideal" Detectors

A 2DEG detector would incorporate a capacitance in series with the kinetic inductance of the 2DEG. We could achieve this through the use of a capacitive mesh filter overlaid on a lattice of 2DEG material. The impedance of the mesh filter would go as

$$\frac{1}{\omega_0 C} = \frac{2}{n_1^2 + n_2^2}(4\omega_0 lncsc\frac{\pi a}{g})^{-1}(\frac{gf}{c\omega_0'} - \frac{c\omega_0'}{gf}) \tag{5.6}$$

where $\omega_0' = \omega_0\sqrt{\frac{2}{n_1^2+n_2^2}}$ [84]. The values a and g refer to the dimensions of the mesh (see Figure 5.16), while n_1 and n_2 are dielectric indices of refraction [86]. In our case, n_1 would be the refractive index of air (1) and n_2 that of the heterostructure

(GaAs, $\sqrt{13}$). The dimensions of the mesh would be chosen such that the detector would resonate at the target frequency ω_T: $\omega_T = 1/\sqrt{L_k C}$.

The low thermal conductance of the 2DEG allows us to use larger dimensions than in other detectors. Where they would use antennae to couple incoming radiation to a small absorber, we could simply make our absorber size on the order of the THz wavelength and allow direct absorption.

We have the options of making either 2DEG HEBs or 2DEG CEBs. While the CEB is our goal, a HEB could also be useful. We could modify our meander design by adding regularly spaced metal islands. These islands would serve as a linear capacitive filter. As Figure 5.14 shows, there will also be capacitance between the straights of the meander path and added capacitance due to the islands themselves.

For a 2DEG CEB, we would deposit a layer of superconductor on top of the islands of the capacitive mesh to serve as readout pads. Which island sites we would use would be determined by τ_s. We would choose islands that allow for multiples thereof.

Chapter 6

Conclusion

In this thesis, the possibility of a new type of THz detector (bolometer) using a semiconductor heterostructure has been explored . The absorbing medium would be a 2DEG created through doping of the heterostructure. Among the advantages of such a bolometer over a germanium one, for example would be increased electron mobility. The increased electron mobility will allow for for detection with a smaller number of electrons, and we could control that number through doping whereas a metal is bound to its $\sim 10^{22} electrons/m^3$. A metal bolometer would be limited by the material properties of the absorber, the only way to minimize the number of electrons would be to apply as thin a film as physically possible. A 2DEG will have an effective thickness of a few angstroms, thinner than is possible for a metal film. Fewer electrons would mean a smaller heat capacity for the 2DEG. In the case of a 2DEG CEB, the heat capacity be even lower due to the decoupling of the electrons and the phonons in the 2DEG system. The photon energy would be primarily shared by the electrons so the large heat capacity that would be contributed by the phonons is bypassed. The small heat capacity would also mean a small time constant, i.e. faster measurements.

A 2DEG CEB could potentially have an NEP $\sim 10^{-19} W/\sqrt{Hz}$ and a time constant ~ 1 μs at an operating temperature of 100 mK. A modern silicon-nitride micromesh bolometer (the same type used on BOOMERANG) described in Woodcraft *et al* [87] had a design goal of time constant of 5.8 ms and an NEP of 1.5×10^{-17} at 100 mK. A TES bolometer described by Hunt *et al* [88] has a time constant of 437μs and an NEP of 2.0×10^{-17} (at 360 mK transition temperature).

We have proven that it is possible to produce suitable heterostructures without using overly specialized MBE systems, but, of course, best results will be obtained from MBE systems optimized for 2DEG heterostructure production. The two most pressing challenges to the development 2DEG bolometer prototype are coupling THz radiation into the 2DEG and devising a sensitive thermometer to measure the electron temperature.

For radiation coupling to the system, we would use current antenna/filter technologies. The real problem is getting the THz energy into the 2DEG. The electron density in a 2DEG is lower than that of a metal, but the 2DEG's DC resistance is comparable to metal because of greater electron mobility. The relative scarcity of the electrons in a 2DEG, however, means that the electron-photon interaction cross-section will be much smaller. In addition, the two-dimensional aspect means that light shining on the surface of the heterostructure, perpendicular to the 2DEG's plane, would not be readily absorbed. Radiation will have to be channeled into the plane of the 2DEG both to enable any electron-photon interaction and to maximize the likelihood that the radiation will find electrons.

There are a number of methods that have been proposed for monitoring the temperature of the electrons in a 2DEG including Shubnikov de Haas oscillations and/or Hall resistance (Komiyama, *et al.* [89]), 1-D thermopower (Appleyard, *et al.* [1]), and superconducting tunnel contacts (Anghel, *et al.* [32]). We have done

simulations to show that superconducting SINIS contacts, if properly engineered, could provide a high sensitivity from a relatively high base temperature.

A great hurdle to overcome in the development of 2DEG detectors is simply to understand the mechanism of their interaction with radiation. The impedance of the 2DEG does appear to be frequency dependent through the inductance, as described in Chapter 5, but we lack an exact description of the mechanics. Kabir *et al* [90] suggests that the resistance of the 2DEG may also be frequency dependent. The uncertainty is primarily due to the relative novelty of THz measurement. Studies of higher and lower frequencies have been made, but there is a gap in the area of the spectrum in which we are interested. The solution to this problem is simply more research, and the promise of THz exploration of our universe has prompted studies.

We hope to eventually provide astronomers and astrophysicists a useful, versatile tool to uncover the information long hidden in the THz spectrum. While the hurdles facing 2DEG detector development are not insignificant, our research shows that neither are they insurmountable. Hopefully, the next thesis that mentions 2DEG detectors will be one primarily concerned with data analysis from observations.

Acknowledgments

"And what of that? Is not a day divided into twenty-four hours, each hour into sixty minutes, and every minute sub-divided into sixty seconds? Now in 86,400 seconds very many things can be done."

From *The Count of Monte Cristo* by Alexandre Dumas

The above is one of my favorite quotes, which probably goes a long way towards describing the magnitude of my capacity for procrastination. That does not make it untrue; in the 365 extra days I've taken to get this thesis done, I've done very *very* many things. This has been easily the most difficult thing I have ever done and I would not have made it if not for the support of a lot of good people who are listed in no particular order. Well, my advisor and the people who gave me money are at the top, but I think that's understandable.

Firstly, I'd like to thank Phil for making this all possible. I've learned a great deal from him and I sincerely hope some of his genius has rubbed off on me. It was also fun being around someone who can do Batman-style disappearing acts. Seriously, I'd look up mid-sentence and he'd be gone - then the phone would ring and it'd be him, calling from Italy. Freaky. I thank Antoinette for being my friend and more for the last 11 years of my life. She's just the greatest. I thought that on the day I met her and time has not diminished my opinion. (Okay, honestly, on the day I met her I just thought she had really nice legs, it took me a couple of weeks to get to the "you're the greatest" thing.) Thanks for supporting me, despite not quite believing I would ever finish. Joe, on the other hand, never doubted I would finish, even when I did. In fact, when the conversation veered even close to the prospect, he'd say "You're going to finish, Ian" in a way that implied he'd break my legs if I didn't. Helluva motivator, that. Martin was kind enough to allow me to use his magnetics

lab for the SdH tests and was of immeasurable help in analyzing it later. He was also a very generous source of information and explanation on many subjects. In that same vein, I must thank Dmitry for his numerous impromptu physics lessons. And I must thank my good friend Kenji for getting me the very interesting job that kept me from starving while I wrote up. It was a dirty job and I was glad to do it.

I'd like to thank my family for the reverential way they spoke to me when I started my big time physics Ph.D. and the scolding, shame-inducing way they spoke to me when it started to drag on. It was wonderful having what amounts to a stadium full of women and three guys cheering me on. Sonia provided a welcome distraction from the grind in the form of conversation and the occasional visit. Aunt Pauline, Uncle Ken, and Vada, my family near London. One of the best things about being in the UK was being able to get to know you all a bit better. Thanks to Vada, I'm a Jedi Chef! Wouldn't have happened in the States. My brother Kai. Really, man, thanks for being born. Six aunts who all had girl children, save Raymond? They'd have made me gay if not for your balancing the hormone levels in our clan. Kai's "virtual prison visits" really got me through the last few months in Cardiff. He knows what I'm talking about. My mother for her unabashed pride in me. She shows me off like a new Jaguar and, Mom, I want you to know I appreciate it. Grandma. You were who I hoped to be someday, except with boy parts. I'm so sorry you didn't live to see me get to the end of this, but I know you knew I would. I miss you terribly, but the pain of missing you will never match the joy of having you in my life.

Finally, and only because money and family trump drinking buddies, the Cardiff Crew. I really wasn't ready for how different it would be in the UK– I mean, guns, people! Where the hell are the guns?– but culture shock didn't overwhelm me thanks to my fellow post-grads being so welcoming. I really appreciated your friendship,

despite my inclination to disappear into small rooms with a book. There are, of course, some especially-like-tos. I'd especially like to thank Douglas for providing 40% of my lodgings in Cardiff, but also for being the only other real proponent for dinner parties in Cardiff and for showing me the joys of interior decorating. (Where my family didn't succeed in making me gay, Douglas did, apparently. Whoa, that didn't come out right...) David, who put the mate in flat mate. The greatest moments were watching Smallville and cruising the mean streets of San Andreas. Thanks for being a good mate. And thanks *a lot* for the thesis assist! Also, David, I'd like to thank you for saying "Right, time for some pimpin'," in a Welsh accent. Honestly, nothing can get me so down that recalling that doesn't make me laugh. The Wasketts, Kat and Tim. Tim, greatest thing, sharing stories. You're the author of one of my favorite short stores ever, What If- Part Two. Hope we do it again someday soon. Kat, greatest thing, sitting closer to you than I probably should have. Do not get me wrong, fun talking to you, too, but, yeah, more fun sitting next to you. Hope we do it again someday soon. Dave and Hannah, thanks for inviting me to your wedding. That was a ridiculous amount of fun and one of the highlights of my time in Cardiff. Themed weddings rock! Cindy and Andrew, your wedding rocked on another level. Also a highlight. Those cakes you guys ordered... I'm still having the dreams.

And with that, I away.

Ian Dean Bacchus. September, 2007.

Appendix A

2DEG Simulation Program

The following Appendix contains the text of the IDL code used to generate the simulations found in Chapter 4:

```
pro tunnelcurrent2deg

;Looking at cooling properties of a two-dimensional
;electron gas using equations from Nahum APL (65) pg. 3123
; and parameters from Appleyard Phys. Rev. Lett (81) 3491.
;Attempting to replicate results from Savin APL (79) 1471

elec=1.602e-19 ;electron charge in Coulombs

;delta=348.e-6 ;2xenergy gap of aluminum at 0K in eV
delta=3050.e-6 ;2xenergy gap of niobium at 0k in eV
;delta=174.e-6 ;energy gap of aluminum at 0K in eV
;delta=1525.e-6 ; energy gap of niobium at 0k in eV
```

```
;delta=500.e-6

de=delta/100.;Integration element

;de2=delta2/100

kb=8.62e-5 ;Boltzmann constant in eV/K

h=4.14e-15 ;Planck constant in eV*s

tl=.3 ;Lattice temperature in K

rn= 100. ;Normal state resistance of the junction in Ohms

ev=2. ;Energy difference between Fermi levels in super-
;conducter and normal metal

mu=1.5e12 ;Central frequency of detector in Hz

eta=0.05 ;Overall transmission of the system, dimensionless

emis=1. ;Emissivity of the background, dimensionless

popt=1.e-12 ;Optical power input in Watts

area=10000. ;Area of absorber material in square microns
```

```
qdot=.25e-17 ;coefficient of electron-phonon interaction in W/(electron)K^5

nel = 2.e3 ; electron density in 1/um^2

sigma = qdot*nel ; coefficient of electron-phonon interaction in W/um^2K^5

photnep=sqrt(2*popt*(h*elec*mu+eta*emis*kb*elec*tl)) ;Photon NEP in units of W
;bacground temperature = lattice temp
;absorbed incident power = optical power


vbias=(dindgen(100)+20)*de ;Bias voltage
energy=(dindgen(1000)+101)*de ;Electron energy
telect=(dindgen(1000)+1)*tl/500.+ de/kb ;Electron temperature

tuncur=dblarr(1000)
powout=dblarr(1000)
powelph=dblarr(1000)
terel=dblarr(100)
tunrel=dblarr(100)
phonep=dblarr(100)
johnep=dblarr(100)
g=dblarr(100)
didte=dblarr(1000)
dpoutdte=dblarr(1000)
```

```
dpelphdte=dblarr(1000)
didp=dblarr(100)

;Want to create a graph of electron temperature vs. bias voltage for a 2DEG.
;In operation, the power input will be equal to the power output; the only
;relevant electron temperatures are going to be those temperatures at which
;the input and output powers are equalized.  The input power is something we
;control via the amount of (optical) energy to which we expose the 2DEG.  The
;output power will be lessened due to energy lost to electon-phonon interaction
;within the lattice.  Hence, we want an equation that reads as follows:
;optical power - electron-phonon power - output power = 0.
; To calculate output power, I am using equaion 2 from Nahum APL vol.65 pg.
;3123, December, 1994.  It's an integral.  For future work, I'm also calculating
;the tunneling current using equation 1 from the same paper.

for i=0, 99 do begin
vb=vbias(i) ;Setting bias voltage value for each iteration of the i-loop

for j=0, 999 do begin
;en=energy(j)
te=telect(j)

fdd2d=1./(exp((energy-vb)/(kb*te))+1.) ;Fermi-Dirac distribution 2DEG
dossc=energy/sqrt(energy^2-delta^2) ;Density of states in superconductor
 d2ddte=((energy-vb)*(exp((energy-vb)/(kb*te)))/((kb*te^2)*(exp((energy-vb)/(kb*te))+1.
;The above is the derivative of fdd2d wrt the electron temperature.
```

```
tuncur(j)=(1./rn)*total(fdd2d*dossc)*de ;Integral for tunneling current
powout(j)=(1./rn)*total((energy-vb)*fdd2d*dossc)*de ;Integral for power
powelph(j)=sigma*area*(te^5-tl^5) ;Equation for electron-phonon power

dpelphdte(j)=5.*sigma*area*te^4 ;Derivative of electron-pnonon power wrt
;electron temperature.

didte(j)=(1./rn)*total(d2ddte*dossc)*de ;Integral for derivative of tunnel cur
;wrt electron temperature.
;stop

dpoutdte(j)=(1./rn)*total((energy-vb)*d2ddte*dossc)*de ;Integral for derivativ
;output power wrt electron
 ;temperature


endfor

relevantte=min(abs(popt-powout-powelph),jmin) ;min function finds minimum of a
;operation contain in parentheses and
;places the location of that value in
;a locator, in this case "jmin."  Again
;we ideally want the sum of the powers
;to be zero.
;Note: Without the comma and locator
```

```
; assignment, min will simply return the
;smallest value in the array.  Note, in
;this case, min is acting on the
;absolute value (abs function) of the
;array operation in the parentheses.


terel(i)=telect(jmin) ;Gives relevant value of electron temperature for the this bias v

tunrel(i)=tuncur(jmin)

didp(i)=didte(jmin)/(dpoutdte(jmin)+dpelphdte(jmin));

g(i)=5*sigma*terel(i)^4*area

phonep(i)=sqrt(4*kb*elec*terel(i)^2*g(i)) ;Phonon NEP

johnep(i)=sqrt(4*kb*elec*terel(i)/(rn*didp(i)^2)) ;Johnson NEP

endfor

plot, vbias, terel,thick=2,$
title= '!8Electron Temperature vs. Bias Voltage',$
xtitle='Bias Voltage (V)',$
ytitle='Electron Temperature (K)'
stop
```

```
;plot, vbias,tunrel,thick=2,$
;title= '!8Current vs.Bias Voltage',$
;xtitle='Bias Voltage (V)',$
;ytitle='Current (Amps)'
;stop

;plot, vbias, didp,$
;title= '!8Responsivity vs. Bias Voltage',$
;xtitle='Bias Voltage (uV)',$
;ytitle='Responsivity (A/W)'
;stop


plot,/ylog, vbias, phonep+johnep,$  ;for partial noise
title= '!8Partial NEP vs. Bias Voltage',$
xtitle='Bias Voltage (uV)',$
ytitle='NEP (Watts/sqrt(Hz))'
stop

;plot,/ylog, vbias, photnep+phonep+johnep,$
;title= '!8NEP vs. Bias Voltage',$
;xtitle='Bias Voltage (uV)',$
;ytitle='NEP (Watts/sqrt(Hz))'
;stop
```

```
set_plot, 'ps'
;device, filename='\\Serpens\spxidb\spie\300mk2degtvsv.ps'
;plot, vbias, terel,thick=2,$
;title= '!NElectron Temperature vs. Bias Voltage (300 mK Lattice Temp.)',$
;xtitle='Bias Voltage (V)',$
;ytitle='Electron Temperature (K)'
;device,/close

;device, filename='\\Serpens\spxidb\spie\50mkiv.ps'
;plot, vbias,tunrel,thick=2,$
;title= '!8Current vs.Bias Voltage (50 mK Lattice Temp)',$
;xtitle='Bias Voltage (V)',$
;ytitle='Current (Amps)'
;device,/close

;device, filename='\\Serpens\spxidb\thesis\4k2degresvsv.ps'
;plot, vbias, didp,thick=2,$
;title= '!8Responsivity vs. Bias Voltage (4K Lattice Temp.)',$
;xtitle='Bias Voltage (uV)',$
;ytitle='Responsivity (A/W)'
;device,/close

;device, filename='\\Serpens\spxidb\spie\300mk2degnepvsv.ps'
;plot, /ylog, vbias, photnep+phonep+johnep,$
;title= '!8NEP vs. Bias Voltage (300mK Lattice Temp.)',$
;xtitle='Bias Voltage (uV)',$
```

```
;ytitle='NEP (Watts/sqrt(Hz))'
;device,/close

set_plot,'win'

;iv=dblarr(2,100) ;making txt file of current and voltage data
;iv[0,*]=vbias
;iv[1,*]=tunrel
;openw, 1, '\\Serpens\spxidb\spie\50mkiv.txt'
;printf, 1, iv
;close, 1
end
```

Bibliography

[1] N. J. Appleyard, J. T. Nicholls, M. Y. Simmons, W. R. Tribe, and M. Pepper, Phys. Rev. Lett. **81**, 3491 (1996).

[2] M. Devlin, *Welcome to BLAST* (Web site of the University of Pennsylvania Physics Department, http://chile1.physics.upenn.edu/blastpublic/scienceintro.shtml, 2006).

[3] S. Kwok, B. J. Hrivnak, and E. F. Milone, Astrophys. Jour. Pt. 1 **303**, 451 (1986).

[4] E. E. Becklin and L. J. Moon, Adv. in Space Res. **30**, 2083 (2002).

[5] René Dändliker, The concept of modes in optics and photonics, in *Proc. SPIE Vol. 3831, Sixth International Conference on Education and Trainin in Optics and Photonics*, edited by J. J. Sanchez-Mondragon, pp. 193–198, 2000.

[6] D. P. Marrone *et al.*, *Observations in the 1.3 and 1.5 THz Atmospheric Windows with the Receiver Lab Telescope* (arXiv.org: from the Cornell University Library, http://www.arxiv.org/PS cache/astro-ph/pdf/0505/0505273v1.pdf, 2005).

[7] C. Leinert *et al.*, Astron. Astophys. Suppl. Ser. **127**, 1 (1998).

[8] M. J. Griffin, B. M. Swinyard, and L. G. Vigroux, SPIRE - Herschel's submillimetre camera and spectrometer, in *Proceedings of the SPIE, Volume 4850, IR Space Telescopes and Instruments*, edited by J. C. Mather, pp. 686–697, 2003.

[9] B. P. Crill *et al.*, Astophys. Jour. Suppl. Ser. **147**, 527 (2003).

[10] P. D. Mauskopf *et al.*, Astrophys. Jour. Lett. **536**, L59 (2000).

[11] P. Ade *et al.*, The balloon-borne large aperture submillimeter telescope (BLAST), in *Proc. SPIE Vol. 5498, Millimeter and Submillimeter Detectors for Astronomy II*, edited by J. Zmuidzinas, W. S. Holland, and S. Withington, pp. 42–54, 2004.

[12] D. J. Haig *et al.*, Bolocam: status and observations, in *Proc. SPIE Vol. 5498, Millimeter and Submillimeter Detectors for Astronomy II*, edited by J. Zmuidzinas, W. S. Holland, and S. Withington, pp. 78-94, 2004.

[13] J. Glenn *et al.*, Current status of Bolocam: a large-format millimeter-wave bolometer camera, in *Proc. SPIE, Volume 4855, Millimeter and Submillimeter Detectors for Astronomy*, edited by T. G. P. Jonas Zmuidzinas, pp. 30-40, 2003.

[14] *BOOMERANG at Cardiff Astronomy Instrumentation Group* (Web site of Astronomy and Instrumentation Group at Cardiff University, http://www.astro.cardiff.ac.uk/groups/instrumentation/projects/boomerang/index.html, 1998).

[15] W. Holmes *et al.*, Preliminary performance measurements of bolometers for the Planck high frequency instrument, in *Proc. SPIE Vol. 4855, Millimeter and Submillimeter Detectors for Astronomy*, edited by W. S. H. Jonas Zmuidzinas and S. Withington, pp. 208–216, 2003.

[16] P. M. Harvey, G. H. Rieke, D. F. Lester, and D. J. Benford, Single aperture far-infrared observatory (SAFIR), in *Proc. SPIE Vol. 4850, IR Space Telescopes and Instruments*, edited by J. C. Mather, pp. 1097–1108, 2003.

[17] D. Leisawitz, Adv. in Space Res. **34**, 631 (2003).

[18] D. Leisawitz, Astrophys. and Space Sci. **269-270**, 563 (1999).

[19] D. Leisawitza *et al.*, Adv. in Space Res. **40**, 689 (2007).

[20] T. Nakagawa and H. Murakami, Adv. in Space Res. **40**, 679 (2007).

[21] L. Heimerl, *Scientific and Technical Information (STI)* (Web site of National Aeronautic and Space Administration, http://www.sti.nasa.gov/tto/spinoff2000/ard6.htm, 2007).

[22] P. L. Richards, Jour. of App. Phys. **76**, 1 (1996).

[23] R. V. Sudiwala, M. Griffin, and A. Woodcraft, Int. Jour. of Inf. Mill. Waves **23**, 545 (2002).

[24] J. C. Mather, Appl. Opt. **21**, 1125 (1982).

[25] R. C. Jones, J. Opt. Soc. Am **43**, 1 (1953).

[26] A. V. D. Ziel, *Noise in Solid State Devices and Circuits* (Wiley-interscience, New York, 1986).

[27] L. Kuzmin, Ultimate cold-electron bolometer with strong electrothermal feedback, in *Proc. SPIE Vol. 5498, Millimeter and Submillimeter Detectors for Astronomy II*, edited by W. S. H. Jonas Zmuidzinas and S. Withington, pp. 349-361, 2004.

[28] L. Kuzmin, I. Devyatov, and D. Golubev, Cold-electron bolometer with electronic microrefrigeration and general noise analysis, in *Proc. SPIE Vol. 3465, Millimeter and Submillimeter Waves IV*, edited by M. N. Afsar, pp. 193–199, 1998.

[29] W. Holland, W. Duncan, and M. Griffin, Bolometers for submillimeter and millimeter astronomy, in *ASP Conf. Ser. 278: Single-Dish Radio Astronomy: Techniques and Applications*, edited by S. Stanimirovic, D. Altschuler, P. Goldsmith, and C. Salter, pp. 463–491, 2002, Provided by the Smithsonian/NASA Astrophysics Data System.

[30] M. Nahum and J. M. Martinis, Appl. Phys. Lett. **66**, 3203 (1995).

[31] M. Nahum and J. M. Martinis, Appl. Phys. Lett. **63**, 3075 (1993).

[32] D.-V. Anghel and L. Kuzmin, Appl. Phys. Lett. **82**, 293 (2003).

[33] A. M. Kadin and M. W. Johnson, Appl. Phys. Lett. **69**, 3938 (1996).

[34] D. Chouvaev, L. Kuzmin, and M. Tarasov, Supercond. Sci. Technol. **12**, 985 (1999).

[35] K. S. Yngvesson, Appl. Phys. Lett. **76**, 777 (2000).

[36] G. N. Gol'tsman *et al.*, Supercond. Sci. Technol. **4**, 453 (1991).

[37] E. M. Gershenzon *et al.*, Superconductivity **3**, 1582 (1990).

[38] A. Skalare *et al.*, A superconducting hot electron bolometer mixer for 530 GHz, in *Proceeding Fifth International Symposium Space Terahertz Technology*, pp. 157–168, 1994.

[39] T. G. Phillips and K. B. Jefferts, Rev. Sci. Instrum. **44**, 1009 (1973).

[40] T. G. Phillips and K. B. Jefferts, Ann. Rev. of Astro. and Astrophys. **20**, 285 (1982).

[41] L. Kuzmin, I. Agulo, M. Fominsky, A. Savin, and M. Tarasov, Supecond. Sci. Tech. **17**, S400 (2004).

[42] I. J. Agulo, L. Kuzmin, and M. Tarasov, Attowatt sensitivity of the cold electron bolometer, in *The 16th Int. Symp. On Space Terahertz Technology*, p. 79, 2005.

[43] L. P. Pfeiffer, K. W. West, H. L. Stormer, and K. W. Baldwin, Appl. Phys. Lett. **55**, 1888 (1989).

[44] K. Hirakawa and H. Sakaki, Phys. Rev. B **33**, 8291 (1986).

[45] E. E. Mendez, P. J. Price, and M. Heiblum, Appl. Phys. Lett. **45**, 294 (1984).

[46] H. L. Stormer, L. N. Pfeiffer, K. W. Baldwin, and K. W. West, Phys. Rev. B **41**, 6863 (1990).

[47] C. Kittel, *Introduction to Solid State Physics* (John Wiley and Sons, New York, 1996 (seventh edition)).

[48] N. W. Ashcroft and N. D. Mermin, *Solid State Physics* (Thomson Learning, London, 1976).

[49] R. L. Liboff, *Introductory Quantum Mechanics* (Addison-Wesley Publishing Company, Reading, Massachusetts, 1992 (second edition)).

[50] S. M. Sze, *Physics of Semiconductor Devices* (John Wiley and Sons, Inc., New York, 1981 (second edition)).

[51] D. J. Griffiths, *Introduction to Electrodynamics* (Prentice-Hall, New Jersey, 1989 (second edition)).

[52] A. Rockett, *Material Science and Engineering: Chapter 3 Solution Set* (Web site of University of Illinois at Urbana-Chanpaign, http://www.eeel.nist.gov/812/hall.html, 2005).

[53] R. A. Bube, *Electrons in Solids* (Academic Press, San Diego, 1988 (second edition)).

[54] D. A. Fraser, *Physics of Semiconductor Devices* (The Universities Press, Belfast, 1986 (fourth edition)).

[55] V. Gavryushin, *The Metal-Semiconductor Junction. Schottky Diode. Ohmic Contacts* (Web site of Vilnius University, http://www.mtmi.vu.lt/pfk/funkc-dariniai/diod/schottky.htm, 2004).

[56] K. C. Lee, J. Res. Natl. Inst. Stand. Technol. **103**, 177 (1998).

[57] H. J. Bühlmann and M. Ilegems, J. Electrochem. Soc. **138**, 2795 (1991).

[58] *Hall Effect* (Web site of National Institute of Standards and Technology, http://www.eeel.nist.gov/812/hall.html, 2006).

[59] Y. Ma *et al.*, Phys. Rev. B **43**, 9033 (1991).

[60] N. Balkan, H. Çelik, A. J. Vickers, and M. Cankurtaran, Phys. Rev. B **52**, 17 210 (1995).

[61] D. R. Schmidt *et al.*, Appl. Phys. Lett. **86**, 053505 (2005).

[62] F. C. Wellstood, C. Urbina, and J. Clarke, Phys. Rev. B **49**, 5942 (1993).

[63] J. Thieman, D. Robinson-Boonstra, and B. Stephenson, *Adventures in Geospace: Electromagnetism* (Web site of National Aeronautic and Space Administration, http://son.nasa.gov/tass/content/electromagnetism.htm, 2006).

[64] D. R. Leadley, *Quantum Hall Effect* (Web site of Warwick University, http://www.warwick.ac.uk/ phsbm/research.htm, 1997).

[65] Y.-W. Tan *et al.*, Phys. Rev. Lett. **94**, 016405 (2005).

[66] P. T. Coleridge, Semicond. Sci. Technol. **5**, 961 (1990).

[67] M. G. Vavilov and I. L. Aleiner, Phys. Rev. B **69** (2004).

[68] D. E. Prober, Appl. Phys. Lett. **62**, 2119 (1993).

[69] E. Figueroa-Feliciano, *Transition Edge Sensors (TES)* (Web site of the Figueroa Group at the Massachusetts Institute of Technology, http://web.mit.edu/figueroagroup/ucal/ucal-tes/index.html, 2007).

[70] B. Cabrera *et al.*, Physica B **280**, 509 (2000).

[71] P. Burke, I. Spielman, J. Eisenstein, L. Pfeiffer, and K. West, Appl. Phys. Lett. **76**, 745 (2000).

[72] D. F. Santavicca, M. O. Reesse, A. B. True, and C. A. S. amd D. E. Prober, Antenna-coupled niobium bolometers for terahertz spectroscopy, in *IEEE Proceedings*, pp. 1–5, 2006.

[73] A. M. Savin *et al.*, App. Phys. Lett. **79**, 1471 (2001).

[74] L. Kuzmin, Micro. Elect. Engn. **69**, 309 (2003).

[75] Y. Kawano, Y. Hisanaga, H. Takenouchi, and S. Komiyama, Jour. Appl. Phys. **89**, 4037 (2001).

[76] E. Ciancio, R. C. Iotti, and F. Rossi, Europhys. Lett. **65**, 242 (2004).

[77] N.-P. Chien, H. J. Ueng, D. B. Janes, J. M. Woodall, and M. R. Melloch, Jour. of App. Phys. **88**, 309 (2000).

[78] M. Missous, E. H. Rhoderick, D. A. Woolf, and S. P. Wilkes, Semicond. Sci. Technol. **7**, 218 (1992).

[79] M. Nahum, T. M. Eiles, and J. M. Martinis, Appl. Phys. Lett. **65**, 3123 (1994).

[80] P. J. Price, Jour. of App. Phys. **53**, 6863 (1982).

[81] A. Babiński, J. Siwiec-Matuszyk, J. M. Baranosski, G. Li, and C. Jagadish, Appl. Phys. Lett. **77**, 999 (2000).

[82] A. Cavalheiro *et al.*, J. Phys.: Condens. Matter **15**, 121 (2003).

[83] S. Kang, P. J. Burke, L. Pfeiffer, and K. West, Solid State Elect. **48**, 2013 (2003).

[84] *Everything You Ever Wanted to Know About Frequency-Selective Surface Filters but Were Afraid to Ask* (Web site of Columbia University's Department of Physics, http://calvin.phys.columbia.edu/group web/filters/filter.pdf, 2005).

[85] J. Pendry, A. Holden, W. Steward, and I. Youngs, Phys. Rev. Lett. **76**, 4773 (1996).

[86] L. B. Whitbourn and R. C. Compton, Appl. Opt. **24**, 217 (1985).

[87] A. L. Woodcraft *et al.*, Int. J. of Inf. and Mill. Waves **23**, 575 (2002).

[88] C. L. Hunt *et al.*, Transition-edge superconducting antenna-coupled bolometer, in *Proceedings of SPIE, Volume 4855 Millimeter and Submillimeter Detectors for Astronomy*, edited by T. G. Phillips and J. Zmuidzinas, pp. 318–321, 2003.

[89] S. Komiyama *et al.*, Sol. St. Comm. **80**, 157 (1991).

[90] N. A. Kabir *et al.*, Appl. Phys. Lett. **89** (2006).